SPECTRODIRECTIONAL SENSORS FOR MONITORING THE AMERICAN TROPICAL DRY FOREST SUCCESSION

Virginia Elena García Millán

Tesis doctoral · 2012

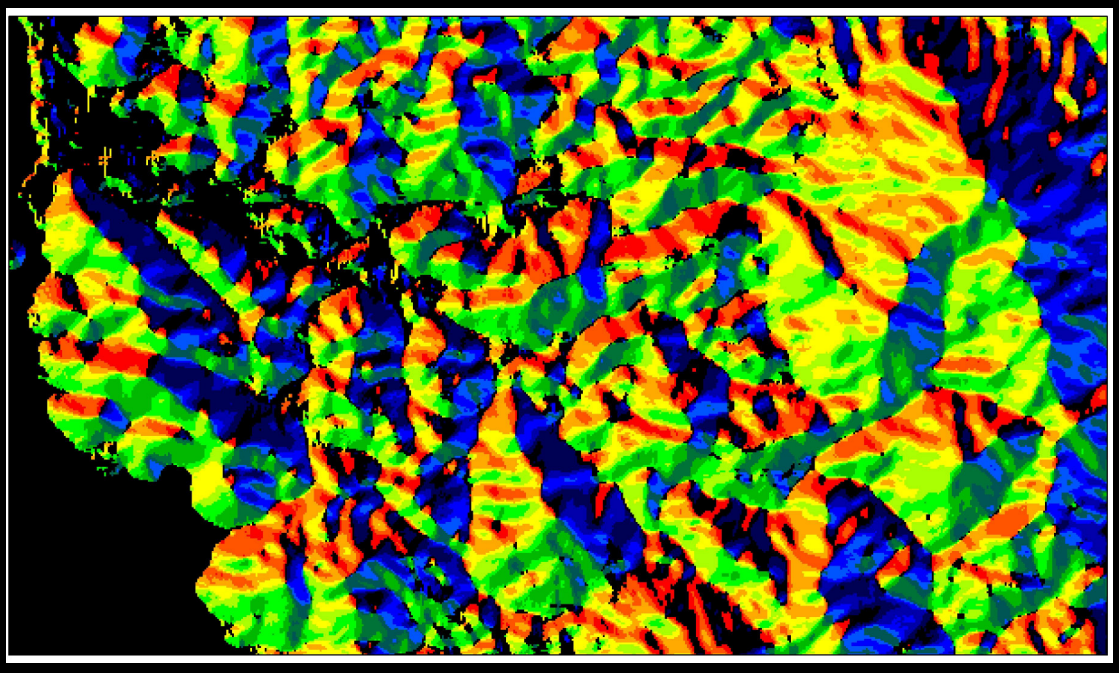

Departamento de Geografía, Historia y Filosofía
Universidad Pablo de Olavide
Sevilla, Spain

SPECTRODIRECTIONAL SENSORS FOR MONITORING THE AMERICAN TROPICAL DRY FOREST SUCCESSION

Memoria presentada por

Virginia Elena García Millán

para optar al grado de Doctora

Con la aprobación de

Dr. G. Arturo Sánchez Azofeifa
Department of Earth and
Atmospheric Sciences
University of Alberta, Canada

Dr. Gonzalo C. Málvarez García
Departamento de Geografía Física
Universidad Pablo de Olavide
Sevilla, España

Universidad Pablo de Olavide, Sevilla
4 de junio de 2012

Caminante, son tus huellas el camino y nada más,
caminante no hay camino, se hace camino al andar.
Al andar se hace el camino, y al volver la vista atrás
se ve la senda que nunca se ha de volver a pisar.
Caminante no hay camino sino estelas en la mar.

Antonio Machado

ACKNOWLEDGEMENTS

I specially would like to show gratitude to my supervisors. I thank Dr. Sánchez Azofeifa for giving me the opportunity to participate in the Tropi-Dry project and guide me in the development of this thesis. It has been very beneficial to me to learn from his scientific and innovative point of view. He showed me the integration of technology and nature conservation by the use of remote sensors. He has been a model to follow and a friend. I thank Dr. Malvarez Garcia for helping me to put science into society, to up-scale our findings into reality. He has always been very supportive and knew the exact words to motivate me.

I would like to acknowledge the Universidad Pablo de Olavide and the University of Alberta for the institutional support. I would like to particularly mention Mei Mei Chong, Donnette Thayer, Antonio Ramírez and Maria del Carmen Martín for the administrative support.

The CHRIS/PROBA images utilized in this thesis were provided by the European Space Agency (ESA) after the Tropi-Dry's project #6036. For this reason, we acknowledge the ESA for the contribution to this thesis. I do a special mention to Peter Fletcher, Ralf Quast and Luis Alonso for their help with CHRIS/PROBA images pre-processing and solving questions about BEAM-Visat operation.

There have been many people that helped in the development of this thesis somehow and in different moments. I would like to thank Dr. Carlos Portillo, Mauricio Yamanaka, Mauricio Castillo, Tao Cheng, Dr. Jilu Feng and Gerard More for their help in data processing, for assisting with the software and with the statistical analysis. We also thank Mauricio Yamanaka for his help in the field work in Mexico and Daniel Costa Paula, Joselandio Santos and Dorim in Brazil. We make a special mention to Dr. Mario Marcos do Espirito Santo for the institutional support in Brazil (Universidad de Montes Claros UNIMONTES). We thank Catalina Maria Smith and Donnette Thayer for their help as proofreaders.

I thank my family, friends and colleagues for their emotional support and patience. This thesis would have not been possible without them.

TABLE OF CONTENTS

LIST OF TABLES

LIST OF FIGURES

Resumen

El bosque tropical seco es un "hot-spot" a nivel mundial no solo por la biodiversidad que engloba, si no por su fragilidad y por estar altamente amenazado por el impacto humano, al ser un ecosistema que provee de diversos servicios ambientales, dadas las características climáticas y ambientales que lo definen.

En comparación con el bosque tropical húmedo, al bosque tropical seco se le ha prestado mucha menos atención en el ámbito científico y legislativo. Es por ello que es prioritario el estudio de este ecosistema a escala de paisaje, para desarrollar estrategias de gestión y conservación.

El bosque tropical seco se ha deforestado durante siglos para ser sustituido por zonas de pastos para ganado, con fines agrícolas o para extraer maderas preciosas. A partir de los informes presentados por el Club de Roma en 1968 acerca del desarrollo económico en curso y los efectos sobre la sociedad y el medio ambiente (presentados en la Cumbre de Estocolmo en 1978), y en el informe Bruntland de la ONU en 1987, que desembocaron en la Cumbre de la Tierra de Rio de Janeiro en 1992 y en Johannesburgo en 2002, la presión internacional acerca del estado del medio ambiente y de la necesidad de preservarlo, llevaron a los gobiernos de muchos países a dictar legislación referente a la protección del medio ambiente dentro de sus territorios nacionales. Gracias a ello, en el caso del bosque tropical seco, se protegieron ciertas zonas dedicadas a la conservación del ecosistema, comenzando así un proceso de regeneración del bosque, o en términos ecológicos, de sucesión ecológica.

Diversos estudios apuntan la necesidad de tener en cuenta el estado de desarrollo del bosque a la hora de estimar los servicios ambientales que pueden proporcionar, y de cara a la gestión de estos espacios. Por eso es necesario determinar la extensión y localización precisa del bosque tropical seco, especificando el estado de sucesión ecológica en el que se encuentra.

La teledetección se erige como una herramienta de alta utilidad para estudios a escala paisaje, especialmente en ecosistemas que no sean de acceso fácil, como el bosque tropical seco. Además, es una herramienta que proporciona un monitoreo continuo a escala temporal y espacial a bajo coste.

Hasta el momento los satélites en órbita eran capaces de identificar elementos de la superficie de la tierra, y en el caso de la vegetación, distinguen diferentes ecosistemas e incluso rasgos fenológicos de la vegetación. Sin embargo, no son

capaces de proporcionar información acerca de procesos ecológicos al detalle, como el estado de sucesión ecológica en el que se encuentra el bosque tropical seco.

Los satélites de nueva generación, como Chris Proba, apuestan por tecnologías hasta el momento poco exploradas, como sensores hiperespectrales y observación del objeto en estudio desde varios ángulos de observación.

En esta tesis, queremos estudiar la capacidad de Chris Proba para indagar más en profundidad en procesos ecológicos como la sucesión ecológica, o la productividad de pastos tropicales.

En una primera aproximación al estudio de las imágenes Chris Proba, se han analizado los valores de reflectancia de imágenes adquiridas para México, Nicaragua y Brasil (cubriendo todo el eje latitudinal de distribución del bosque tropical seco en el continente americano). Se han utilizado imágenes de la época seca y la época de lluvias con cinco ángulos de observación diferentes (-55º, -36º, 0º, +36º, +55º). Las áreas de trabajo corresponden con tres estadios sucesionales dentro del bosque tropical seco secundario (temprano, intermedio y maduro), que fueron caracterizados a partir de su estructura y composición florística.

Las técnicas estadísticas empleadas incluyen un análisis de las firmas espectrales para cada ángulo de observación, estadio sucesional y estación del año y análisis de la varianza para cada una de las 18 bandas espectrales del sensor. Además se realizó un análisis multidimensional con las 18 bandas que ofrece este satélite y estudios estadísticos de separación espectral de los estados sucesionales del bosque tropical seco.

Los resultados apuntan a que Chris Proba es capaz de distinguir los tres estadios sucesionales del bosque tropical seco en los tres puntos del continente americano estudiados en función de sus características espectrodireccionales, especialmente durante la época seca.

Una vez demostrada la potencialidad de Chris Proba para la discriminación de estados sucesionales del bosque tropical seco (capítulo 2), se hace necesaria la elaboración de mapas de distribución de dichos estados sucesionales, que supondrá una herramienta real para la gestión de este tipo de espacio.

Para el desarrollo del capítulo 2, se han utilizado imágenes del bosque tropical seco brasileño, por el alto conocimiento de campo que se tiene del área. Para la generación de mapas de clasificación, se han empleado modelos estadísticos no paramétricos, que se adaptan mejor a las características de la ecología del

bosque tropical, que no se definen por una distribución normal de datos. Se han utilizado árboles decisionales como método estadístico. Se han analizado diversas combinaciones de variables a introducir en el modelo estadístico (nº de ángulos de observación y nº de estaciones del año) para dilucidar cuál es la mejor opción en la creación de un mapa de clasificación de estados sucesionales del bosque tropical seco, en función de los resultados de precisión de los mapas resultantes.

Una vez habiendo explorado las técnicas apropiadas para generar un mapa de estados sucesionales de bosque tropical seco en área planas, nos enfrentamos al reto de elaborar un mapa de similares características en México, donde existe la dificultad añadida de la topografía del área.

En el mundo de la teledetección, no se ha logrado una corrección radiométrica de los valores de reflectancia de píxeles afectados por sombras que crea el relieve con una precisión adecuada. Sin embargo, es del todo necesario tener mapas de los estados sucesionales del bosque tropical seco para la gestión del mismo, por lo que la limitación de la topografía debe ser superada, y éste es el interés de nuestro estudio. Para Chris Proba, además, se debe considerar el efecto del ángulo de observación en la iluminación de la superficie terrestre.

Una vez las imágenes Chris Proba fueron corregidas atmosféricamente y ortorectificadas, se aplicó un algoritmo que utiliza el coseno del ángulo de incidencia solar para rectificar el efecto de las sombras generadas por el terreno.

Se realizaron mapas de clasificación usando las imágenes Chris Proba antes y después de aplicar dicho algoritmo para cuantificar el error producido por las sombras en la identificación de los estados sucesionales del bosque tropical seco.

La presente tesis presenta por primera vez mapas de sucesión del bosque tropical seco americano, una herramienta indispensable para la gestión de este ecosistema amenazado. Se abre una línea de trabajo en la monitorización de este fenómeno ecológico, puesto que una vez determinada la técnica más apropiada para realizar mapas de clasificación de los estados de sucesión del bosque seco, se podrán realizar mapas cada cierto tiempo para monitorizar y estudiar el progreso de la regeneración del bosque seco y la tasa se crecimiento del bosque.

Tras los experimentos conducidos en la presente tesis, se ha llegado a la conclusión de que son necesarias técnicas más complejas de teledetección para monitorear y cartografiar fenómenos fenológicos, como la sucesión ecológica del bosque tropical seco.

Queda demostrado que los sensores multiespectrales son insuficientes para la identificación de estados sucesionales del bosque tropical seco, mientras que los sensores hiperespectrales sí lo logran. Además, la observación multiangular que ofrecen pocos satélites (como Chris Proba), aportan nueva información acerca de la estructura del bosque tropical seco, que ayuda a la discriminación de estados de sucesión.

Los resultados de esta tesis animan a continuar en estas líneas de trabajo (hiperespectrabilidad y multiangularidad), de cara al diseño de satélites y planificación de misiones espaciales en el futuro.

Abstract

In a world of rapid global change, it is necessary to understand the underlying causes and mechanisms of these changes. Unfortunately, many of the driving processes that control global change occur at local scales. For this reason, it is necessary to investigate from the local to the global scale. Remote sensing is a suitable tool for this, since current offer of space-borne and air-borne platforms covers all scales in a continuous spatial and temporal mode. This thesis focuses on a particular ecosystem, the tropical dry forest. For this aim, the spectral, angular and temporal domains of Chris remote sensor on board of PROBA-1 are examined in three study sites within the Americas.

The outline of this thesis is conFigured in five chapters that are briefly introduced as follows:

Chapter 1 – introduces general concepts about the tropical dry forests and remote sensing of forests. A description about the American tropical dry forest and its conservation status is provided, as well as technical description of CHRIS/PROBA satellite and reference research on remote sensing of forests worldwide.

Chapter 2 – presents an exploration of spectral, angular and temporal CHRIS/PROBA data in the discrimination of three successional stages (early, intermediate and late) within secondary tropical dry forests in three study sites in the Americas (Mexico, Nicaragua and Brazil).

Chapter 3 – investigates optimum methods for mapping succession within a tropical dry forest in a flat area in Brazil considering the spectral, angular and temporal domains of CHRIS/PROBA data. Non-parametric decision trees are used for classification.

Chapter 4 – analyzes the implications of CHRIS/PROBA's radiometric correction in the accurate discrimination of three successional stages of a tropical dry forest in a mountainous area in Mexico, considering the angular particularities of the sensor and the phenology of the ecosystem.

Chapter 5 – presents general conclusions extracted from core chapters 2 to 4 and suggestions for future research.

Chapter 1.

REMOTE SENSING OF FORESTS, AN OVERVIEW

Remote sensing of forests

In a scenario of increasing awareness about the state of forests and climate change, it is crucial to have data about the forest extent and health status, distinguishing between different forests biomes and primary and secondary forests (Wright, 2005, Saatchi et al. 2010). Maps about forest extension, succession, biomass and health are fundamental tools for environmental management. Remote sensors provide unique opportunity for mapping, since they collect optical data of the Earth surface in a spatial and temporal continuum. In addition, remote sensing overcome traditional mapping techniques because (1) it is possible to retrieve information of remote areas that cannot be reached in field surveys, (2) satellite images are more affordable than field campaigns and (3) maps generated with aerial photos or satellite images are more accurate than maps derived from extrapolated field data (Asner et al. 1998, Braswell et al. 2003).

Many forests maps have been done for the American continent to date. The United States created the National Land Cover Data (NLCD) from Landsat TM 30m spatial resolution (Stehman et al. 2003). In the same line, Mas et al. 2002 produced a land cover map for Mexico using Landsat ETM+. The collaboration of seven research groups resulted in the generation of unified Ecosystem Map for seven countries of Central America (Vreugdenhil et al., 2002). Eva et al. 2004 produced a land cover map of South America by the combined used of 1600 images of several satellites: the Along Track Scanning Radiometer (ATSR-2), Systeme Pour l'Observation de la Terre (SPOT) and the JERS-1 L band radar. For the scope of our study, the most remarkable contribution is a land cover map of Neotropical dry forests for the Americas generated with Landsat ETM+, MODIS and the Digital Elevation Model (DEM) of Shuttle Radar Topography Mission (SRTM) (Portillo & Sanchez-Azofeifa, 2010). However, these coarse-scale resolution maps derived from multispectral imagery (e.g. Advanced Very High Resolution Radiometer AVHRR, SPOT and MODIS provide an insight of forest distribution at a regional level, but they do not grant enough resolution for monitoring ecological processes and accurate estimate biomass and carbon stocks.

Until date, studies on tropical forests have pointed out limitations in the characterization of secondary forests and successional stages (Sanchez-Azofeifa et al. 2003a): (1) confusion of advanced stages of succession (more than 15 years) and primary forests (Vieira et al. 2003), (2) difficulties to discriminate early stage of succession from plantations, crops and shrubs (Helmer et al. 2000), and (3) wrong classification of successional stages of succession in mountainous areas due to shadows

produced by topography (Fahsi et al. 2000). Up to year 2005, many authors proposed medium-resolution multispectral sensors (e.g. Landsat, SPOT, Advanced Spaceborne Thermal Emission and Reflection Radiometer, ASTER) as the most appropriate for mapping secondary forest and succession (Arroyo-Mora et al. 2004, Kalacska et al. 2005a, 2005b). Nevertheless, the progress in spectrodirectionality suggests that better forest characterization can be achieved from hyperspectral sensors and multi-angular observations (Schaepman et al. 2009).

As stated in the previous section, structure and composition varies along successional stages of TDFs. Hyperspectral sensors arise as suitable tools for biochemical identification of vegetation components, while multiangular observations provide accurate characterisation of forest structure (Barnsley et al. 2004, Kneubühler et al. 2008, Schaepman et al. 2009). Motivated by the promising results of spectrodirectional space-borne platforms, we decided to explore the study of tropical dry forests succession using CHRIS/PROBA imagery.

a. Hyperspectral sensors in the study of forests

The term "hyperspectral" refers to sensors which offer high spectral resolution by covering a certain range of the spectra with a continuous or semi-continuous large collection of narrow bands (around 10 nm width). The advantage of hyperspectral bands in front of broad bands of multispectral sensors is the individualization of biochemical properties of vegetation in narrower bands. For instance, Landsat ETM+ band 5 covers the spectral range between 1550-1750 nm, which coincides with absorption peaks for lignin (1690 nm) and nitrogen (1730 nm) (Fourty et al., 1996).

Hyperspectral sensors have been used in the study of vegetation at several scales, from leave to canopy. At the leave-scale, these sensors have demonstrated to prevail over multispectral sensors in discriminating leaf pigments, water content, and chemical composition of green leaves (e.g. chlorophyll, nitrogen) (Curran 1994; Martin and Aber 1997; Townsend et al. 2008, Blackburn, 1999, Gastellu-Etchegorri et al. 1995) as well as other non-photosynthetic elements of vegetation (e.g. lignin) (Roberts et al. 1990, 1993, Ustin et al. 1992, Gao et Goetz, 1994). At a canopy-scale, structural parameters such as canopy closure, LAI or stand density have been determined using hyperspectral sensors on board of air-borne or space-borne platforms (Asner et al. 2003). Composition features such as chlorophyll content, nitrogen, lignin and water content (Dennison and Roberts, 2004) helped in the identification of forest types (Kayitakire et al.

2006, Johansen et al. 2007), tree species (Levin et al. 2007, Rocchini, 2007, Martin et al. 1998), invasive species and plagues in the early stage of invasion (Underwood et al. 2003, Lass et al. 2002, Bachmann et al. 2001).

Even though hyperspectral sensors have existed in orbit for more than 20 years with the launch of MODIS (220 bands) in 1999, environmental studies that used this kind of sensors are limited. Most of these studies have been developed with NASA's Airborne Visible / Infrared Imaging Spectrometer (AVIRIS) (Green et al. 1998). Several are the causes for the low exploitation of hyperspectral sensors (Nagendra & Rocchini, 2008, Thenkabail et al., 2004a, Schaepman et al. 2009):

1. There is a small number of hyperspectral sensors in orbit (Table 1.1.).
2. Acquisition of hyperspectral images is expensive or depends on the affiliation of a project into a global research schedule (e.g. AVIRIS, CHRIS/PROBA).
3. Hyperspectral space-borne and air-borne platforms do not have a regular orbit, but depends on demand. Though, there is not a temporal series of hyperspectral images of sites worldwide and image acquisition requires pre-scheduling.
4. Due to the high number of bands, there is a high volume of data collected, which requires large storage and downlink capacity, plus computational effort and timing.
5. A complex and specific knowledge on software and techniques are needed to correct and analyze hyperspectral images. Usually, required software is expensive.

Given the large number of landscapes, habitats, species and stages of growth and succession, plus the complex structure of the canopy of tropical forests (Nagendra 2001), hyperspectral sensors are especially useful in the characterization and monitoring of this biome. Despite this, there is a little number of publications on tropical areas that used hyperspectral sensors. In tropical forests, hyperspectral sensors have been used for trees and lianas species identification (Cochrane 2000, Castro-Esau et al. 2004, Clark et al. 2005, Kalacska et al. 2007a, 2007b, Sanchez-Azofeifa et al. 2009), forest structure description (Thenkabail et al., 2003), biomass estimation and land cover classification (Thenkabail et al. 2004b). To our knowledge, any study has focused in the determination of the biomass or the land cover classification of tropical dry forests with hyperspectral sensors.

CHRIS on board of PROBA-1 was designed to overcome some of the limitations that previous hyperspectral sensors presented. CHRIS spectral

resolution covered the entire wavelength range in an almost continuum in 62 bands for Mode 1. However, it was able to capture a subset of a smaller number of bands (37 or 18 bands) for a selected target (e.g. water, chlorophyll, land, aerosols) by previous configuration, on key wavelength of the spectra. This feature reduced the acquired data easing the computational work and storage. For studies different to atmosphere, bands of water vapour and oxygen absorption were neglected. CHRIS images were delivered free of charge, because PROBA-1 was an experimental mission. Although CHRIS/PROBA was subdued to an acquisition plan that was scheduled many months in advance, it could be eventually modified to image environmental disasters (e.g. tsunamis or volcano explosions). Moreover, the ESA developed an open-source user-friendly interface to pre-process raw CHRIS/PROBA images that allow initial exploration, BEAM-Visat (Alonso et al. 2009).

b. Multiangular observations for the study of forests

Natural targets on Earth's surface scatter sunlight diffusely in several directions, with the exception of a mirror-like surface of a calm water body, which reflects it in a preferential direction (Diner et al. 1999). The angular reflectance pattern into which solar radiation is scattered from an observed target is also known as Bidirectional Distribution Reflectance Function (BDRF) (Nicodemus et al. 1977). It is determined on the sun and the sensor viewing geometry, and depends on the wavelength (Asner et al. 1998). Its magnitude and shape is governed by the composition, density and geometric structure of the reflecting medium (Diner et al. 1999). The BRDF of most natural targets is anisotropic (especially vegetation and atmosphere), meaning that sunlight do not reflects/emits with the same intensity in all directions (Asner et al. 1998) (Figure 1.2.).

BRDF of vegetation is determined at leaf, canopy and landscape level. At the leaf level, the BRDF is a function of leaf biochemical composition (e.g. chlorophyll, water, lignin, cellulose, starch and nitrogen), geometry and orientation (Myneni et al. 1989). At a canopy level, the BRDF depends on vegetation and understory's texture and composition (Jacquemoud et al. 1992), as well as the leaf are index (LAI), the leaf angular distribution (LAD), foliage clumping and the distribution of shaded and illuminated leaves and branches (Ross, 1981, Goel, 1988, Myneni and Asrar, 1993, Chen and Cihlar, 1995, Li et al. 1995). At a landscape level BRDF is determined by the configuration of different vegetation types, tree morphology and ground coverage (Li and Strahler, 1985, Li et al. 1995).

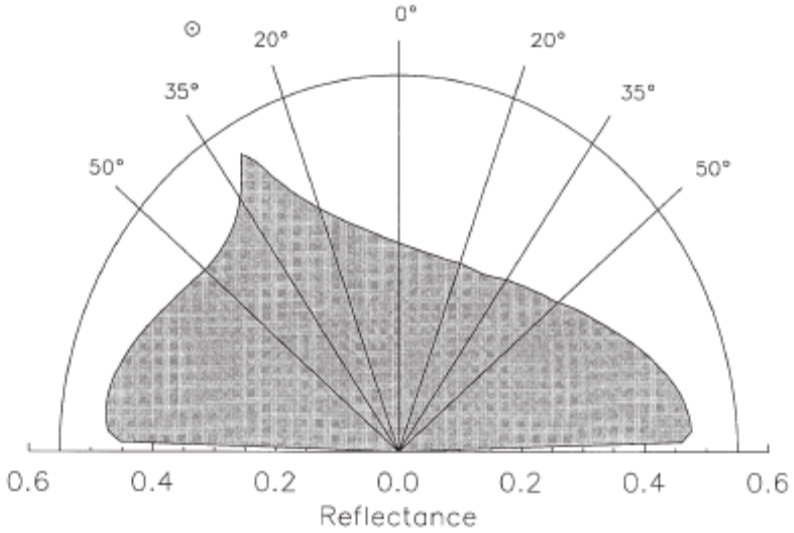

Figure 1.2. BRDF representation along the solar principal plane (the plane defined by solar inclination and normal angles). After Asner et al. 1998.

Since the launch of ESA ATSR-1 on ERS-1 in 1991, there are satellites equipped with more than a single-pointing camera. Nevertheless, their multi-angle capability has not always been used to explore the BRDF of observed targets (Diner et al. 1999). It has been used for different purposes, such as enlarging the swath width and better characterize atmospheric parameters (e.g. MODIS, AVHRR) (Asner et al. 1998) or to build up Digital Elevation Models (e.g. ASTER). These satellites did not succeed in the study of BRDF because multi-angle images were acquired in a sequential manner (Diner et al. 1999, Braswell et al. 2003). The sequential imaging consists in taking an image of an Earth area during an overpass and taking another image of the same area in the successive overpass from a different angle. The temporal gap between the first and the second acquisition can be of several days or weeks; therefore there could be changes in the observed target (e.g. phenological changes in vegetation) and especially in atmospheric conditions (Diner et al. 1999). The assembling of both images with different angle of observation for the characterization of BRDF results inaccurate (Diner et al. 1999, Barnsley et al. 2004). A second generation of multi-angle satellites (e.g. MIRS on board of Terra or POLDER on board of ADEOS, both launched in 1999) acquires quasi-simultaneous images at different angles of observation along the flight direction by a battery of cameras pointing at different directions (Figure 3). The reconstruction of the BRDF of a ground target is possible in the overlapping areas of consecutive images. However, the real simultaneous acquisition of multi-angle images has not been achieved until

the launch of PROBA-1 in 2001, which focuses a single ground target and takes images of it from five different angles as it progresses in its across-track orbit (Figure 1.3.).

Two other important limitations of most satellites with multi-angular pointing are (1) the low spectral resolution and (2) the coarse spatial resolution. Chris on board of PROBA-1 overcame these two limitations (Barnsley et al. 2004). For instance, compared to MIRS (5 broad bands covering VNIR), Chris provided 18 to 62 hyperspectral bands of a wavelength range of 400-1050 nm. Chris' pixel size ranges between 17 to 34 m depending on the acquisition mode, in front of 250 m (red band) to 1100 m (rest of bands) of MIRS (Table 1.2.).

Structure have been proved to play an important role in the characterization of forests and other vegetation types worldwide, helping in the discrimination of forest types, successional stages of growth, biomass and carbon sequestration (Widlowski et al. 2004, Chopping et al. 2006). Remote sensing multi-angle observations are intended to collect information about structural parameters of the observed target, particularly about the structure of the forest canopies (Braswell et al. 2003). Most of Earth Observation satellites offer a single-angle observation (generally nadir pointing), which have been demonstrated to be insufficient for the retrieval of structural elements. Since forests' BRDF is anisotropic (Asner et al. 1998) (Figure 2), single-angle sensors are missing part of the optical information of the target. Until the launch of multi-angle satellites, vertical structural parameters (e.g. LAI) were estimated indirectly using nadir observations as a function of other parameters (e.g. NDVI, fraction of Absorbed Photosynthetic Active Radiation (fAPAR)) (Asner et al. 1998, Diner et al. 1999, Kalacska et al. 2005a, 2005b). Nowadays, multi-angle satellites allow the direct and accurate characterization of structural parameters, such as leaf angle distribution, tree height (Kimes et al. 2006, Chopping et al. 2008a, 2009, Heiskanen et al. 2006), tree density (Sabol et al. 2002, Wessels et al. 2004, Chopping et al. 2006, 2008, 2009), LAI (Diner et al. 1999, Pocewicz et al. 2007), fAPAR (Running et al. 1994), canopy clumping (Ustin el at. 2004, Chen et al. 2005a, Leblanc et al. 2005), gap fraction (Barker-Schaaf and Strahler 1994, Li et al. 1995, Gerard and North 1997) and canopy heterogeneity (Widlowski et al. 2001, Pinty et al. 2002). Most of these findings have been performed with NASA's Multi-Angle Instrument Radiometric Spectrometer (MIRS). The only paper that focused on tropical dry forest from a multiangular point of view is Liesenberg et al. 2007, who studied the Brazilian *cerrado* using MIRS.

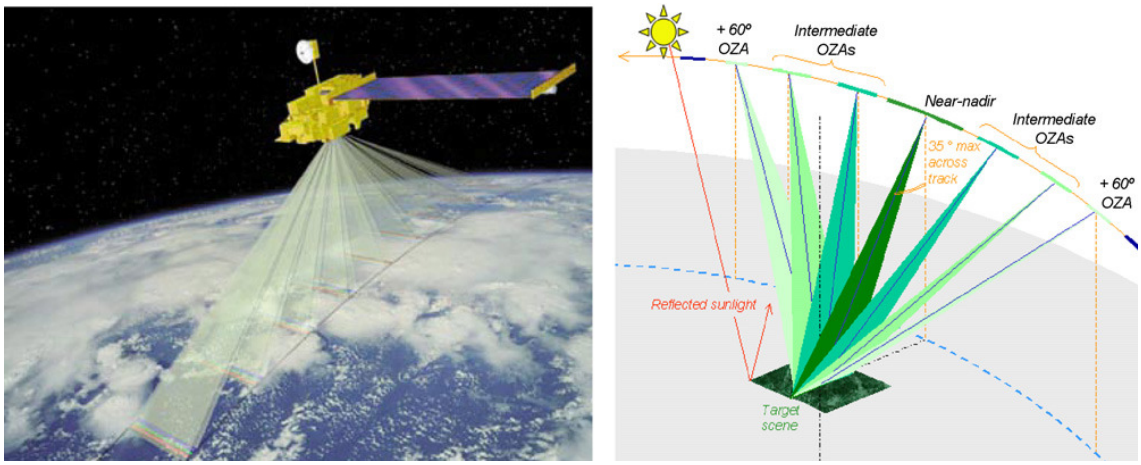

Figure 1.3. Two different acquisition methods of directional information using either nine cameras pointing at different locations (left) (NASA MISR), or by using an agile platform (right) (SPECTRA, 2005 after Schaepman et al. 2007).

The avant-garde on satellites. The case of CHRIS/PROBA

a. Basic description

The Compact High Resolution Imaging Spectrometer (CHRIS) instrument is the principal payload on the European Space Agency (ESA) small satellite platform PROBA-1 (Project for On-Board Autonomy). When PROBA-1 was launched on October 2001, it was originally intended to be a one-year experimental mission to test the technical configuration of SPECTRA mission (Barnsley et al. 2004, Cutter & Sweeting, 2007). Nevertheless, it has been working during almost 11 year and provided more than 10 000 images for different research purposes. In February 10th 2012, PROBA-1 was orbiting in a different orbit than originally planned, so illumination conditions were different to those for its nominal operational plan. Up to this, the constant radiation affected the spacecraft attitude and pointing control systems. For these reasons, until new order, CHRIS/PROBA is not functioning anymore.

PROBA-1 is a small platform of 60cm×60cm×80cm that weights around 100 kg, including payloads. It has a sun-synchronous orbit, with an equatorial crossing time at launch of 10:30. Its orbit is near elliptical, with an altitude varying from about 550km to about 670km. The spacecraft attitude is controlled by a set of four reaction wheels, which are integrated to the satellite structure. These allow the satellite to be manoeuvred in each of the three planes (i.e. roll, pitch and yaw). This characteristic was intended to: (1) enlarge the area to be visualized on Earth surface, (2) to increase the possibilities of avoiding clouds bodies in scene and sun glint over water bodies, (3) improve the signal-to-noise ratio by increasing the

integration time (by slowing the pitching while image acquisition) (4) to increment the re-visit period (to acquire more that one image of a Earth's target per week) and (5) to provide images at different five view angles in the same overpass (Figure 4). This last property was designed to support research on Bi-directional Reflectance Distribution Function (BRDF) (especially of vegetation and atmospheric aerosol targets) and to generate digital elevation models through stereo photogrammetric reconstruction. PROBA-1 takes a first image when the platform reaches a position at -55º respect to the ground target, and repeats the imaging at -36º, 0º, +36º and +55º as it progresses in its along track (Figure 1.4.). This process takes around three minutes.

Regarding the re-visit period, the probability of acquiring successive images within a short time period depends on the orbit of PROBA-1 although is elevated in higher latitudes. Close to the equator, it is possible to acquire images of the same ground target in three consecutive days: one from the west, one on top of the target and another from the east (Barnsley et al. 2004).

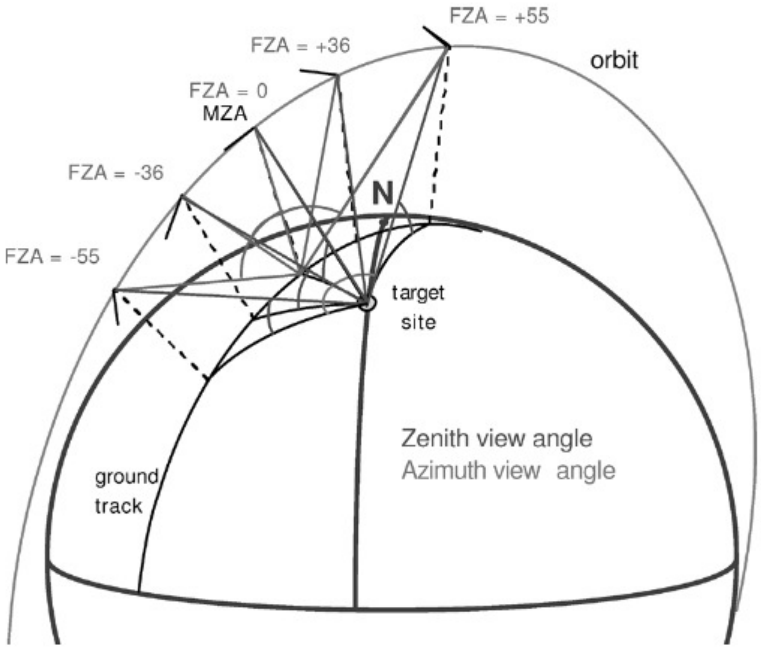

Figure 1.4. Scheme of PROBA/CHRIS acquisition geometry (after Guanter et al. 2004)

Among the several instruments on board of PROBA-1, our interest is centred in CHRIS push-broom sensor. CHRIS is a hyperspectral imager, consisting on a telescope and an imaging spectrometer, attached to a CCD-array (Charge Coupled Device) detector system. It weighs approximately 14kg and occupies a volume of 0.79m×0.26m×0.20m. The spectral

resolution of CHRIS is limited to the visible and near-infrared wavelength between 400 and 1050 nm, of narrow band-width between 5 to 11 nm. CHRIS can deliver images of nominal swath up to13 km, at two spatial resolutions: 17 m or 34m. The main particularity of CHRIS is that output images can be layout in five modes with different spatial and spectral resolution (Barnsley et al. 2004) (Table 1.3.):

TABLE 1.3. CHRIS Nominal Operating modes after Cutter & Sweeting, 2007.

Mode	Nº of bands	Pixel size	Swath width	Application
1	62	34 m	Full (13 km2)	Aerosols
2	18	17 m	Full (13 km2)	Water
3	18	17 m	Full (13 km2)	Land
4	18	17 m	Full (13 km2)	Chlorophyll
5	37	17 m	Half (7 km2)	Land

Mode 1. Full Swath, Reduced Spatial Resolution. This mode provides the larger nominal swath (13 km) and broader spectral range (400–1050 nm) covering in an almost continuous mode the entire spectrum with 62 spectral bands. In detriment, it can only offer the half spatial resolution, so the pixel size is 34 m.

Mode 2 – 4. Full Swath, Full Spatial Resolution. This mode keeps the full swath (13 km) and spatial resolution (17 m) by a reduction of the number of bands (18 bands). Depending on the scope of the research, the offered bands cover different wavelengths (Figure 1.5.).

Mode 5. Half Swath, Full Spatial Resolution. This mode is offered in half swath (7 km) in the endeavour of having the full spatial (17m) and spectral resolution (62 bands).

In the present thesis, CHRIS/PROBA Mode-4 was selected for the three study sites, at different acquisition dates.

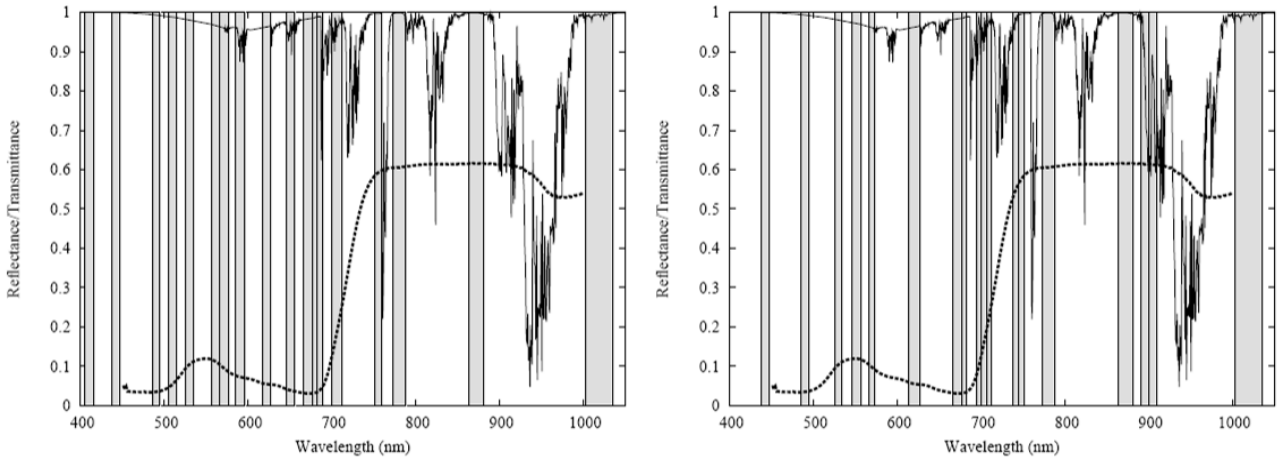

Figure 1.5. CHRIS/PROBA Mode 2 and Mode 3 band sets, with typical atmospheric transmittance (continuous line) and vegetation spectral reflectance (dashed line) curves superimposed (after Barnsley et al. 2004).

b. CHRIS/PROBA images. Data pre-processing

CHRIS/PROBA data are delivered as Level 1b top-of-atmosphere radiance data. Since the scope of this thesis is the spectral analysis of TDFs, it was necessary to transform CHRIS/PROBA data into a reflectance product (Level 2). Moreover, we pursued the comparison of different angles of observation of the same study site, so an accurate geometric correction, ortho-rectification and co-registration were required.

Because of the particularities and uniqueness of CHRIS/PROBA, the European Space Agency (ESA) funded the implementation of a set of CHRIS/PROBA-specific pre-processing tools, in collaboration with Brockmann-Consults. The CHRIS/PROBA tool-box was integrated in BEAM, an open-source software developed to exploit Earth Observation data. CHRIS/PROBA tool-box offers four modules of correction: (1) noise reduction (Gomez-Chova et al. 2008), (2) cloud screening (Gomez-Chova et al. 2006), (3) atmospheric correction (Guanter et al. 2005), and (4) geometric correction (Alonso et al. 2004).

BEAM's noise reduction module is intended to eliminate noise caused by drop-out pixels and vertical striping, in this order. CHRIS/PROBA's channel 2 generates wrong pixels randomly, so-called drop-outs. Since they are easily identified as outliers in the image histogram they can be removed off the scene. Push-broom sensors such as CHRIS/PROBA are affected by vertical striping, a multiplicative noise that affects some image columns. It is caused by irregularities in the coupling between the entrance slit and the

CCD-array system in the across-track direction. Vertical striping appears as a gain in radiance of certain image columns in a non-periodic pattern. This kind of noise is related to temperature at the moment that the CHRIS/PROBA image was captured, which is recorded in the metadata. The relationship between the vertical striping and the temperature is described in look-up-tables (LUT) allowing the characterization of the noise and its correction (Gomez-Chova et al. 2008).

Optical sensors like CHRIS/PROBA are not able to skip clouds, in contraposition to other remote sensors such as radar or Lidar. Because of that, clouds in CHRIS/PROBA images (covering the visible and infra-red spectrum) must be identified and removed. The cloud screening module designed by BEAM's team is not a simple cloud mask. This module provides a cloud probability of each pixel in the scene by the definition of identified cloud pixels. To start, the module considers illumination parameters in the moment of acquisition (day of the year and satellite position respect to the sun). An unsupervised Expectation-Maximization (EM) clustering algorithm is used for the identification of cloud pixels. Pixels with whiteness, brightness, water vapour and oxygen absorptions are considered as "high probability" to be a cloud cluster in the EM classification. Afterwards, a Fully Constrained Linear Spectral Unmixing (FCLSU) is applied to the image to calculate the fraction of cloud contained in each pixel. Cloud pixels are removed of the image together with the cloudy fraction inherent to cloudy pixels. Cloud screening is a non-mandatory step in the atmospheric correction of CHRIS/PROBA images. It is only applied if clouds are present in the scene (Gomez-Chova et al. 2006).

The atmosphere correction module in BEAM is intended to correct the added radiation and scattering effects produced by the atmosphere. The atmosphere, located between CHRIS/PROBA and Earth's surface targets, is the main interference in the signal arriving to Chris sensor. Specifically, aerosols and water vapour are the main features that distort the surface reflectance. Aerosols affect the entire CHRIS/PROBA spectral range, with the largest distortion in the shortest visible wavelengths. Water vapour only affects certain spectral bands around 940 nm, which is not included for CHRIS/PROBA mode-4. To determine the effect of the atmosphere, it is necessary to model the atmospheric conditions in the moment of the image acquisition by the definition of several parameters, such us: (1) the spectral calibration of the sensor, (2) the Top-Of-Atmosphere (TOA) radiance, (3) the Aerosol Optical Thickness (AOT), (4) the Column Water Vapour (CVW) (not for CHRIS/PROBA's modes 2 to 4) and the (5) surface reflectance. These parameters are inputs of the MODerate resolution

TRANsmittance (MODTRAN-4) atmospheric radiative transfer model. This model assumes a Lambertian reflectance, since frequently field data do not exist about the bidirectional reflectance distribution factor (BRDF) for the location and time of acquisition. AOT data is extracted of dark pixels within the scene, where it is assumed that there is not ground reflectance (Guanter et al. 2005).

For CHRIS/PROBA ortho-rectification a second order polynomial model was used in ERDAS. Geometric correction enables the co-registration of the 5 acquisition angles and the projection onto a reference cartographic system. To ensure multi-angular and multitemporal comparison, five CHRIS/PROBA angles of observation and all acquisition dates of the same study site were co-registered with an RMSE under one pixel.

c. Contributions of CHRIS/PROBA to the study of forests

Since PROBA-1 was launched to the space on 2001, many researchers have taken the advantage of its hyperspectral and multi-angular properties to investigate structural and biochemical qualities of forests worldwide by:

(1) better characterizing HRDF and BRDF (Verhoef & Bach, 2007, Barducci et al. 2009);

(2) improving BRDF models by the addition of angular, biophysical and biochemical parameters to the models (Koetz et al. 2005, Verrelst et al. 2008, Kneubühler et al. 2008);

(3) retrieving structural and biochemical parameters about forest canopy and understory by the direct exploration of CHRIS/PROBA data (Rautianien et al. 2008, Knyazikhin et al. 2009, Mottus & Rautianien, 2009) or by extracting forests features by the inversion of radiative transfer models (Huber et al. 2010, Laurent et al. 2011a);

(4) identifying forest tree species (Dyk et al. 2006); and

(5) generating forest maps about forest cover, succession (Galvao et al. 2009, Liesenberg et al. 2009) and biomass (Ponzoni et al. 2010).

The areas of interest have focused mainly in coniferous or deciduous-mixed forests of the Northern hemisphere (Koetz et al. 2005, Dyk et al. 2006, Verhoef & Bach 2007, Verrelst et al. 2008, Kneubühler et al. 2008, Barducci et al. 2008, Rautianien et al. 2009, Knyazikhin et al. 2010, Huber et al. 2010, Laurent et al. 2011a 2011b). Only few studies have focused in

tropical areas (Galvao et al. 2009, Liesenberg et al. 2009, Ponzoni et al. 2010). Because of the scarce investigation on tropical areas and particularly in tropical dry forests, the aim of this thesis is to contribute in the study of TDFs' succession using CHRIS/PROBA images.

Tropical dry forests

a. *A general overview*

The potential biogeography of tropical dry forests (TDFs) worldwide is comprised between the tropics of Cancer and Capricorn. Approximately the 54% of TDFs develop in the Americas (Miles et al. 2006). In this region, the mean annual temperature is >25ºC (ranging from 14ºC to 27ºC), the total mean annual precipitation is 1048 mm (ranging between 700 and 2000 mm), and there are three or more dry months every year (precipitation < 100 mm) (Olson et al. 2001, Sanchez-Azofeifa et al. 2005).

Several definitions about TDFs exist; in this thesis, we adopt the one defended by Portillo & Sanchez-Azofeifa, 2010. In the geographic distribution of the world's biomes, TDFs are catalogued into the category of "tropical and subtropical dry broadleaf forests" (Olson et al., 2001). TDFs are defined as a vegetation type typically dominated by deciduous trees where at least 50% of trees present are deciduous during the dry season (Olson et al. 2001, Sanchez-Azofeifa et al. 2005). Under this description, there are other vegetation types associated to TDFs, such as savannas, gallery forests, coastlines and mangroves that can occur within the matrix of tropical dry forests (Sanchez-Azofeifa et al., 2005). Some American forests, such as caatinga, cerrado and campos ruprestres (in Brazil), dry Chaco (in Argentina), Beni-savannas (in Bolivia) and Llanos (Venezuela) are considered as shrub formations, deciduous forests or savannas by other authors (Queiroz, 2006, Olson et al., 2001). In this thesis we include these vegetation types under the TDFs' description since they are within the potential distribution of TDFs and considering the historical fragmentation that Neotropical forests have experienced (Portillo & Sanchez-Azofeifa, 2010, Gentry 1995, Eva et al. 2004, Fajardo et al. 2005, Pennington et al. 2000, 2006). These other vegetation types are under the classification of "tropical and subtropical grasslands, savannas and shrublands" or "Desert and Xeric shrublands" biomes (Olson et al. 2001).

TDFs are considered environmental hotspots not only because of the biodiversity they shelter, but also because of the high level of threaten they support (Janzen, 1988, Hoekstra, 2005). TDFs have been deforested to

open areas for cattle ranching, timber logging, fine woods extraction and urbanization, since the area these forests occupy are very attractive for its moderate climate and good edaphic properties (Sanchez-Azofeifa et al. 2005). Nowadays, American TDFs appear as fragments of a continuous belt that reached Mexico to northern Argentina along 15 countries of Latin America (Portillo & Sanchez-Azofeifa, 2010).

Little attention has been paid to this ecosystem in comparison to tropical rainforests (Sanchez-Azofeifa et al. 2005, Gillespie et al. 2003, Mayaux et al. 2005). TDFs present a lower biodiversity in number of species, genera and families in comparison to tropical wet forests (Gentry, 1995, Fajardo et al. 1995). Nonetheless, TDFs shelter a high diversity and a high number of endemisms (Janzen, 1988, Rzedowski, 1991, Gentry, 1982, Joly, 1970). In opposition to tropical wet forests, biodiversity in TDFs decreases as they approach the equator (Chazdon and Denslow, 2002); the most diverse TDFs have been reported in Mexico, Argentina, Brazil, Bolivia and Paraguay) (Gentry, 1995). Moreover, the most diverse TDFs are the driest; a higher number of species have been described for drier areas such as Chamela (Mexico) and Quiapaca (Bolivia) than in moister areas such as Guanacaste (Costa Rica) (Gentry, 1995, Lobo et al., 2003).

Besides, TDFs hold important environmental services for the 40% of the Latin American population by providing freshwater, protecting fertile soils from erosion, and offering alternative sources of income to local communities (e.g. ecotourism, payments for environmental services) (Sanchez-Azofeifa et al., 2005, Fajardo et al. 2005). Because the interaction of humans with TDFs, the 48.5% have been converted into other land uses at a global scale (Hoekstra et al. 2005). For Latin America, it is estimated that the 66% of the initial extension of TDF has been deforested by the timber industry, indigenous fuel-wood extraction, and the expansion of cattle ranching and the remaining 44% exists in fragmented areas (Portillo & Sanchez-Azofeifa, 2010, Fajardo et al. 2005). Deforestation of TDFs is unbalanced along the American continent: in North and Central America, 72% of TDFs have disappeared, while South America lost the 60% of its extent and the Caribbean Islands the 66% (Portillo & Sanchez-Azofeifa, 2010). Fragmentation is also unequal depending on the country. The most affected TDFs by fragmentation are located in Nicaragua, Guatemala, Ecuador, Costa Rica and Peru, while the largest fragments are found in Bolivia, Brazil and Mexico (Portillo & Sanchez-Azofeifa, 2010).

The lack of interest and little knowledge about TDFs is reflected in the scarce protection provided by international and governmental institutions and legislation. In South America, only the 6.6% of TDFs are protected in

nature reserves, of which the 64% are found in Bolivia and Brazil. In Central America, it is only the 0.4% of TDFs that are under some level of protection, and practically all reserves are in Costa Rica or Mexico. This data have to be interpreted carefully and considering the extent of protected areas related to the actual extent of TDFs in a country. Then it is observed that i.e. Costa Rica is protecting the 15% of their TDFs, while Mexico only protects its 0.2%. The Caribbean Islands protect a 10.2% of its current extent. However, the severity of protection is higher in continental America, where most of TDFs are protected under the "National Park" status (IUCN Protected Area Category II), while in the Caribbean Islands most of them are protected under "Sustainable Management areas" (IUCN Protected Area Category VI) and a smaller percentage under the "National Park" category (Portillo & Sanchez-Azofeifa, 2010).

b. Ecological succession within tropical dry forests

The estimation of the extension of TDFs worldwide and particularly in America is necessary as a starting point for environmental management (Sanchez-Azofeifa et al. 2005, Portillo & Sanchez-Azofeifa, 2010). Beyond this requirement, it has also been pointed out the need of distinguishing primary and secondary TDFs for an accurate estimation of environmental services and carbon stocks (Saatchi et al. 2010). Primary and secondary forests do not present the same structure and species composition, thus their ecological dynamics are different, in terms of the biodiversity they shelter (Wilson, 1989), the carbon they absorb (Grace et al., 1996) and how they regulate the climate (Gedney & Valdes, 2000). A secondary forest is composed of pioneer species that grow in a faster rate in comparison to stabilized primary forests, motivated by the different availability of light, water and nutrients that occur in an area that has been previously deforested. A younger tree grows faster and has a higher photosynthetic:non-photosynthetic ratio than an old tree, conditioning secondary forests accumulate more carbon and present different carbon fluxes with other components of the carbon cycle than primary forests do (Canadell et al., 2007, Eaton et al. 2009, Uhl et al. 1988, Brown et al. 1993, Dixon et al. 1994, Fearnside and Guimaraes 1996).

This thesis aims to the estimation of the extent of successional stages of TDFs in America via remote sensing. The ecological succession is the process by which an ecosystem starts the colonization of a bare area (Opler et al. 1986). In our case of study, we focus in the ecological recovery of a potential forested area after a disturbance, such as deforestation or fire, which have been the most often cause of clearance in TDFs in America

(Janzen 1988). Intuitively, successional stages of re-growth shall be defined by age or "time since last disturbance". Nevertheless, several authors found difficult to determine the chronological age of a forest because of gaps in historical data (Kimes et al., 1999) or uncertainties in age definition of the successional stages (Sader et al. 1989, Helmer et al. 2000). It is only recommended to use this "age approach" when the knowledge about the age since abandonment is truthful and a structural description of the forest is provided (Steininger 2000). Moreover, successional stages defined by age are not comparable to other forests of the same age in different geographical areas because the growth rate depends on local climatic conditions, edaphology, topography or last land use and its intensity (Lucas et al. 2000, Castro et al., 2003, Foody et al. 2003). For this reason, some authors prefer to characterize forests' successional stages in terms of forest structure and composition.

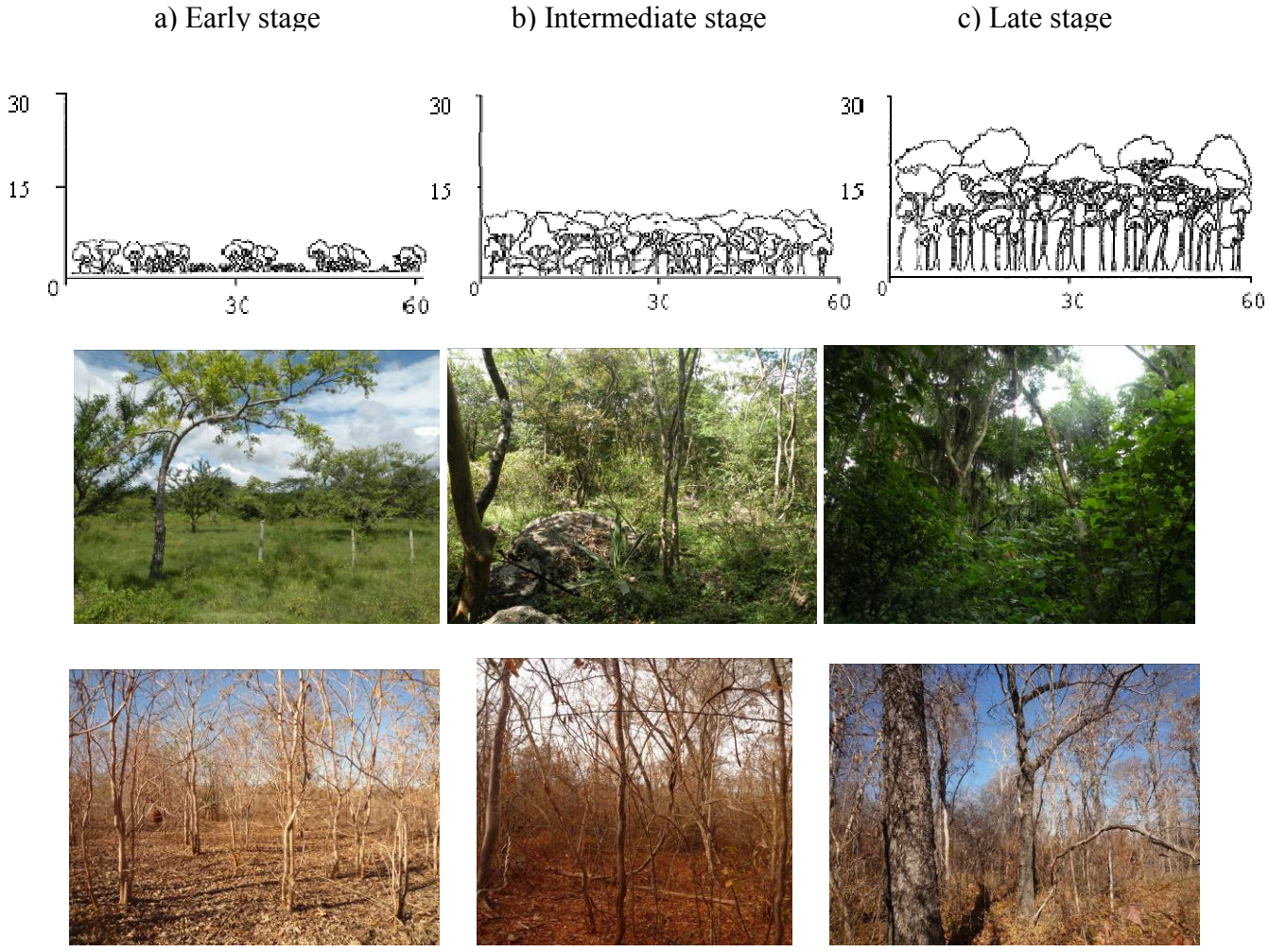

Figure 1.1. Scheme of the three successional stages of Tropical Dry Forest adapted after Kalacska et al. 2004a (upper line); stages of succession in TDFs during the wet season in Nicaragua (middle line) and dry season in Brazil (bottom line).

In all experiments conducted for the thesis, three successional stages have been defined in terms of forest structure and species composition: early, intermediate and late stage (Figure 1.1.). A detailed description is found in Arroyo-Mora et al. 2005 and Kalacska et al. 2005a after Ewel 1977 and Pacheco 1998. The structure of TDFs is defined in both vertical and horizontal axis. From a vertical point of view, as a TDF grows, the number of canopy layers increases in a vertical profile and trees become taller. The physical parameters that define vertical structure are tree height and leaf area index (LAI). In the horizontal plane, the structure of the forest is based on tree density and distribution of tree crowns. The horizontal structure is defined by basal area, diameter of trees at breast height (DBH), number of stems per area and canopy openness. In earlier stages of succession, the number of stems per area is relatively small (around 50 trees per 0.1 ha). Most of trees are young and though they are short (5–8 m height) and their DBH and basal area are thin, leaving large open areas between them. As the succession progresses, a second generation of trees settle in the open areas, therefore in an intermediate stage of succession there are two or more canopy layers and the tree density increases (around 150 trees per 0.1 ha). The upper canopy can reach up to 10–12m. There is an affluence of lianas and saplings, making the canopy openness practically null. Since there is more than one generation of trees, there is a higher variance of basal area, DBH and tree height. In a late stage of succession, the competition for nutrients and light defined a more selected plant community, populated by higher well-developed trees that reach the upper canopy layer. Though, there is a cleaner understory where saplings can only develop in open gaps where an old tree fell. In comparison to the intermediate stage, in the late stage there is a decrease of the number of stems per area (around 120 per 0.1ha) but an increase in the DBH and basal area. At a bird's-eye view, the upper canopy is a continuum reaching an averaged height of 15–18m. From the vertical point of view, though, it is possible to observe spread emergent trees standing out the main canopy layer around 20–25m. This is an important difference respect to tropical wet forests, were there is a single upper canopy with no emergent trees (Figure 1.1.).

On the other hand, as the ecological succession progresses, the presence and the relative abundance of species change (Kalascka et al., 2004a). In earlier stages of succession, there is a predominance of pioneer species and there are a small number of families and species that compose the predominant vegetation classes. In an intermediate stage of succession, the pioneer species already created a less stressing environment allowing some other species with higher environmental requirements to colonize the area. For this reason, the intermediate stage presents the highest number of

species and families. As described by Kalascka et al. 2004b, the present species in late stage are not very different to the ones observed in the intermediate stage, but the dominant species differs in both stages. While in the early stage of succession the number of predominant families was small, in the intermediate and the late stage of succession the diversity dominance is shared by a larger number of species and families.

Most of species present in TDFs drop their leaves during the dry season, but there is certain asynchrony in leaf-flushing depending on the successional stage. Species present in the early stage of succession usually start losing their leaves at the beginning of the dry season and the plant community is conformed by deciduous species that lose all their leaves. In the other extreme of the gradient, in late stage forests there are certain evergreen species that keep their leaves the entire year, and most of trees drop their leaves in different moments during the dry season. The species within the intermediate stage of succession present an intermediate phenology between the early and late stages, where about of the 80% of the species are deciduous (Kalacska et al. 2004b, Arroyo-Mora et al. 2005).

c. Measuring structure and composition of Neotropical dry forests

The main objective of this thesis is to map succession of TDFs in America using remote sensing. For this reason, three study sites were selected covering a latitudinal gradient along the continent: Chamela-Cuixmala Biosphere Region, in Mexico (North America), Los Naranjos in Nicaragua (Central America), and Parque Estadual da Mata-Seca, in Brazil (South America). Three successional stages of succession within these TDFs were defined in terms of structure and species composition. A secondary objective of the thesis is to verify that this characterization of successional stages based on structure and composition is repeatable along the continent and suitable for remote sensing monitoring. To enable comparison between study sites, field data collection in the three study sites was done under the same procedure, after the methodology applied in Tropi-Dry network.

According to Tropi-Dry's Manual of Methods and Kalacska et al. 2005b, forest structure and composition is inventoried in 20 × 50 m (0.1 ha) plots for each successional stage for all woody stems with DBH $\geq$ 5 cm. The plots were located within a matrix of homogeneous vegetation with a margin of at least 50m around. At least three plots were delimited for each successional stage at each country.

Among the structural parameters, number of stems, DBH, basal area, tree height and LAI and canopy openness were measured. Tree height was

measured with Impulse 200 Laser Ranger (Laser Technology Inc. Colorado, USA). LAI was estimated with a Li-Cor 2000 instrument and hemispherical photos (Nikon CoolPix 995). Canopy openness was calculated using hemispherical photos. Basal area was calculated considering the DBH and the area of the plot. Tree density was defined as the number of stems per area, considering the area of the plot.

Family, genera and species composition was determined by the accounting of stems of each species by the expertise identification of taxonomists. As an integrated measurement of structure and composition, the Complexity Index of Holdridge was calculated (Holdridge et al. 1971) considering only stems with DBH > 0.5 cm, as modified by Lugo et al. (1978) for measuring complexity of secondary forests. This index is defined as:

$$HCI = \frac{H \cdot G \cdot D \cdot S}{1000} \qquad (1)$$

where H is canopy height (m), G is basal area (m2/ha), D is the number of stems, and S is species density (number of species per 0.1 ha).

TABLE 1.1. Example of space-borne and air-borne sensors for vegetation monitoring

Sensor name	Platform or mission	Launch date	Swath width	Temporal resolution	Number of bands	Band width	Wavelength region (nm)	Spatial resolution
Medium-resolution multispectral sensors								
MSS (MultiSpectral Scanner)	Landsat 4-5	July 1972	185 km	16 days	7	60-270 nm	VNIR B1-B4:450-900	30 m
							SWIR B5&B7:1550-2350	30 m
							TIR B6: 10410-12600	60 m
ETM+ (Enhanced Thematic Mapper)	Landsat-7	April 1999	185 km	16 days	7	60-270 nm	VNIR B1-B4:450-900	30 m
							SWIR B5&B7:1550-2350	30 m
							TIR B6: 10400-12500	60 m
							PAN: 520-900	15 m
HRVIR	SPOT-5	May 2002	60 km	26 days	5	70-230 nm	VNIR B1-B3:500-890	10 m
							SWIR B4:1580-1750	20 m
							490-690 (PAN)	2.5-5 m
ASTER (Advanced SpaceborneThermal Reflection Radiometer)	TERRA	December 1999	60 km	16 days Potentially scheduable up to 5 days	14	40-100 nm	VNIR B1-B3:520-860	15 m
							SWIR B4-B9:1600-2430	30 m
							TIR B10-B14: 8125-11650	90 m
High-resolution multispectral sensors								
IKONOS	IKONOS	September 1999	11.3 km	On demand Potentially scheduable up to 3 days	5	71-96 nm	VNIR B1-B4:445-853	4 m
							450-900 (PAN)	1 m
BGIS-2000	Quickbird	October 2001	16.5 km	On demand Potentially scheduable up to 1 – 4 days	5	70-140 nm	VNIR B1-B4:450-890	2.5 m
							450-900 (PAN)	0.70 m
Hyper-spectral sensors (satellites)								
AVHRR (Advanced Very High Resolution Radiometer)	NOAA-METOP	June 1979	6400 km	Twice daily	6	100-1000 nm	VNIR B1-B2:580-1000 SWIR B3-B4: 1580-3930 TIR B5-B6: 10.000-12.500	1100 m

(continued)								
MODIS (Moderate Resolution Imaging Spectrometer)	TERRA	December 1999	2 330 km	1 – 2 days	36	10-15 nm	VNIR 620--880 SWIR 890-1390 TIR 3660-14385	250 m 500 m 1000 m
Hyperion	EO-1	November 2002	7.7 km	On demand	242	10 nm	400-2500 nm VIS (35 bands) NIR (35 bands) SWIR (172 bands)	30 m
MERIS (Medium Resolution Imaging Spectrometer)	ENVISAT†	February 2002	1150 km	3 days	15	3.5 – 20 nm	VNIR: 412-900	250 m
CHRIS (Compact High Resolution Spectrometer)	PROBA-1†	October 2001	13 km	On demand	18-37-62	5-11 nm	VNIR 400-1050	17 or 34 m
ALI (Advanced Land Imager)	EO-1	November 2002	37 km	On demand	10	20-270 nm	VNIR B1-B5:400-890 SWIR B6-B10:1200-2350 PAN: 480-690	30 m 30 m 10 m
Hyper-spectral sensors (airborne)								
AVIRIS (Airborne Visible / Infrared Imaging Spectrometer)	NASA	1998	4 km 11 km	On demand	224	10 nm	VNIR-SWIR: 380-2500	4 m 20 m
CASI (Compact Ariborne Spectrographic Imager)	Borstad	1994	1-2 km	On demand	288	3 nm	VNIR: 400-946	2-4 m
HyMap	HyVista (Australia)	1998	1.5 - 5 km	On demand	128	15-20 nm	VNIR: 450-1350 SWIR: 1400 -2500	3-10 m
APEX (Airborne Prism Experiment)	ESA	2009	4-10 km	On demand	300-500	1.5 nm	VNIR 380-1000 SWIR 1000-2500	2-5 m

† Not operating anymore

TABLE 1.2. Satellites Instruments capable of Multiangle Sampling

Sensor name	Platform	Launch date	Angular resolution	Sampling method	Swath width	Temporal resolution	Spectral resolution	Spatial resolution
AVHRR	NOAA-METOP	May 1991	0º ± 55º	Across-track Temproal compilation	6400 km	Twice daily	6 bands 100 nm width λ: 580-1000 nm	1100 m nadir 4000 m ± 55º
ATSR-2 (Along-Track Scanning Radiometer)	ERS-2†	April 1995	0º ± 55º	Along track	512 km	On demand	7 bands 20 nm λ: 550-1200nm	1 km nadir 1.5x2 km ± 55º
POLDER -2 (Polarization and Directionality of the Earth's Reflectances)	ADEOS†	December 2002	0º ± 42º ± 51º	Across track (± 42º) Along track (± 51º) Temporal combination	2400 km	4 days	9 bands 10-40 nm width λ: 444 – 860 nm	6 x 7 km
MODIS	TERRA	December 1999	0º ± 55º	Across-track FOV Temproal compilation	2 330 km	16 days	36 bands 10-15 nm width λ: 620-14385 nm	VNIR 250 m SWIR 500 m TIR 1100 m
MISR (Multiangle Resolution Imaging Spectroradiometer)	TERRA	December 1999	0º ± 26º ± 45º ± 60º ± 70º	9 fixed cameras Across-track Quasi-simultaneous acquisition	360 km	16 days	4 bands 20-40 nm λ: 446-867 nm	275 m 1100 m
ASTER	TERRA	December 1999	0º -28º	Along-track	60 km	14 days	14 bands 10-40 nm width λ: 520-12500 nm	VNIR 30 m SWIR 60 m TIR 90 m
CHRIS (Compact High Resolution Imaging Spectrometer)	PROBA-1†	October 2001	0º ± 36º ± 55º	Along-track Simultaneous acquisition	13 km	On demand	18-37-62 bands 5-11 nm width λ: 400-1050 nm	17 or 34 m

† Not operating anymore



Chapter 2.

QUANTIFYING TROPICAL DRY FOREST SUCCESSION IN THE AMERICAS USING CHRIS/PROBA

Abstract

To date several studies have proven the limitations of multispectral imagery to characterize ecological succession in tropical environments. This study explores the possibility of estimating different stages of ecological succession in tropical dry forests using CHRIS/PROBA hyperspectral satellite images. Tropical dry forests in the Americas are considered the most threaten ecosystem in the continent given its location in areas of high soil fertility which promotes fast deforestation rates. Three successional stages (early, intermediate and late) are studied in sites throughout a latitudinal gradient of tropical dry forests in the Americas. Sites are located in Mexico, Nicaragua and Brazil. Reflectance values of CHRIS/PROBA Mode-4 were extracted for these sites for the dry and wet season and analyzed using scatterplots, nD visualization and Transformed Divergence separability test. Our results confirm the utility of CHRIS/PROBA as a critical tool for environmental planning in tropical environments.

Monitoring secondary forests using remote sensors

With present world trends of increasing population and an expanding global economy, conservationists and policy makers are pointing out the need to identify factors that threaten forest cover now and in the future (Wright, 2005). In tropical areas, forests have been cut-logged or otherwise degraded to open pasturelands for cattle or to extract fine woods or timber (Janzen, 1988, Sanchez-Azofeifa et al. 2003b). Once these activities are abandoned, a secondary forest occupies the area. The rate of reforestation depends on local environmental conditions (e.g. climate, soil properties, intensity and type of last land use). This ecological process is known as succession (Opler et al., 1980).

Although deforestation rates in the tropics are alarming, secondary forests and protected areas provide some mitigating effects, reducing the impact of decreasing forest cover by providing shelter to threatened flora and fauna, promoting biodiversity and carbon sinks (Wright, 2005, Perz & Skole, 2003, Achard et al. 2002). Furthermore, studies suggest that secondary forests sequester carbon dioxide at a higher rate than do primary forests, depending on the species composition and the age of the secondary forest (Uhl et al. 1988, Brown et al. 1993, Dixon et al. 1994, Fearnside and Guimaraes 1996). However, current methods assess carbon fluxes from total forest coverage without discerning primary from secondary forests (Lawrence et al., 2007, Eaton et al., 2009, Canadell et al., 2007). As such, there is a need to distinguish between primary and secondary forests, and from this first binary classification, develop efforts to characterize secondary forests' stage of succession, so proper carbon estimations can be achieved (Sanchez-Azofeifa et al. 2003a).

Because of their importance to the global water and carbon cycle, most deforestation and regeneration studies have centred on the Amazon Basin or other rainforests worldwide, while little attention has been paid to tropical dry forests. However, secondary dry forests are important providers of ecosystem goods (e.g. firewood, charcoal and non-timber and timber for domestic use) to 60% of Latin American nations (Murphy & Lugo 1986, Redford et al. 1990, Mares 1992, Gillespie, 1999, Laurance, 1999, Cincotta et al., 2000, Sanchez-Azofeifa et al. 2003b).

Satellite data have been proven to provide more accurate estimates of forest cover and deforestation than field surveys, and are emerging as useful mapping tools for primary and secondary forests (Achard et al. 2002, Hansen and DeFries, 2004, Wright and Muller-Landau, 2006). In remote sensing studies, ecological succession has been traditionally described in

terms of "years since its last disturbance" (Saldarriaga et al., 1988; Uhl et al., 1988, Helmer et al. 2000, Lu et al. 2003, Vieira et al. 2003, Galvao et al. 2009). This concept has been highly criticised in the literature since it fails to consider local environmental factors, such as soil, climate or previous land use (Lucas et al. 2000, Castro et al., 2003). A better approach to look at linkages between remote sensing and ecological theory suggests that secondary forest age should not be considered a sole determinant of successional stage. Instead, ecosystem structure and species composition have been suggested as better descriptors of remote sensing observations of ecosystem regeneration (Moran et al. 2000, Castro et al. 2003, Kalacska et al. 2004a, Arroyo-Mora et al. 2005). Changes in structure and composition along a given ecological succession path implicate changes in the spectral behaviour that can be captured by remote sensors (Ruiz et al., 2005, Kalacska et al., 2007a, Feeley et al., 2005, Gamon et al., 2005, Gillespie et al. 2006).

Due to the ecological complexity of tropical forests in terms of tree diversity, coarse-spatial resolution or multispectral sensors are not appropriate to discriminate stages within a successional gradient (Jensen 2000a). The Compact High Resolution Imaging Spectrometer (CHRIS) on board of space platform Proba-1, intends to overcome the limitations of previous studies about natural targets by offering narrower hyperspectral bands, higher spatial resolution and multi-angle observations (Barnsley et al., 2004). The pixel size (17 m) offered on its vegetation mode (mode-4) is appropriate for research on ecological processes (Castro et al., 2003). The hyperspectral information of CHRIS/PROBA's sensor reflects biochemical and biophysical properties of vegetation canopies, whereas the directional component provides information on canopy structure (Kneubühler et al. 2008).

The objective of this study is to discriminate three successional stages within a TDF ecosystem (early, intermediate and late stages) along a latitudinal gradient in the Americas (Mexico, Nicaragua and Brazil) using CHRIS/PROBA. CHRIS/PROBA's multi-angularity capability is tested by assessing its ability to identify vertical and horizontal structural parameters such as canopy height, canopy openness and basal area. The sensor's hyperspectral properties are used to study the discrimination of sub-pixel elements (e.g. understory vs. canopy) and species composition that characterize each successional stage. CHRIS/PROBA's reflectance values are analyzed in band-by-band and 18-dimensional approaches as a function of seasonality (wet vs. dry season) and five CHRIS/PROBA's angles of observation.

Measuring spectrodirectional properties of tropical dry forests succession in America

a. The tropical dry forest in a latitudinal gradient in the Americas

Three TDF sites were selected based on their latitudinal distribution (Portillo & Sanchez-Azofeifa, 2010; Figure 1): a) the Chamela-Cuixmala Biosphere Reserve in Mexico, b) The Pacific region Los Naranjos in Nicaragua and c) The Parque Estadual da Mata-Seca in Minas Gerais, Brazil.

The selected TDF areas have two very well delimited seasons each year, mostly defined by water availability: a rainy season from October to March, and a dry season for the rest of the year. From a topographic point of view, both the Nicaragua and Brazil study sites are flat, while Mexico presents significant relief (between 0 and 500m altitude for the study site).

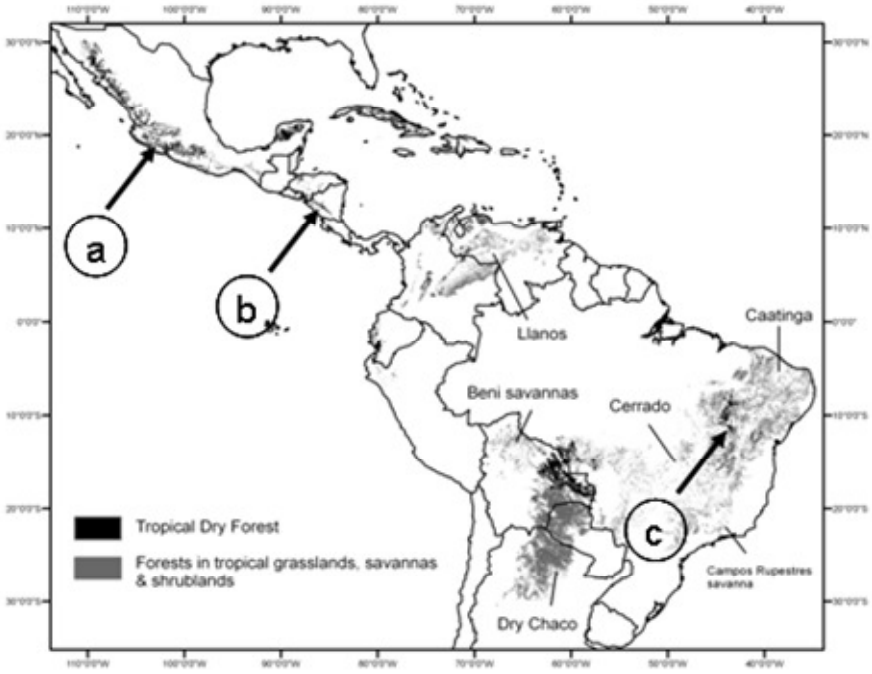

Figure 2.1. Study sites locations (after Portillo & Sánchez-Azofeifa, 2010): (a) Chamela-Mexico, (b) Los Naranjos-Nicaragua and (c) Mataseca-Brazil.

The selected sites provide no exception to the rule of deforestation, land degradation, and secondary growth processes observed across the Americas (Portillo and Sanchez-Azofeifa, 2010). For all study sites, forest cover was replaced early in the 1960s and 1970s by pasture lands aimed to support extensive cattle ranching, which were eventually abandoned in the 1990s as

a result of varying socio-economic processes (Sanchez-Azofeifa et al, 2007; Castillo et al. 2009; Calvo-Alvarado et al. 2009). In the case of Brazil and Mexico, conservation policies at the state (Brazil) and national (Mexico) levels motivated the acquisition of the land at the study sites to promote secondary regeneration and biodiversity conservation. For Nicaragua, Los Naranjos study area is located in the buffer area of the Protected Terrestrial Landscape of Miraflor-Moropotente, but it is not considered a priority area for conservation.

Mexico's site is the most preserved of all sites studied in this paper, in this region primary forest is dominant and continuous, while in Nicaragua the forest is highly fragmented with only small patches remaining. The Mata-Seca site is a mosaic of forests under different successional stages. In table 1, three sites are described and compared.

TABLE 2.1. Description of the study sites.

Site	Coordinates lat / long	Country	Rain (mm)	Temp (^{o}C)	Topography	Land use
Chamela-Cuixmala Biosphere Reserve	19º29'55" N 105º02'39" W	Mexico	919	24	Mountainous	Cattle, Fine woods extraction
Pacific Los Naranjos region	13º11'39"N 86º20'07"W	Nicaragua	874	21	Flat on the study site	Cattle, Timber extraction
Parque Estadual da Mata-Seca	14°50'50.52"S 43°58'43.74"W	Brazil	916	24	Flat	Cattle

In this chapter our analytical emphasis focuses on the three levels of forest successional stage: early, intermediate and late, which are present at the selected sites per Kalacska et al. (2004b). At each successional stage 3 field plots of 20 x 50m (0.1 ha) were identified, marked and sampled for ecosystem structure and composition.

b. Image acquisition and pre-processing

For each site, images were acquired for both the dry and the wet season (Table 4), with the purpose of analysing the behaviour of the vegetation as a function of phenological responses. In Figure 3, a phenology sequence of the forest is shown for each site, extracted of MODIS NDVI product (https://daac.ornl.usgs.gov/MODIS/modis.htlm), and acquisition dates are pointed out on the Figure.

TABLE 2.2. Acquisition dates for CHRIS/PROBA images for each study sites.

	Dry season	Wet season
Mexico	31st March 2006	25th April 2010
Nicaragua	19th February 2009	19th April 2010
Brazil	18th September 2009	24th May 2010

CHRIS/PROBAMode-4 images (Figure 2.3.) were atmospherically corrected using CHRIS/PROBA Tool-Box in BEAM-Visat 4.6.1 (Alonso et al. 2009) and geometrically corrected and co-registered in ERDAS.

(a)

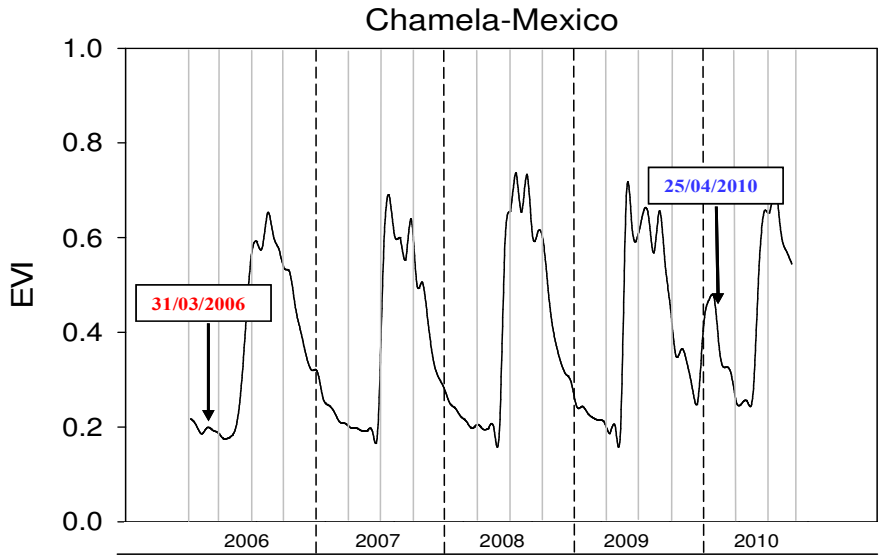

(b)

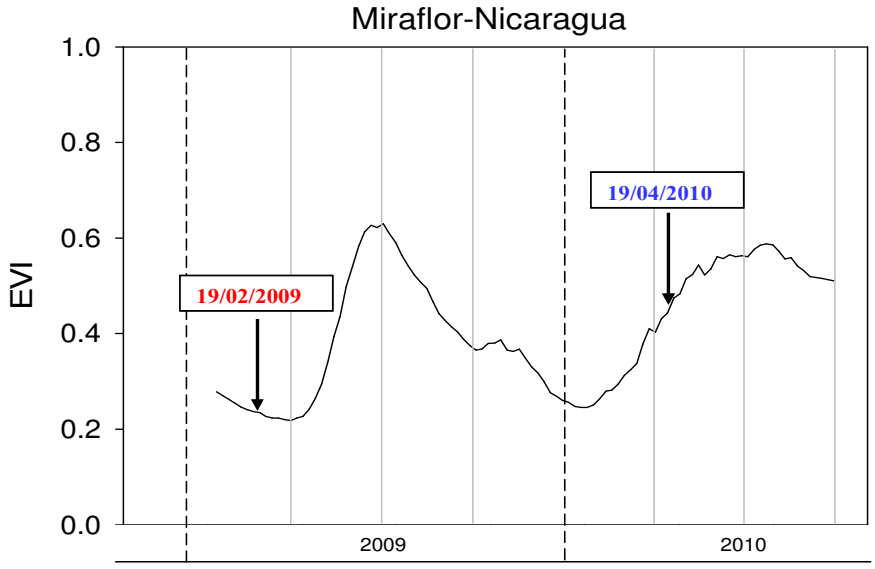

(c)

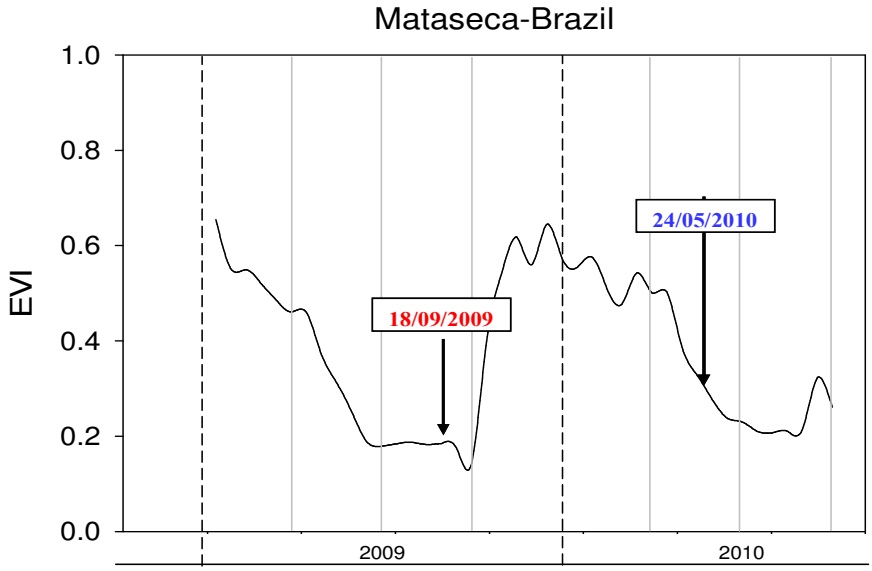

Figure 2.2. MODIS NDVI product for (a) Chamela, Mexico, (b) Los Naranjos, Nicaragua, (c) Mataseca, Brasil. The arrows point out the acquisition dates of CHRIS/PROBA scenes for the dry and wet season.

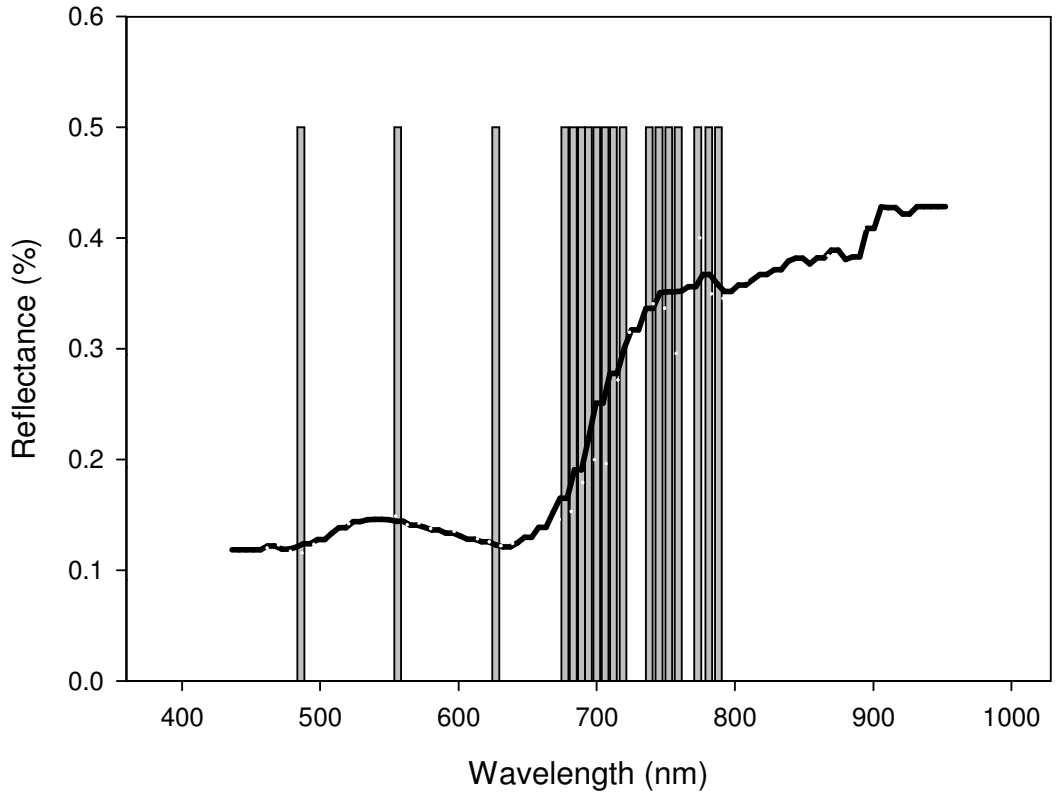

Figure 2.3. CHRIS/PROBA Mode 4 (chlorophyll mode) covers spectrum range from 489 to 792 nm by 18 bands of 10-12 nm width.

c. Statistical tests

For each of the CHRIS/PROBA images, a one-way ANOVA was performed to test the spectral differences between successional stages as a function of the angle of observation and seasonality, in a band-by-band approach. The ANOVA is based on the null hypothesis that there are no differences among groups (early, intermediate and late successional stages, in our case) (Fisher, 1918):

$$H_0: \eta_n\,(i) = \eta_{n+1}\,(i)$$

where η_n is the median reflectance for successional stage number n = 1, 2, 3. . . (N_1), and i = 1, 2, 3. . .i is the wavelength band.

The null hypothesis was tested using the F-test at a significance level of α = 0.01. The F statistic is a ratio used to gauge the differences of the effects (Snedecor & Cochran, 1989). If there are no missing data, F is calculated as:

$$F = \frac{\text{estimated population variance between groups}}{\text{estimated population variance within groups}} = \frac{\text{MSbetween}}{\text{MSwithin}}$$

If the F ratio is around 1, it can be concluded that there are no differences among successional stages (the data are consistent with the null hypothesis). If F is a large number, the variability among successional stages' means is larger than expected from random variability, meaning there are differences between successional stages. In other words, high F-values indicate that the spectral variance within successional stages is smaller than between them, so successional stages belong to separated groups, while F values around 1 show similar differences between and within groups, so groups are not well defined. In cases where normality and/or equal variance tests failed, a Friedman test was performed (Friedman, 1940).

The F-test rejects the null hypothesis when at least one successional stage is spectrally different from the other two, but this statistical method does not specify which groups are different, or evaluate the magnitude of these differences. Multiple comparison tests perform pairwise comparisons, identifying which successional stages are spectrally separate and quantifying the magnitude of the spectral differences between groups. The Holm-Sidak test (Sidak, 1967) was used to conduct multiple pairwise comparisons measured with t-test. The t-test provides similar comparisons to the F-test, but it compares successional stages two-by-two instead of evaluating all three successional stages at one time.

A p-value for significance is used to determine the accuracy of both the F-test and the t-test. p-values higher than α at some spectral locations indicate that the spectra of different successional stages are very similar as none of them is statistically separable from the group. On the other hand, where the derived p-value is smaller than the classic 0.05 α threshold, there is only a 5% chance that the pairwise difference has occurred by chance. Below-threshold p-values in this study suggest that at least one pair of successional stages is statistically different.

d. Separability Analysis

We used the Transformed Divergence test to evaluate spectral separability pairwise between successional stages as a function of the angle of observation and seasonality. It measures the spectral intra-variability of a successional stage and the spectral inter-variability of two successional stages considering the mean values and data dispersion of each successional stage.

The transformed divergence is based in the Euclidean spectral distance between two mean vectors corresponding to a pair of pixel clusters in an n-

Dimension space. It considers the covariance and the mean of the spectral values. The Transformed Divergence test is a variation of the standard Divergence test, intended to minimize the increase of the average divergence value in well-separated classes that mislead the divergence measure. It uses the standardized form of the Divergence test, but scales the divergence values to a maximum value of 2.0. (Swain & Davis, 1978, Richards, 1993).

Transformed Divergence values fall within a range between 0 and 2.0. Values greater than 1.9 indicate good separability between classes. Values below 1.7 show poor class separation, and values under 1.0 suggest that the two classes are effectively only one class.

The transformed divergence measure follows the same principle as other separability tests such as the Bhattacharyya (Bhattacharyya, 1943) and the Jeffries-Matusita (Richards & Jia, 2005) analyses, but it does not assume the Gaussian distribution of the data (Gunal & Edizkan, 2008).

The transformed divergence (TD) is defined as:

$$TDij = 2000\left(1 - \exp\left(\frac{-Dij}{8}\right)\right)$$

where Dij is the divergence, which considers the variance and mean of each class, represented by i and j, to determine the distance of each class to a reference vector.

e. n-Dimensional analysis of the reflectance values

In order to visualize potential separation between forest successional stages as a function of the entire CHRIS/PROBA Mode-4 spectra (18 bands), ENVI's n-Dimensional Visualizer was used in this paper (Boardman et al., 2005). The n-dimensional visualizer is an interactive scatter plotting technique that allows real-time rotation of scatterplots in n-dimensions. The n-dimension analyzer is a technique that allows the exploration of all the bands of interest, avoiding noise derived by the correlation between neighbour bands (Boardman et al., 2005). The observed spectral reflectance data were cast as a scattering of points in an n-dimensional Euclidean space, where n is the number of spectral channels. Each spectral channel was assigned to one axis of the space, all being mutually orthogonal. It is the shape of the n-D scatterplot, the patterns within it and the configuration of its exterior that can be used to understand and analyze the spectral information in the data (Boardman et al., 1995). An n-dimensional

visualization of reflectance values was performed for each site and successional stage for dry and wet seasons (Figures 8 and 9).

Quantifying spectrodirectional properties of tropical dry forests' succession

a. Spectral analysis of the successional stages

The analysis of spectral signatures of the selected pixels (Figures 4 and 5) permitted the verification of the phenological state of the observed targets (e.g. presence or absence of leaves) at the moment of the acquisition of CHRIS/PROBA's images. For dry season's images, TDF's spectral signatures represent a mixture of woody elements, litter fall, dry pasture and bare soil (Figure 4). For the same pixels in wet season's images (Figure 5), a classic spectral signature of green vegetation is observed, presenting low reflectance in blue and red bands, and high reflectance in near-infrared bands.

Apart from seasonal traits, spectral signatures are similar for the three geographic sites and angles of observation (Figures 4 and 5). The spectral signature of Mexico's wet season differs slightly different from that of Nicaragua and Brazil in that the red edge (700-750 nm) is not as vertical for the latter two, probably due to low rainfall during the 2010 study year (Figure 5).

In general terms, the early successional stage presents the highest reflectance values and the late successional stage the lowest reflectance values in dry season scatterplots. In contraposition, wet season scatterplots do not show a repeatable pattern relating reflectance and successional stage. We found some anomalies concerning the shape of the spectral signatures for angle, namely, anomalies occurred at 55º in Nicaragua for both the dry and wet season, and in Brazil for the dry season only. We suspect that the anomalies might be the result of a high proportion of shadows within the respective pixels (Figures 4 and 5). For the wet season (Figure 5), the three successional stages only show separability in the infrared bands (742-792 nm). In the case of Mexico, they also separate in the red edge (700-750 nm), especially at the early stage.

For a wavelength analysis, we performed a band-to-band one-way ANOVA to evaluate successional stage separation. F-values displayed in Figures 4 and 5 compare the three successional stages concurrently for a given spectral band. Significant cases with $p < 0.05$ have been represented in

light gray. Multiple pair-to-pair comparisons between successional stages have also been performed. CHRIS/PROBA bands that presented a t-test with $p < 0.05$ for all pairwise comparisons (early-intermediate, early-late and intermediate-late) has been represented in dark grey in Figures 4 and 5.

For most of the cases, significance using the F-test achieved $p < 0.001$ significance, meaning that at least one successional stage is spectrally different from the other two stages independently of the season and the angle of observation (Figures 4 and 5). Higher F-values are observed for ±55º in Brazil and Nicaragua and +36º in Mexico in the dry season (Figure 4). Nevertheless, F-values for the wet season are much smaller than for the dry season, and approach a value of F=1 in many cases, meaning successional stages' spectral values are not well discriminated in the wet season (Figure 5).

The multiple comparisons t-tests indicate that the three successional stages clearly separate along the entire spectral range of 18 CHRIS/PROBA'sbands in all dry season cases (Figures 4 and 6) with some exceptions. In Mexico, early and intermediate do not separate at +55º for bands 1 to 6; in Nicaragua, intermediate and late do not separate at +36º for bands 12 to 18; and in Brazil, intermediate and late stages do not separate at +36º for bands 1 to 7, 9, 11 and 15 (Figure 4 and 6). T-test values for the wet season do not agree with the visual analysis of spectral signatures (Figures 5 and 7), since intermediate and late stage do not separate in Mexico (all angles of observation), Nicaragua (±55º and +36º) and Brazil (+36º) according to the t-test, but they did appear to be separate in the spectral signature. In addition, the t-test indicates that early and intermediate stages do not separate in Nicaragua (-36º and 0º; infrared bands), and Brazil (+36º, the red edge; and +55º in the visible bands). The same is true for early and late stages in Brazil (0º), which do not appear separate at visible bands (Figures 5 and 7).

As extracted from t-test analysis, there is an order in the separation of successional stages that is preserved in all dry season images. For the dry season, late and early stages show divergence more readily than do early and intermediate successional stages, with the least divergence discernable for comparisons of late and intermediate successional stages (Figure 6). The exception is found in Mexico for off-nadir angles of observation, where late and intermediate successional stages show the greatest divergence, and early and intermediate stages the least (Figure 6). T-values are smaller in Mexico than in Nicaragua, while Brazil presents the highest t-values; the former suggesting that separation between successional stages is more pronounced in Brazil and less pronounced in Mexico (Figures 4

and 6). The highest t-values for specific angles of observation among the sites are as follows: Mexico (+36º), Nicaragua (±55º) and Brazil (±55º), in agreement with observed with F-values (Figures 4 and 6). In the wet season, most successional pairs do not significantly separate, as explained by t-test (Figures 5 and 7). Moreover, t-values are smaller in wet season images than they are in the respective dry season counterpart for pairs where $p < 0.05$.

F-values and t-tests that failed normality or equal variance validations are represented in red in Figures 6 and 7. Failing the normality test implies a more complex and disperse distribution of spectral data, due to species diversity and leaf orientation in the wet season's images, and a higher sub-pixel mixture of shadows, non-photosynthetic and soil targets in +36º in the dry season's images. For the wet season, a larger number of spectral bands failed normality or equal variance tests in comparison to the dry season (in red, Figure 7). We observed that most of pairwise comparisons that failed normality and / or variance tests occurred in the wet season and in Mexico (-55º), Nicaragua (+36º) and Brazil (+36º) in the dry season (Figure 7).

The complex structure and high species composition characteristic of TDFs results in complex spectral responses, therefore spectral values do not follow a normal statistical distribution. When the data do not match a normal distribution, non-linear statistical procedures (e.g. n-Dimension Visualizer and Friedman test) are recommended for a better spectral separation of successional stages. During the wet season, the spectral complexity increases because of the presence of leaves. From a biochemical point of view, there is an incremental difference in spectral signatures depending on the species and the health status of each tree. From a structural point of view, leaves are oriented in several directions, increasing light scattering.

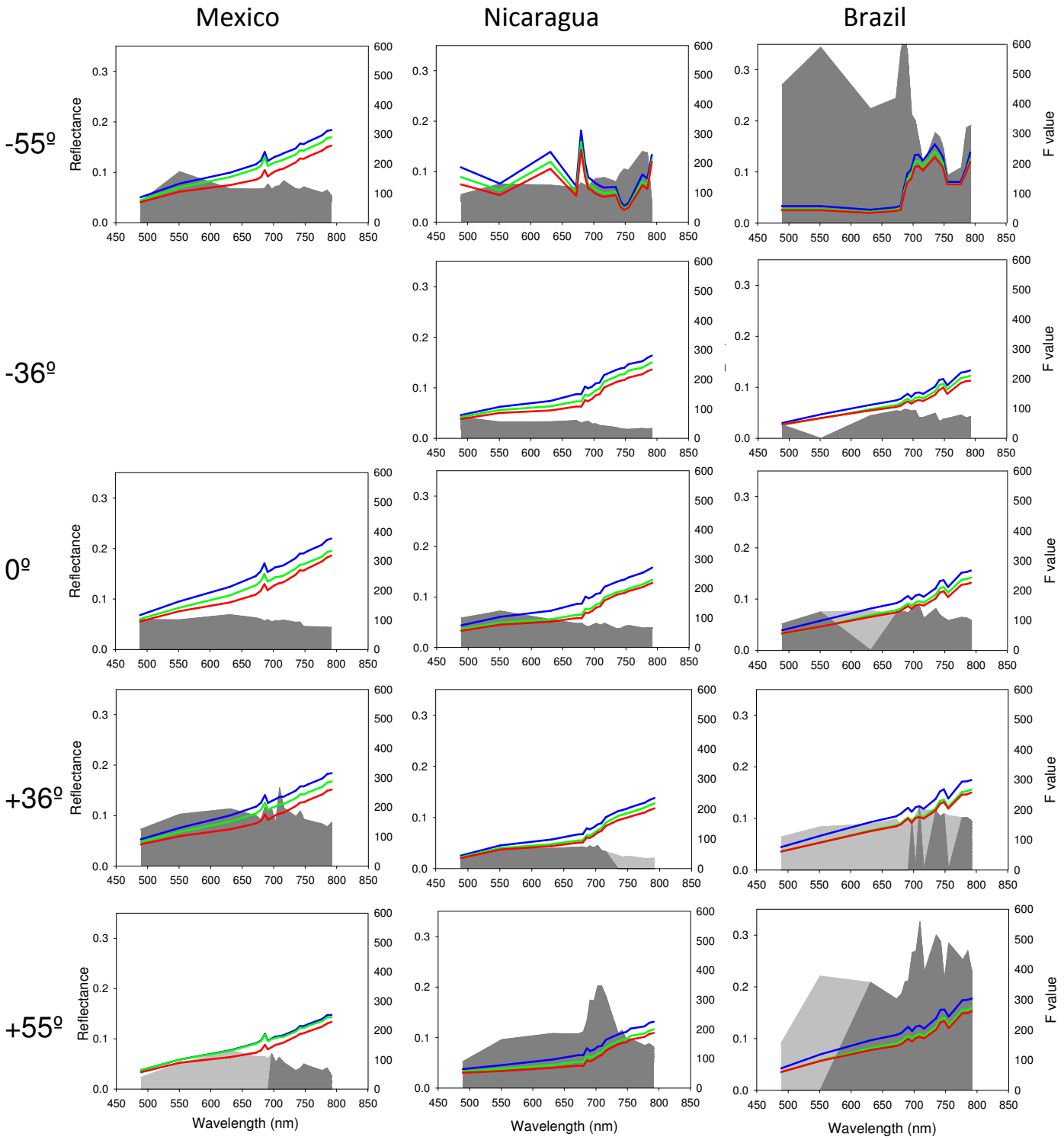

Figure 2.4. Spectral signatures for Chamela, Los Naranjos and Mataseca sites for the dry season. Early stage is represented in blue, intermediate stage in green and late stage in red. F-values of significant bands ($p < 0.05$) are presented in the background in light grey. Bands with significant t-test for all pairwise comparisons are represented in dark grey.

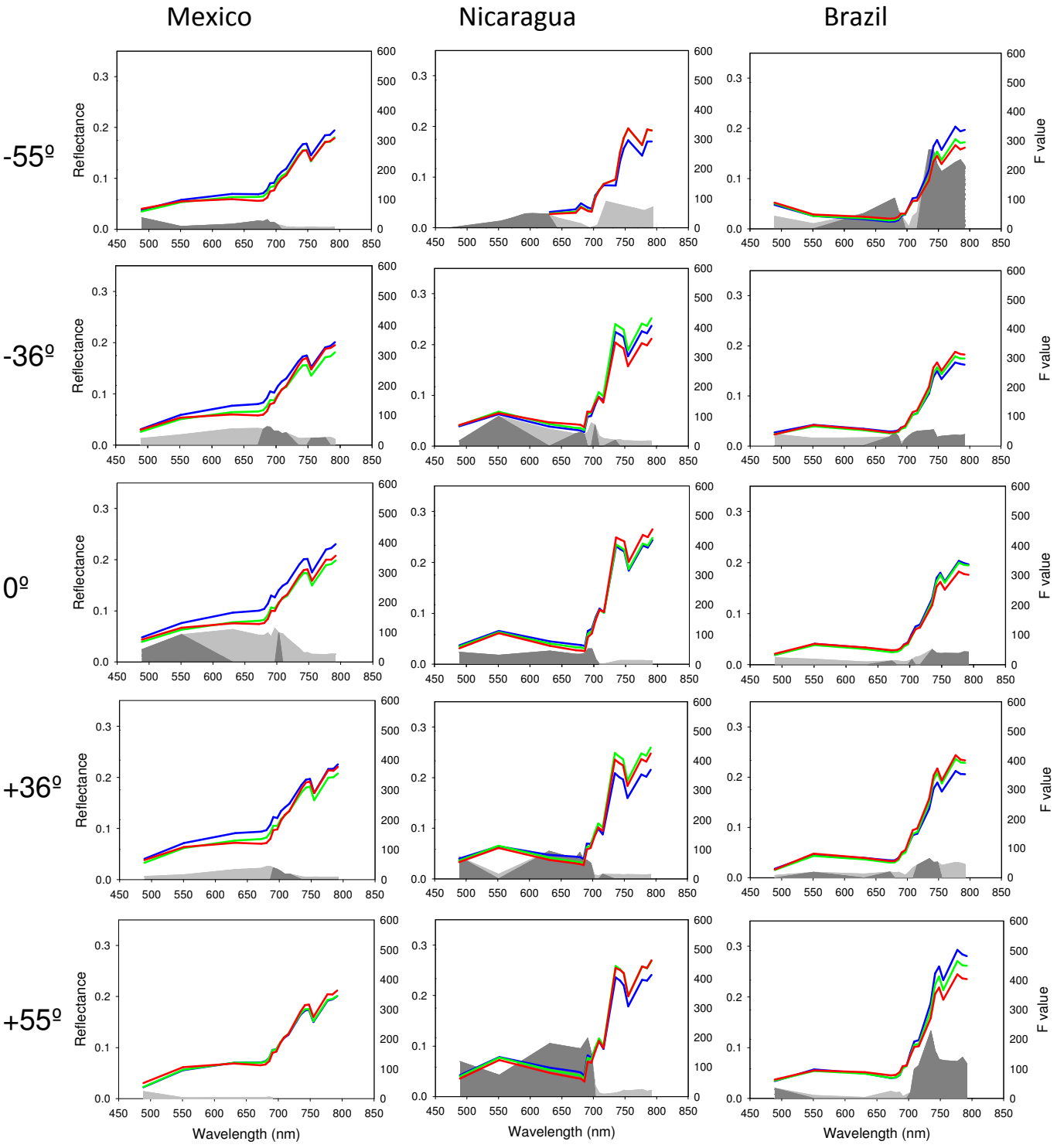

Figure 2.5. Spectral signatures for Chamela, Los Naranjos and Mataseca sites for the wetseason. Early stage is represented in blue, intermediate stage in green and late stage in red. F-values of significant bands ($p < 0.05$) are presented in the background in light grey. Bands with significant t-test for all pairwise comparisons are represented in dark grey.

b. n – dimensional analysis of the reflectance values

Figures 8 and 9 embody a snapshot of an image in rotation of a hyperspace of 18 axis, one for each CHRIS/PROBA band. For an easier interpretation and comparison of the data, all graphs are presented in the same position and orientation. The presented 18D scatterplots intend to show the highest clustering and separation of successional stages, after exploring all the perspectives in the rotating animation.

The spectral data contained in the 18 CHRIS/PROBA bands of the three successional stages are clearly separated in dry season images, especially in Nicaragua (Figure 8). The integrated spectral values for the 18 bands are positioned on a single diagonal in a repeatable order for all angles of observation and study sites; the intermediate stage falls between the late and the early stages. A slight overlapping between successional stages' spectra is observed in some cases: late and intermediate stages coincide for angles 0º in Mexico and for angles -36º, 0º, +36º and +55º in Brazil. There is also overlapping between intermediate and early stages in Mexico at 0º and +55º. For Nicaragua, all stages are clearly separated at all angles, especially at -55º, -36º and +55º. For Brazil and Mexico, a -55º angle shows the clearest discrimination of stages.

In wet season cases, only Nicaragua (+55º) shows a pattern of distribution similar to the dry season's scatterplots (Figure 9). A good spectral separation is also observed in Brazil at -55º and +55º, although there is slight overlapping between intermediate and late stages. As opposed to spectra observed in dry season images, the spectra of the successional stages are not distributed in a single line. For example, the early stage forms a cluster separated from the intermediate-late stages in Nicaragua at -55º and +36º and Mexico at 0º. Also, the late stage is separated in Nicaragua at -36º and 0º and in Mexico at -55º, -36º and +55º.

In Mexico's 18D plots (Figures 8 and 9), we can observe two sub-clusters for each successional stage. For the dry season, this fact does not interfere in the separation of successional stages, but for the wet season sub-clusters of different successional stages overlap.

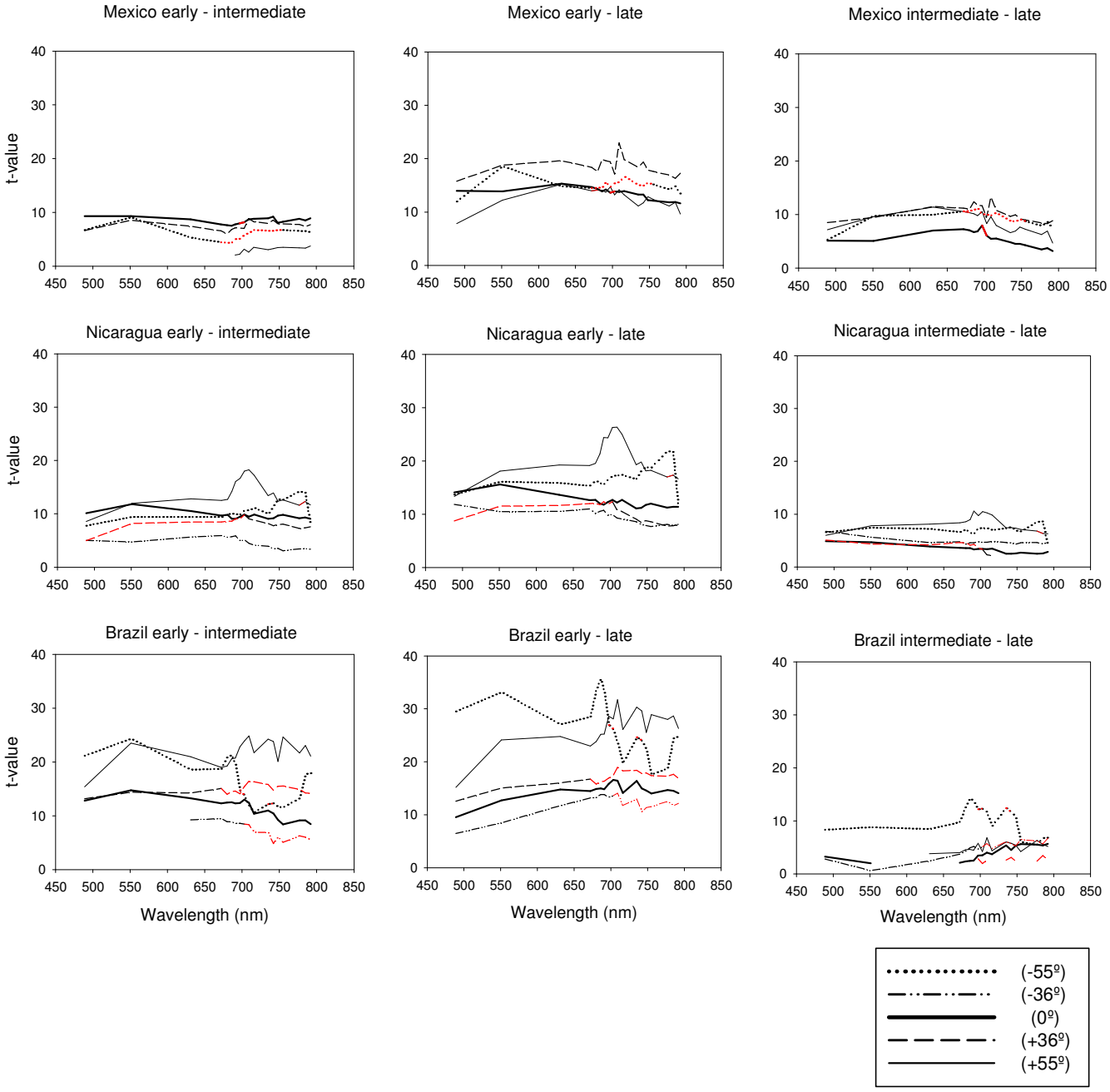

Figure 2.6. Multiple comparison test for successional stages pairwise for Chamela, Los Naranjos and Mataseca sites for the dry season. Only t-values of significant bands ($p < 0.05$) are represented. Values that failed normality or equal variance tests are represented in red.

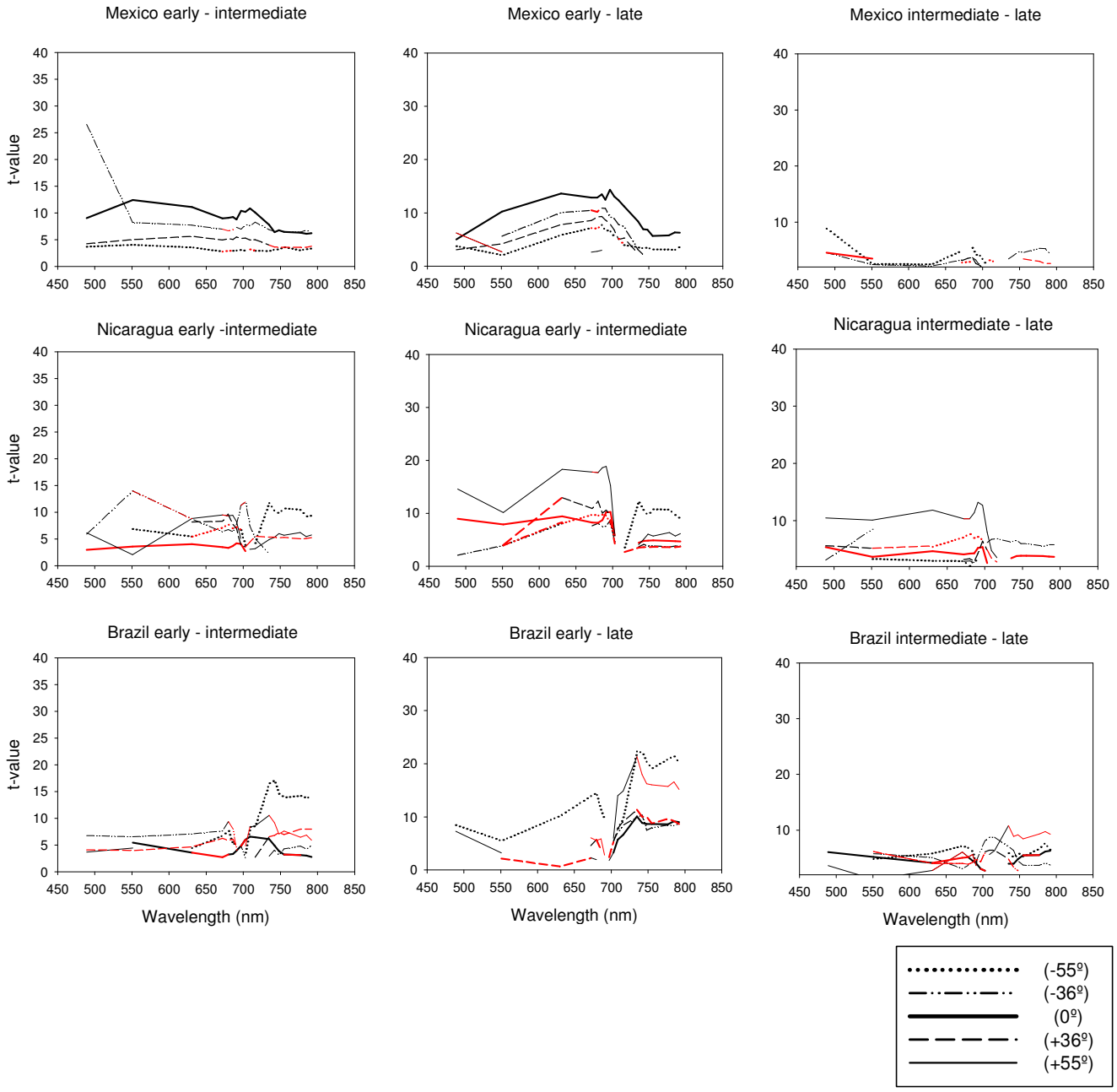

Figure 2.7. Multiple ANOVA for successional stages pairwise for Chamela, Los Naranjos and Mataseca sites for the wet season. Only t-values of significant bands ($p < 0.05$) are represented. Values that failed normality or equal variance tests are represented in red.

c. Separability analysis

The results of the separability test show different results from the ones observed in sections 3.2., were spectral overlapping of two or more successional stages were observed in wet season scatterplots. The Transformed Divergence test considers mean value of each successional stage, but also data distribution in a Euclidean space. Therefore, transformed divergence values offer a more accurate ability to discriminate among successional stages than the n-dimensional visualization (Landgrebe, 1997). All successional stages' pairwise comparisons reached a transformed divergence value above 1.9, independently of season, angle of observation or study site variables. These results imply that when using 18 CHRIS/PROBA bands, it is possible to spectrally discriminate the three successional stages in any case. Lower transformed divergence values are observed for Brazil.

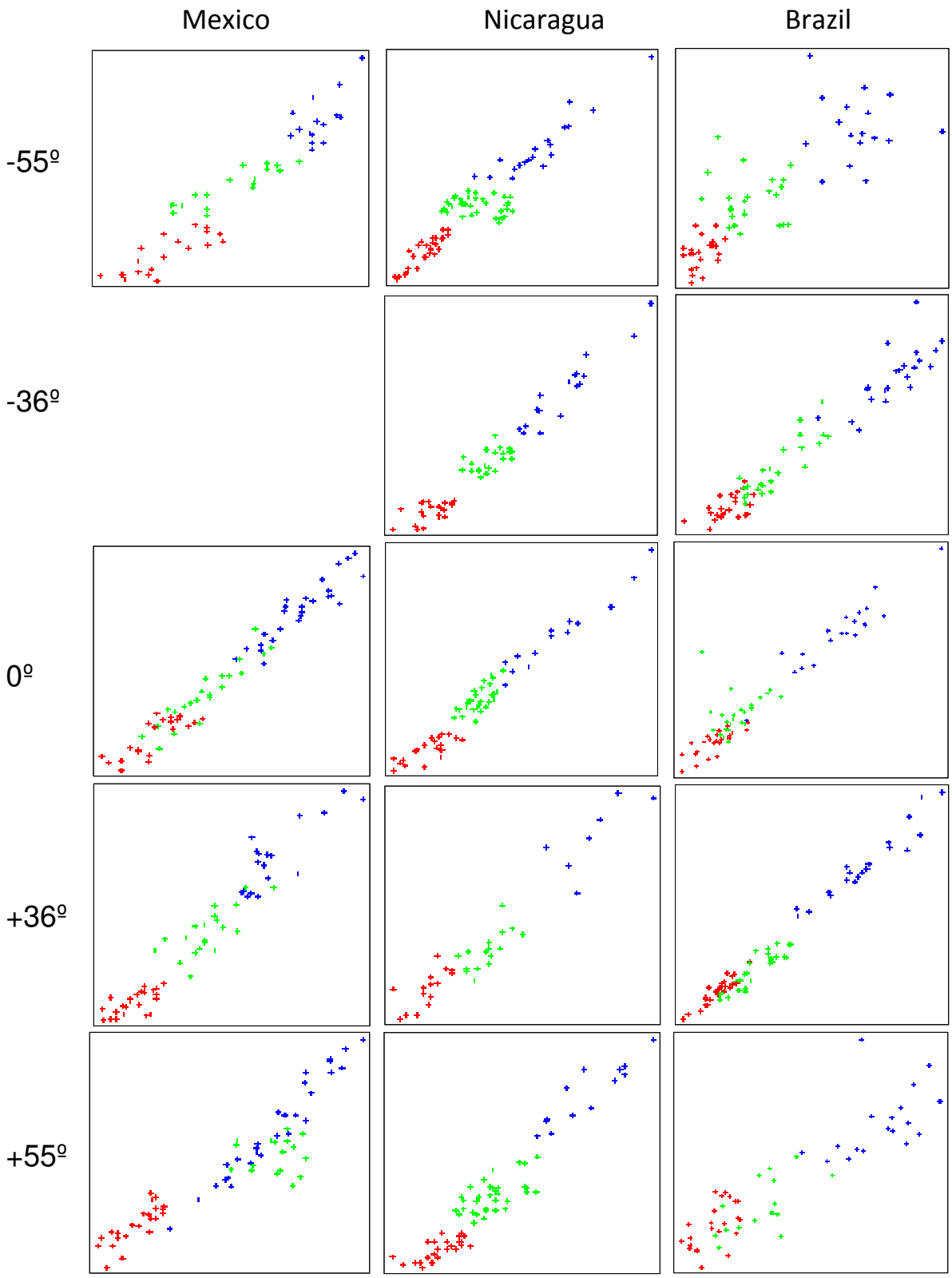

Figure 2.8. 18-Dimensions graphs for 5 observation angles and for dry season in each study site. Early stage is represented in blue, intermediate stage in green and late stage in red.

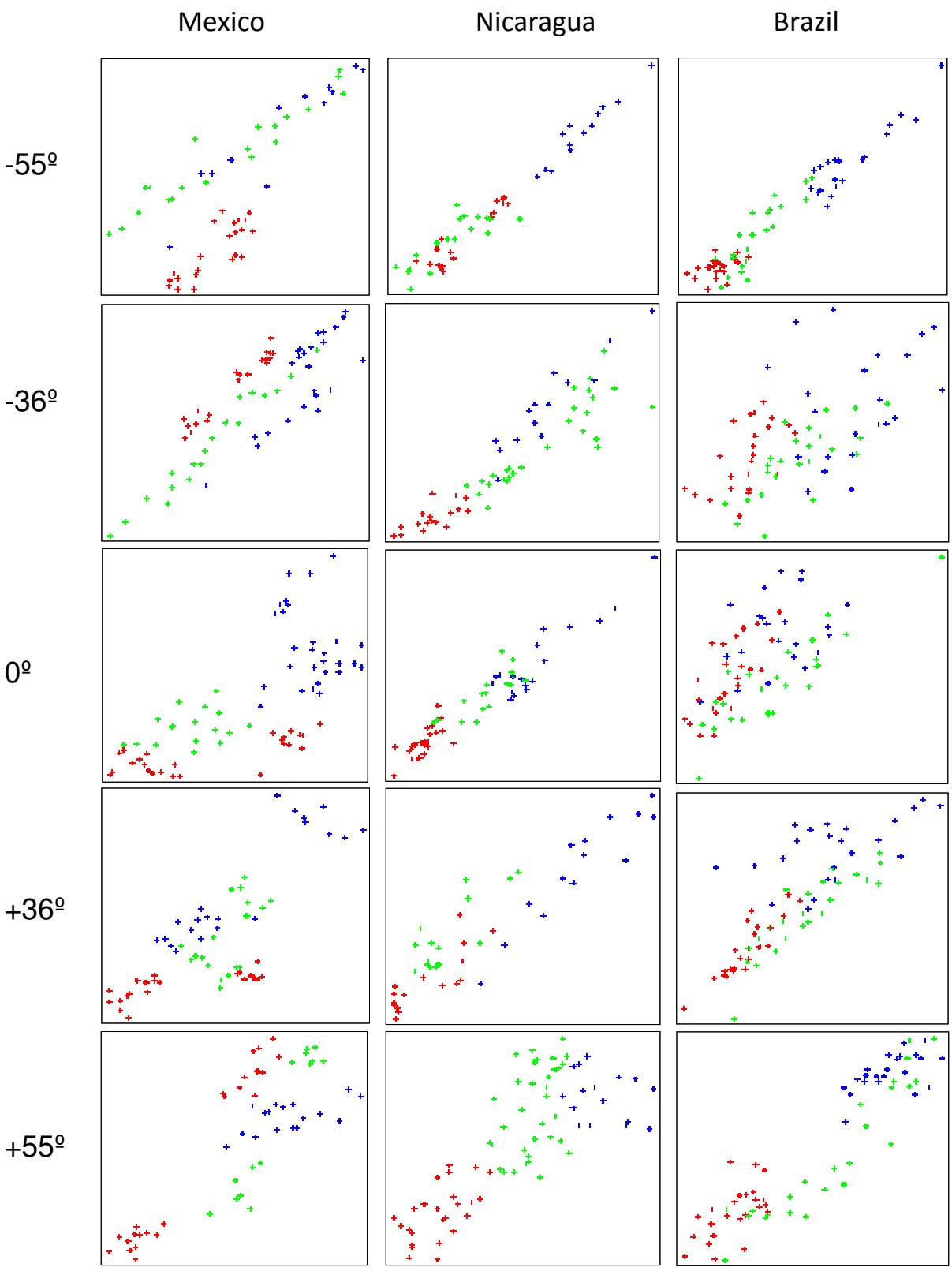

Figure 2.9. 18-Dimensions graphs for 5 observation angles and for wet season in each study site. Early stage is represented in blue, intermediate stage in green and late stage in red.

d. Overview on statistical analysis

Our results in band-by-band analysis indicate that in CHRIS/PROBA's images, the spectral separation of successional stages is more evident during the dry season, suggesting that non-photosyntetic components of the forest and the understory better define the three stages of succession, from a spectral point of view, than the photosynthetic vegetation present in the wet season. During the dry season, it is possible to discern certain structural forest features (e.g. canopy openness, tree height and basal area) depending on the angle of observation. For the dry season, it is CHRIS/PROBA's multiangular component which discriminates succession. In this season, CHRIS/PROBA's hyperspectral sensor is capturing differences in non-photosynthetic components (e.g. understory composition, bare soil, litter and woody components) that characterize successional stages. These results are in agreement with previous studies in TDFs (Arroyo-Mora et al. 2005, Kalascka et al. 2005, Liesenberg et al. 2007). In fact, during the wet season the green canopy masks structural and compositional differences among stages and increases light scattering, which hinders spectral separation. Regarding F-test and t-test values, optimal wet season spectral separation has been reported for extreme angles of observation, suggesting that tree height and Leaf Area Index (LAI) highly conditions the stages' reflectance at CHRIS/PROBA's given pixel size. Backward angles showed better spectral separation than forward angles and nadir. Only +55º reported good spectral separation in both seasons, meaning that sunlit trunks and tree shadows are both defining differences between successional stages.

Band-by-band analysis also demonstrated that many spectral bands failed normality and/or equal variance tests (Figures 6 and 7), suggesting that linear statistical approaches are not appropriate for spectral analysis of our data. Non-parametric statistics (e.g. Friedman F-test, Holm-Sidak t-test, n-dimension analysis and Transformed Divergence test) provide a more flexible and suitable technique to identify spectral differences among successional stages.

In contrast to the band-by-band analysis that showed statistical significance for spectral separation of successional stages only during the dry season, transformed divergence values achieved significant results in both the dry season and the wet season when using CHRIS/PROBA 18 bands together. These results suggest that different compositional elements are reflected in different regions of the spectra, helping in the discrimination of the successional stage. As stated in previous paragraphs, during the dry season, non-photosynthetic components define spectral differences within TDF dry season succession, while wet season reflectance values are largely a

product of composition. As explained before, non-parametric statistics such as Transformed Divergence test enhance the spectral separation of successional stages.

Implications of spectrodirectional separation of successional stages within tropical dry forests

It has been proven that multispectral sensors and observations in nadir show little spectral separation of successional stages of both dry and humid tropical forests (Helmer et al. 2000, Foody and Curran 1994, Moran et al. 1994, Steininger, 2000) if there is no strong ancillary data (Viera et al. 2003), support of other sensors (Arroyo-Mora et al. 2005), or multitemporal images (Kimes et al. 1999, Lucas et al. 2002). CHRIS/PROBA's potential with respect to vegetation studies rely on its hyperspectral resolution and spectro-directionality (Diner et al. 1999, Verstraete et al. 1996, Schaepman et al. 2007). Angular observations have been demonstrated to improve land cover classification because of the spectral information on vegetation structures and textures (Braswell et al. 2003, Liesenberg et al. 2007), while hyperspectral data provides biophysical and biochemical information about vegetation species (Kneubühler et al. 2008). CHRIS/PROBA has the capacity to combine these two resources. In this paper, we evaluated the angular and spectral ability of CHRIS/PROBA in discriminating ecological stages of succession in three TDF locations.

Our results indicate that CHRIS/PROBA is able to discriminate successional stages of the TDF band-by-band in five angles of observation during the dry season (Figures 4, 6 and 8), confirming previous observations that have been limited to nadir observations (Kalacska et al. 2004a, 2007a, Arroyo-Mora et al. 2005). The separation of three successional stages in the wet season is only achieved when using all 18 CHRIS/PROBA bands concurrently, as confirmed by results obtained with transformed divergence. In the cases of Brazil and Nicaragua, the best separation is shown in ±55º, both in dry and wet seasons. For Mexico the best separation corresponds to -55º, 0º and +36º for the dry and wet seasons, respectively (Figures 4, 6 and 8).

As stated in the results section, Mexico shows the weakest spectral separation, while Brazil the highest (t-test and transformed divergence). The limitation found in the Mexican case may be linked to the particularly high number of stems in this region, which mask some structural parameters such as canopy openness and leaf area index, reducing spectral

differences between stages (especially intermediate and late stages) (Table 2).

Spectral differences between successional stages are a function of seasonality and the angle of observation of the sensor. In nadir observations, during the dry season, CHRIS/PROBA captures structural differences between the three successional stages corresponding to basal area, tree density and understory conditions including canopy gaps and area between trees. The early succesional stage produces better spectral separation because the reduced tree density allows superior exposure of the understory to sensors (Arroyo-Mora et al., 2005, Kalacska et al. 2007a). Early stage understory consist of higher percentages of bare soil or pastures that present a very different spectral signature in comparison to the intermediate and late stages of succession, where the predominant reflectance of both successional stages correspond to woody elements. The divergence in reflectance values of the early stage 18D plots, in comparison to intermediate and late stages (Figure 8), is due to the heterogeneity of early stage elements at a sub-pixel level, where trees, pasture and soil are present (Arroyo-Mora et al. 2005). The intermediate stage canopy has more openness than the late stage canopy, and intermediate stage increased canopy openness allows for observations of understory litter fall, shrubs and lianas (Sanchez-Azofeifa et al. 2009). In the late stage the canopy is nearly homogenous and the most useful information to reach the sensor involves bare branches.

During the wet season at nadir, the forest is seen as a homogeneous green carpet, hiding canopy gaps, trunks, branches and understorey, therefore masking differences between successional stages. Canopy gaps are larger in the early stage and the sensor can still catch reflected light coming from the understorey, this justifies the fact that the early stage is clearly differentiated from the rest in 18D plots and statistically as shown by t-test (Figures 5, 7 and 9).

In off-nadir angles, vertical structural parameters become relevant, such as tree height and leaf area index (LAI) (Asner et al. 1998, Heiskanen 2006, Chopping et al. 2008a). Late and early stages differ in no more than 10 meters in height, but CHRIS/PROBA is able to grasp this difference at its spatial resolution of 17 m. In the late stage, taller trees and higher tree densities translate into a higher light absorption, resulting in a lowered reflectance. On the other hand, in the early stage, lower tree density absorbs little light, particularly in comparison to late stage. The decrease in vegetation absorbance together with a higher soil reflectance results in a higher total reflectance for the early stage (Figures 4 and 5).

Hyperspectral sensors like CHRIS/PROBA are especially proficient at capturing species diversity (Castro-Esau et al. 2006, Kalacska et al. 2004a). During the wet season, the spectral variability within a certain successional stage increases due to the high number of species present in tropical forests, while the inter-variability between groups is reduced because of the many species present in all three successional stages (Kalacska et al. 2004b). In 18D plots, this increment of spectral variability results in a cloud of pixels where the three successional stages share the same spectral hyperspace. Intermediate and late stages possess an even larger number of common tree species and families in comparison to the early stage, hindering their spectral separation from one another (Arroyo-Mora et al. 2004, Liesenberg et al. 2007). For this reason, intermediate and late stages usually overlap, while the early stage is more easily separated from the rest (Figures 8 and 9). Nevertheless, non-linear statistics are able to address these limitations, since Transformed Divergence test was able to discriminate the three successional stages by using all 18 CHRIS/PROBA bands together, independently of the season and the angle of observation.

The intensity and purity of the light signal reaching the sensor is also compromised by seasonality and the angle of observation. Sunlight reaching the forest during the wet season scatters in a Lambertian mode due to the multiple orientations of leaves in the green canopy, weakening the light beam bouncing back to the sensor (Kimes, 1983). The relatively leafless state during the dry season produces images where branches form the dominant reflectance feature, reducing surface scattering, making this reflectance aspect less important and the signal reaching the sensor less contaminated. In off-nadir angles, the sensor mainly captures vertical non-photosynthetic structures such as trunks and branches, simpler surfaces that reflect sunlight in a preferential direction, providing a stronger and clearer signal to the sensor and reducing the noise-to-signal ratio. Moreover, in extreme angles there is less interference of understory and other elements, reducing the mixing at a sub-pixel level. Therefore, there is less pixel mixing and light scattering in off-nadir angles, enhancing the differentiation of successional stages in comparison to nadir observations. An exception is found in the spectral signature corresponding to -55º in Brazil and Nicaragua that present an odd pattern in comparison to the rest of angles since the reflectance might be influenced by shadows in the backward position of the satellite.

The reflectance interpretation becomes more complex with the effect of topography, since more surfaces are added to the observed system, as illustrated by the case of the Mexican study site. In an attempt to control for

differential reflectance in shadowed and sunlit faces, some other authors selected pixels in flat areas or areas with similar orientation to improve the classification of vegetation types (Verrelst et al. 2010) or did a sub-classification within a certain forest type –i.e. sunlit primary forest and shadowed primary forest– (Helmer et al., 2000, Thenkabail, 1999). Even though we selected pixels in flat areas within the Mexico site in order to avoid slope shadowing, we observed the spectral data within a given successional stage split in two sub-groups that did appear to be related to slope and shadowing. Probably the effect of shadows is not limited to mountain slopes, but also affects flat areas nearby mountains. For the wet season field plots, two sub-clusters of different successional stages often overlap, such as late and intermediate or intermediate and early, and in these mixed successional vegetation areas, the effect of the topography on the reflectance may provide an even stronger effect than successional differences. Selection of pixels in flat areas or sub-classification based on light exposure worked for mentioned authors since they studied broad vegetation categories, such as primary and secondary forest, but those techniques are insufficient when dealing with vegetation analysis at a finer scale, which includes evaluating successional stages within a secondary forest. As previously noticed by Kneubühler et al. 2008, further radiometric correction efforts are needed in mountainous terrain for the CHRIS/PROBA instrument.

Our results partially differ from some other multi-angular studies in tropical humid areas (Gobron et al. 2000, Galvao et al. 2009), which reported better separation of succesional stages in backward (positive) angles, when targets are sunlit. In our case, best successional discrimination is found mostly in forward observations, suggesting that shadows are a factor in the discrimination of successional stages (Gerard & North, 1997, Goodin et al. 2004, Verreslt et al. 2008), a finding corroborated by the results reported for the Brazilian cerrado (Liesenberg et al. 2007). In our study case, trees are taller in the late successional stage and shorter in the early stage (see Table 2), so it is predictable that late stage patches project thicker and longer shadows than the early and intermediate stages, depending on the position of the sun and the sensor.

Spectrodirectional patterns of tropical dry forests' succession in the Americas

The regeneration of TDFs after deforestation is a matter of crucial importance for ecological management, particularly under conditions of climate change. Remote sensors can facilitate the monitoring of

regeneration processes in large areas, providing a continuous map of the state of succession of forested areas, especially in those spots that are difficult to reach in field surveys.

Three TDF successional stages (early, intermediate and late stages) have been spectrally separated using CHRIS/PROBA's space-borne sensor in three study sites along a latitudinal gradient in the Americas: Mexico, Nicaragua and Brazil. CHRIS/PROBA's discrimination potential relies on its hyperspectral and multi-angular components, which provide information about composition and structure of the forest, respectively, the two parameters selected to characterize successional stages in this paper.

Topography remains a concern in the interpretation of light reflectance of vegetation since it particularly interferes in the spectral separation of successional stages. Differences in reflectance due to topography have been reported in this study to be more significant than spectral differences between successional stages, masking the potential of CHRIS/PROBA in discriminating succession within TDFs in mountainous areas, so further investigation is recommended.

In this study, similar spectral behaviour has been reported for three pan-American sites confirming that the classification of successional stages in terms of structure and species composition is appropriate for remote sensing monitoring. These results suggest a need for the development of a common protocol to monitor TDFs in the Americas using remote sensing tools. We recommend the use of hyperspectral data and multi-angular observations and non-parametric statistical analyses of the data.

Chapter 3.

MAPPING TROPICAL DRY FOREST SUCCESSION WITH CHRIS/PROBA HYPERSPECTRAL IMAGES USING NON-PARAMETRIC DECISIONAL TREES

Abstract

Most satellites for environmental monitoring point ground targets from a perpendicular position to the terrain, also known as nadir. CHRIS/PROBA platform provides four extra angles of observation, plus nadir pointing: -55º, -36º, 0º, +36º and +55º. In this chapter, we compare the contribution of multi-angular observations to classical nadir observation for the discrimination of three successional stages of tropical dry forest and riparian forest in Parque Estadual de Mata-Seca, Brazil. The importance of phenology in succession's spectral separation is also evaluated, by the generation of vegetation maps using dry season's images, wet season's images or both seasons together. Principal component analysis provided input variables for classification. Non-parametric decisional trees were used to build up classification. The purpose of the study is to find out the best combination of season and angle of observation to generate a land cover map that satisfies the classification of all vegetation types under study.

Mapping forests succession: achievements and challenges

Remote sensing is considered an important tool for forest monitoring because of the possibility of generating land cover maps in a spatial and temporal continuum, through the optical behavior of forests canopy (Stoms & Estes, 1993). Its use is especially recommended for remote areas were it is not possible to conduct field surveys. Actual techniques and satellite data allow the generation not only of forest cover, but also about certain forest traits, such as canopy height, aboveground biomass, forest health and forest succession. We are particularly interested in the differentiation of primary and secondary forests because their different implications in carbon sequestration in climate change (Eaton et al. 2009). For this reason, in this study the objective is the generation of ecological succession maps for tropical dry forests (TDF).

Coarse spatial and temporal resolution remote sensors, such as Landsat or MODIS (Moderate Resolution Imaging Spectroradiometer), resulted insufficient for the identification of species or ecological processes (Foody, 2003, Castro et al., 2003, Clarck et al., 2005, Ingram et al., 2005), such as forest succession. Hyperspectral sensors are more sensitive tools in the discrimination of different vegetation types, such as growth stages of secondary forests, and useful when extracting biophysical information such as structure and composition (Jensen 2000b, Thenkabail et al. 2004b). Also multi-angular observations help in the identification of structural traits of forests related to the definition of forest succession (Diner at al. 1999, Gobron et al. 2000, Schaepman et al. 2005, Mahtab et al. 2008). Proba is a hyperspectral sensor on board of platform Chris, which acquires images of ground targets at different pointing angles.

To date, many authors have proposed different approaches to vegetation mapping using CHRIS/PROBA images (Barnsley et al. 2004, Cutter & Sweeting, 2007). In 2008, Kneubühler et al. observed an improvement on map accuracy proportionally related to the addition of CHRIS/PROBA's angles of observation into the classification of Alpen boreal forests. CHRIS/PROBA has also been used in tropical areas for the identification of successional stages of re-growth within Indonesian rainforests (Liesenberg et al. 2009). They used a single image of the wet season and evaluated map accuracy of classifications performed by the use of single CHRIS/PROBA angle in front of multiangular classification (four CHRIS/PROBA angles together). In 2009, Galvao et al. observed that primary forests and three successions of re-growth in Brazilian Amazon rainforest were better differentiated when using two CHRIS/PROBA angles in front of a single CHRIS/PROBA angle.

In the present study the contribution of seasonality in successional stages' discrimination is also evaluated, by the comparison of land cover maps

generated when using one season or two seasons together (dry and wet season). The use of multi-temporal images in classification has been proved to enhance vegetation mapping due to the different phenology of each vegetation cover (Lo et al., 1986, Wolter et al., 1995, Shriever & Congalton, 1998, Guerschman et al. 2003). The optimum number of images within a year needed to differentiate vegetation classes depend on the phenology of classes involved, which is related to environmental conditions such as climate, soil and distance to water, as well as species diversity and representation in the scene (More & Pons, 2007). The distribution of the acquired images along the year also matters (Pax-Lenney & Woodcock, 1997). The use of more than one angle of observation and more than one season have been proved to provide better separation of vegetation in agricultural and urban areas, among other classes (Jin et al. 2012, Duca et al. 2008). CHRIS/PROBA's multitemporal and multi-angular components have been tested together in land cover mapping.

In this study, we evaluate the contribution of CHRIS/PROBA's spectrodirectional data in the discrimination of three successional stages of tropical dry forest. Map accuracy is evaluated for maps generated using different combinations of CHRIS/PROBA's angles of observation (0º, ±36º, ±55º) and TDFs seasons (dry and wet seasons). Class accuracy is also evaluated to evaluate the angle/season combination that comprehends the best classification of three successional stages within TDFs.

Evaluating tropical dry forests' succession classification maps

a. Parque Estadual de Mata-Seca, Brazil

The Parque Estadual da Mata-Seca is a conservation area of integral protection created by expropriation of farmlands in 2000. The Park has an area of 10 281 ha and is located in the valley of the São Francisco River (the second largest river in Brazil), Minas Gerais state, Brazil, between 14°48'36" – 14°56'59" S and 43°55'12" – 44°04'12" W. The potential vegetation of the park is the tropical dry forest, which develops on plain and nutrient–rich soils. These forests are dominated by deciduous trees, with almost 100% of leaf drop during the dry season (May-October). In areas close to water mass, the predominant vegetation is the riparian forest. The climate of the region is considered as tropical semi-arid (Köppen's classification), characterized by the existence of a severe dry season during the winter. The average temperature of the study region is 24.4ºC, and the average annual precipitation is 871 mm. The main economic activities in the area before protection were cattle ranching and bean and corn plantations. Approximately 1525 ha of the area are covered with

abandoned pasture fields in different regeneration stages, while the remaining area supports secondary and primary dry forests. (tropi-dry.eas.ualberta.ca).

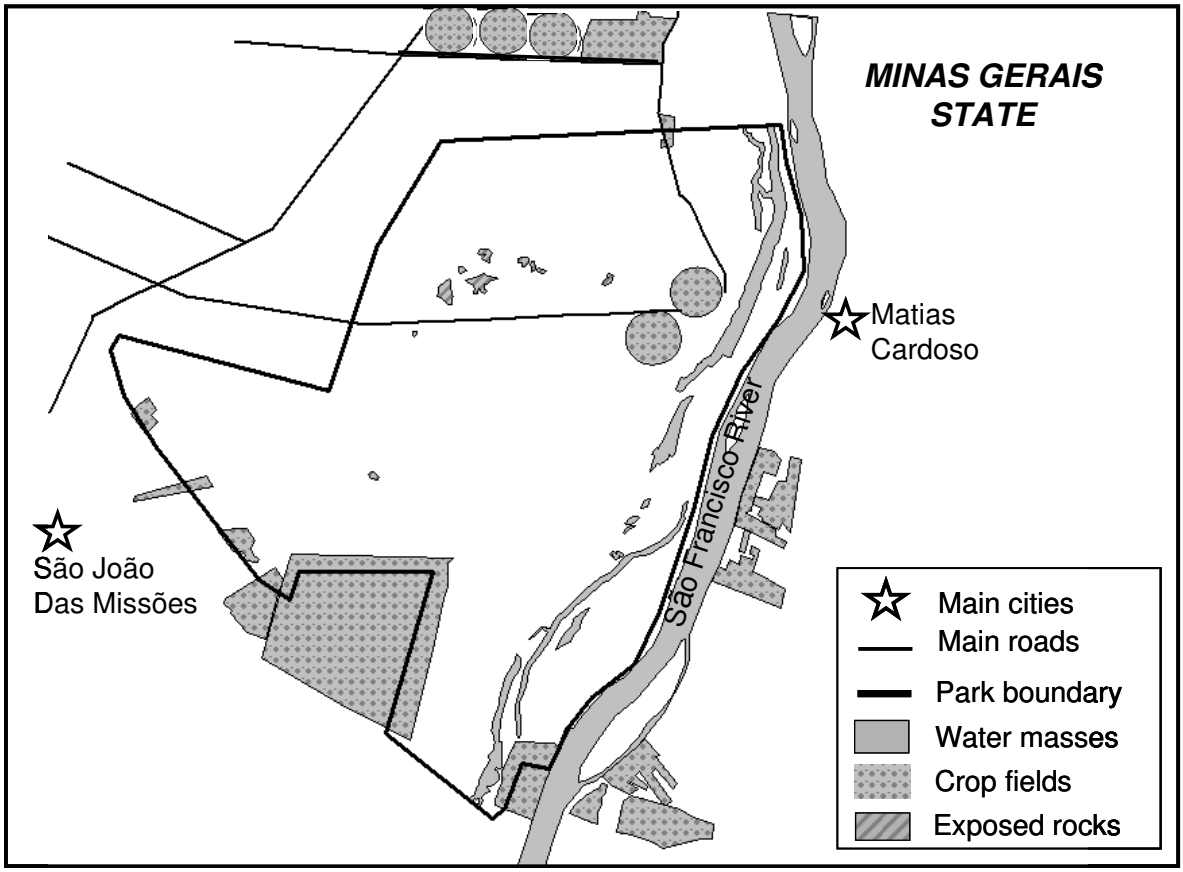

Figure 3.1. Parque Estadual de Mata-seca, Minas Gerais, Brazil

Three successional stages were identified within Mata-Seca's tropical dry forest under study: early, intermediate and late. Successional stages are defined in terms of structure and composition (Kalacska et al., 2004b). (Table 3.1.). In the case of tropical dry forests, the phenology presents two very-well delimited states during the year. During the wet season, all species are dressed up, while most of species lose their leaves during the dry season (Alves, 2008). The transition from wet to dry season is smoother and trees can drop their leaves in some weeks, but the transition from dry to wet season is dramatic, and all trees become green in few days after the first rains (Figure 3.2.). Riparian forests remain green the entire year, because of their proximity to water masses.

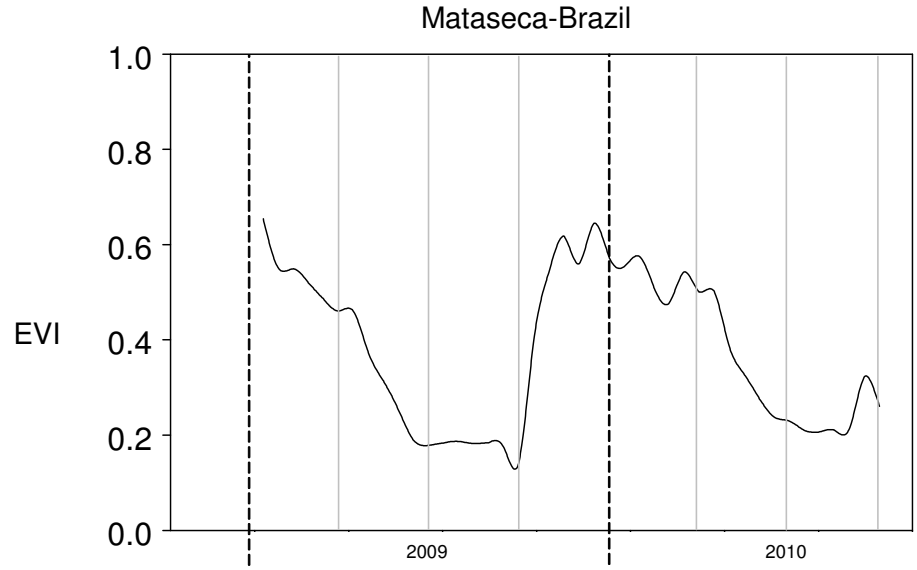

Figure 3.2. Phenology pattern of Mata-Seca study site (Brazil). MODIS EVI product. (https://daac.ornl.usgs.gov/MODIS/modis.htlm)

TABLE 3.1. Structure and composition parameters of three successional stages within Mata-Seca's dry forest.

	Early stage	Intermediate stage	Late stage
# stems (0.1 ha)	49.3 ± 21.0	109.0 ± 11.6	115.3 ± 15.8
# species (0.1 ha)	8.0 ± 1.3	20.2 ± 2.1	19.6 ± 1.7
# families (0.1 ha)	4.3 ± 2.1	12.0 ± 0.9	12.3 ± 2.7
Averaged Height (m)	3.4 ± 0.3	8.0 ± 2.0	11.8 ± 1.7
Averaged Basal Area (m^2/ha)	0.006 ± 0.001	0.009 ± 0.001	0.012 ± 0.003
Dominant Family (%)	Caesalpiniaceae (59.1)	Bignoniaceae (34.1)	Bignoniaceae (34.0)
Dominant Species (%)	Senna spectabilis (40.5)	Tabebuia roseo – alba (20.5)	Tabebuia ochracea (24.3)
HCI	0.008 ± 0.003	0.15 ± 0.04	0.33 ± 0.1

b. Image acquisition and pre-preprocessing

CHRIS/PROBA Mode-4 was selected for the study on scope. For the study site, images were acquired for wet season (May 24th, 2010) and the dry season (September 17th, 2010) (Figure 3.3.).

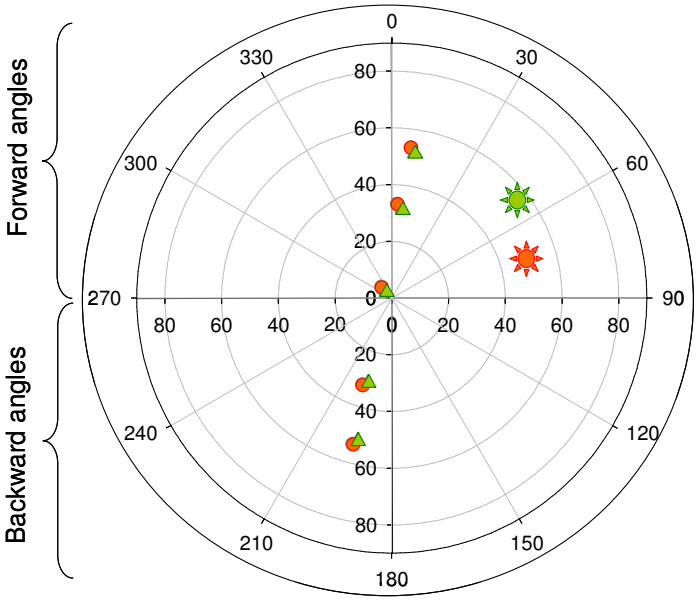

Figure 3.3. Sun position respect to CHRIS/PROBA satellite during the acquisition time for five angles of observation.

All acquired CHRIS/PROBA images were atmospherically corrected using BEAM 4.6.1. CHRIS/PROBA Box 4.7.1. software. Dry season's nadir image was geometrically rectified using a 1 meter resolution Quickbird image as reference. Rest of CHRIS/PROBA images involved in the study were co-registered using this first nadir image as reference. The root mean square error (RMSE) value was smaller than one pixel in all cases.

c. Image preparation

In order to reduce spectral anisotropy and to enhance differences between vegetation classes in the classification process, all non-forested spectral classes were masked (water, roads, crops and clouds). Buffer areas of 50 m both sides of roads were removed to avoid edge effects. In edging areas, light scatters in a different manner than within a homogeneous area (e.g. a forest type), thus pixels in edges present an odd reflectance that introduces noise into the classification.

Four vegetation classes present in the study site were used as training areas for classification: three successional stages of tropical dry forest (late, intermediate and early) and riparian forest. In order to enhance spectral differences between vegetation groups, remove spectral noise and reduce computational time, a forward principal component analysis (PCA) was performed for each angle of observation and season. Principal components (PC) with a percentage of

explanation over 1% were used as input variables for map classification (Table 3.2.). In all cases, maximum variability was captured by the first two PCs (PC1 and PC2). The percentage of explanation of each PC is an adjustment of eigenvalues for each PC, relative to the total sum of eigenvalues for a certain CHRIS/PROBA image, calculated by the ratio:

$$\frac{PCeigen_i}{\sum_{i=1}^{q} PCeigen}$$

where *PCeigen* is the eigenvalue of PCi, *q* is the number of PC for a certain CHRIS/PROBA image and *i* the case PC.

TABLE 3.2. PC adjusted eigenvalues for CHRIS/PROBA's images.

	Angle of observation	% PC1	% PC2	% PC 1+2
Dry season	-55º	55.2	43.4	98.6
	-36º	54.3	44.2	98.5
	0º	62.0	36.8	98.8
	+36º	60.0	38.9	98.8
	+55º	57.0	41.9	98.9
Wet season	-55º	91.5	6.4	97.9
	-36º	86.6	10.8	97.4
	0º	87.6	10.5	98.1
	+36º	86.7	11.4	98.1
	+55º	86.1	11.8	98.0

d. Spectral separability analysis

A first data statistic exploration was done by the analysis of data means, range and standard deviation for each CHRIS/PROBA image, for PC1 and PC2 (Figures 5 and 6), intended to observe the feasibility of each PC to discriminate vegetation types in order to be used as input variables in classification.

Since both PC1 and PC2 are used together as input variables for a single CHRIS/PROBA image, we also wanted to explore potential vegetation types' discrimination when using both PCs together. For that purpose, the Transformed Divergence was used for testing. As other classic separability tests, transformed divergence consider covariance and mean of the studied data. The transformed divergence is a variant of the divergence formula, intended to minimize the increase of the average divergence value in well-separated classes that mislead the divergence measure. It uses the standardized form of the divergence but

scales the divergence values to a certain range (Swain & Davis, 1978, Richards, 1993).

The basis of the transformed divergence measure is the same as other separability test, as Bhattacharyya (Bhattacharyya, 1943) or Jeffries-Matusita (Richards & Jia, 2005), but it does not assume the Gaussian distribution of the data (Gunal & Edizkan, 2008). The transformed divergence (TD) is defined as:

$$TDij = 2000\left(1 - \exp\left(\frac{-Dij}{8}\right)\right)$$

where Dij is the divergence, which considers the variance and mean of each class, represented by i and j, to determine the distance of each class to a reference vector. In this formula, the transformed divergence is scaled to a range of 2.0. The Transformed Divergence values range between 0 and 2.0. Values greater than 1.9 indicate good separability between classes. Values under 1.7 are considered a bad separation, and values under 1.0 suggest the two classes shall be considered as the same one (Gunal & Edizkan, 2008).

e. Image classification

Ten CHRIS/PROBA images were used for classification, corresponding to the wet and dry seasons and five angles of observation. For each vegetation class, a set of 400 pixels surrounding GCPs were used for classification, splitting the 60% of them for training and the 40% for the validation. Pixels on scene were randomly selected from a larger group of pixels to avoid neighbor correlation. To provide an independent validation, training and validation data belonged to different geographical areas within the scene. Non-parametric classification was performed using NLCD-ERDAS with the support of a decisional tree performed in See5.0. Overall map accuracy and accuracy per vegetation class have been evaluated using kappa coefficient (Figures 8 and 9).

The purpose of this study is to Figure out the combination of CHRIS/PROBA's angles of observation and season that better discriminate successional stages in Mata-Seca, Brazil. For this reason, 54 land cover maps were generated by the combination of angles of observation and season, as shown table 3.3. As a first experiment land cover maps using a single-angle and single-season's image into classification were generated. In a second experiment we used more than one CHRIS/PROBA's angle of observation in combinations of two, three or five angles. The rationale of angle's grouping was based on illumination (Figure 3.3.). We grouped CHRIS/PROBA's angles of observation in sunlit angles (backward scattering, -36º and -55º), shaded angles (forward scattering, +36º and +55º), close-to-nadir angles (±36º) and extreme angles (±55º). Moreover,

these groups of angles were tested alone or in combination with nadir (0º) (Table 3.3.). In a third experiment, we explored the effect of multi-temporal classification, by combining CHRIS/PROBA images of both wet and dry season, following the same angle's combination as in experiments 1 and 2. Assuming different angles of observation and seasons provide different spectral information about vegetation targets, our question is whether the anisotropy of information provided by a certain combination of CHRIS/PROBA images enhances classes' discrimination or introduces confusion into the classification.

TABLE 3.3. Combinations of angles of observation as incomes for Mata-Seca's vegetation cover classification.

1 angle	2 angles	3 angles	5 angles
-55º	0º/-55º		0º/±36º/±55º
-36º	0º/-36º		
0º			
+36º	0º/+36º		
+55º	0º/+55º		
	+36º/+55º	0º/+36º/+55º	
	-36º/-55º	0º/-36º/-55º	
	±36º	0º/±36º	
	±55º	0º/±55º	

f. Accuracy assessment

To evaluate the combination of angles of observation and season that better classify vegetation classes within Mata-Seca's study site, classification accuracy was measured by kappa coefficient (Congalton et al. 1983, 1991).

Kappa coefficient is defined as:

$$\kappa = \frac{P_c - \sum_{i=1}^{q} P_{i+} P_{+i}}{1 - \sum_{i=1}^{q} P_{i+} P_{+i}}$$

where Pc is the overall proportion of area correctly classified, defined as $P_c = \sum_{i=1}^{q} P_{ii}$, P_{i+} is defined as $P_{i+} = \sum_{k=1}^{q} Pik$ and $P_{+i} = \sum_{k=1}^{q} P_{ki\cdot}$, q is the number of land-cover categories, and i and k represent classes.

The kappa analysis is a discrete multivariate technique used in accuracy assessment to statistically determine if the selected classification approach is significantly better than a random classification. The kappa coefficient is a

more objective measure than overall accuracy or Tau coefficient because it contains information about the off-diagonal cell values, or the errors of commission and omission (Jensen 1996, Stehman 1999). A high kappa coefficient points out the class under study is correctly classified and it is not confused with a different class. In other words, that the class it is neither underestimated nor overestimated.

A class that achieved low kappa accuracy in classification shall be masked by another class that reached a very high kappa value, resulting in a high overall kappa value. The purpose of the study is to achieve a land cover maps where all vegetation class under study are well-represented. To avoid maps where one vegetation class has been weakly classified, kappa coefficient has also been calculated for each vegetation type, providing partial kappa estimations

On the search of a classification rule for tropical dry forests' succession

a. Data exploration

As referred in the methods, the two first principal components (PC) were used as input variables in the non-parametric classification of Mata-Seca's site for each angle of observation and season. According to PC's adjusted eigenvalues (Table 3.2.), in dry season's images the most of data information is contained in PC1 and PC2, having both PCs similar importance (PC1 around 50-60% and PC2 around 40-50%). The exception is found at +36º and 0º, where PC1 is relative more important than PC2. For wet season's images, most of the data information is contained in PC1 (around 85%) and a small percentage is contained in PC2 (around a 10%), especially in – 55º, which more than 90% is supported by PC1.

Field surveys permitted the interpretation of data contained in each selected PC. For dry season's images, PCA allowed a better discrimination between the four vegetation types within Mata-Seca (three stages of tropical dry forest and riparian forest), while in wet season's images PCA enhanced areas with different soil humidity (Figure 3.4). When visually analyzing dry season's PC1, it is observed that at angles of observation 0º, -36º, +36 and +55º darker pixels correspond to riparian areas (Figure 3.4.a.), while bright pixels correspond to tropical dry forest, especially early stage, which look even brighter. At -55º, the opposite situation is observed (Figure 3.4.b.). In PC2 the discrimination between vegetation types is not that clear. At 0º, -36º, +36 and +55º angles dark pixels correspond to riparian forest or early stage of tropical dry forest, while bright pixels correspond to intermediate and late stages of TDF (Figure 3.4.e.). At -55º, dark pixels correspond to riparian forest, brighter pixels to early stage of TDF and the rest of pixels, to intermediate and late stages of TDF (Figure 3.4.f.).

For wet season's images PC1, bright pixels correspond to wet soil areas at sunlit angles (positive angles) and nadir (0º), while shaded angles point to drier areas, especially those with open canopy, like early stages and areas close to crops and the Park's boundary (Figure 3.4.c.). In the case of shaded angles of observation (negative angles), the information contained in PC1 is inverted respect to sunlit and nadir observations (Figure 3.4.d). PC2 is practically a negative shot of PC1: at negative angles, bright areas correspond to wet soil areas and dark areas to dry and open-canopy areas (Figure 3.4.g), while at positive and nadir angles, wet soil areas match to dark pixels and dry and open areas correspond to bright pixels (Figure 3.4.h.).

PC1

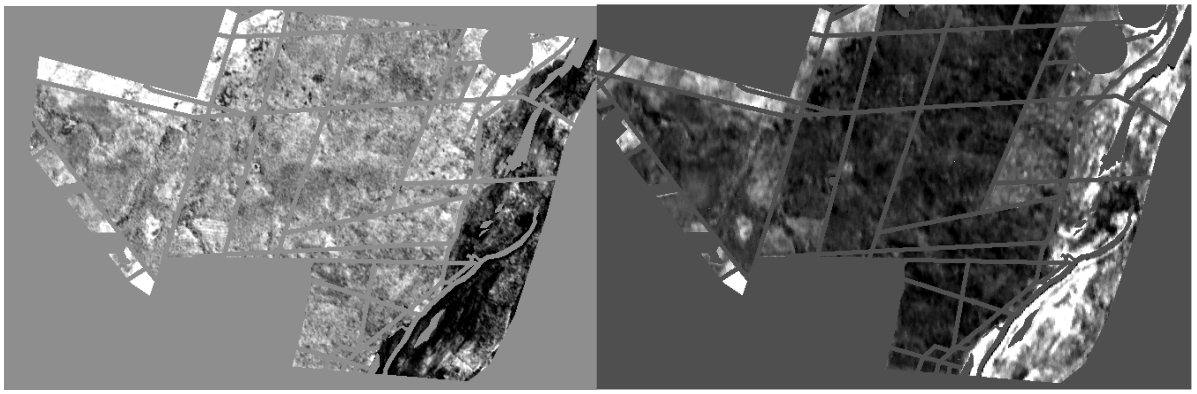

a) Dry season (0º) b) Dry season (-55º)

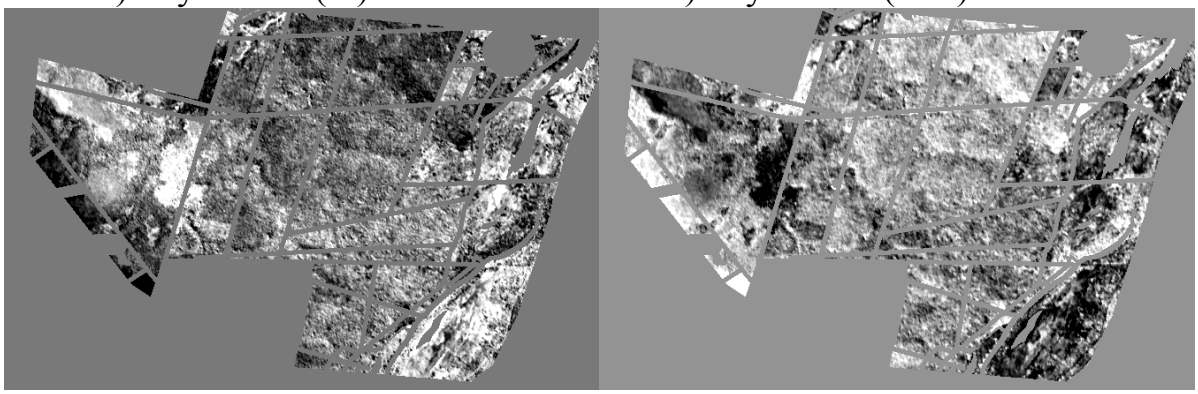

c) Wet season (0º) d) Wet season (-36º)

PC2

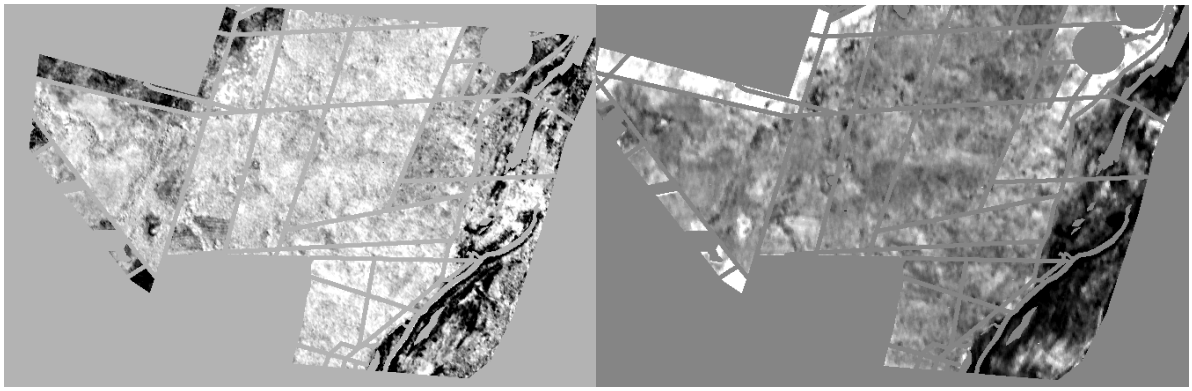

e) Dry season (0º) f) Dry season (-55º)

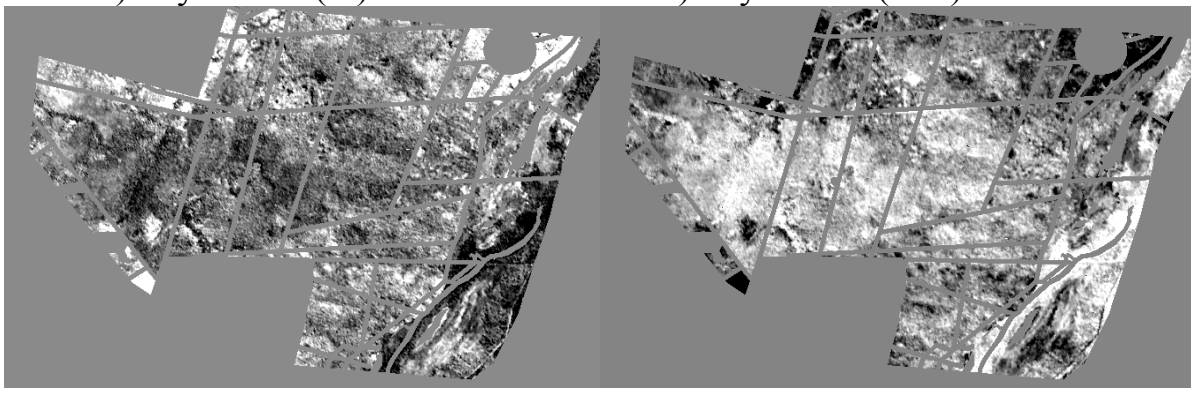

g) Wet season (0º) h) Wet season (-36º)

Figure 3.4. PC1 and PC2 visualizations for the dry season and wet season.

b. Spectral separability

PC1 and PC2 spectral data mean, range and standard deviation are presented for CHRIS/PROBA's angles of observation and seasons, for the four vegetation types under study (Figure 3.5 and 3.6).

For PC1 dry season's images, it is observed that three successional stages of TDF present a small range of variation while riparian forest presents a larger data range. Depending on the angle of observation, some vegetation types share similar spectral range. At -55º, the four vegetation types are perfectly separated. At -36º and 0º, riparian forest and late stage of TDF share spectral values, while intermediate and early stages' spectra totally coincide. At +36º, intermediate and early stages spectra partially overlap, while at +55º they are late and early stages' spectra that partially coincide (Figure 3.5. left).

For PC1 wet season's images, three successional stages of TDF and riparian forest present similar data distribution. Vegetation types' data means never coincide, but data range overlap. For -55º, early stage is totally separated from the rest, late and intermediate stages' data range overlap, as well as intermediate and riparian forest. At 0º and -36º, late stage overlaps with intermediate stage, intermediate with early and early with riparian forest. At positive angles (+36º and +55º), late and intermediate stages and early and riparian overlie, but not intermediate and early stages (Figure 3.5. right).

Dry season's PC2 also presents a small data range for TDF's successional stages and for riparian forest at extreme angles (± 55º). Data means never coincide for any angle of observation and vegetation type, with the exception of early stage and riparian forest at 0º. Nevertheless, there is certain overlapping in data ranges; at -55º early and intermediate stages' spectra overlap, while at 0º and ±36º there is overlapping between intermediate stage and riparian forest as well as between early stage and riparian forest. At +55º all vegetation types separate perfectly (Figure 3.6. left).

For wet season's PC2, data ranges are very small and the four vegetation types present similar spectral range within a certain angle of observation. The only exception is found at +55º, where intermediate stage's spectra separates form the rest (Figure 3.6. right).

In table 3.4., results of the Transformed Divergence test are presented, when analyzing together PC1 and PC2 for a certain CHRIS/PROBA image. In bold, those scores above 1.9 that indicate separation between two vegetation types are shown. For dry season's images, riparian forest represents a different spectral category respect to the rest of TDF's successional stages, for any angle of

observation. The early stage of TDF spectrally separates of intermediate and late stages only in extreme angles of observation (± 55º) and also for -36º for the pair early-late stages. Intermediate and late stages of succession are considered as very similar spectral classes, for all angles of observation.

In the case of wet season's images, all vegetation types' pair comparisons provides values under 1.0, meaning that they belong to the same spectral class. The only exception is found for early and late stages of TDF at -55º, which spectrally separate (Table 3.4.).

In Figure 3.7., PC1 and PC2 scores are confronted to graphically illustrate spectral separation of vegetation types under study, for each angle of observation and season. For dry season's images, it is possible to distinguish the four vegetation groups, although they overlap. Three successional stages of TDF present a linear trend in a different direction than riparian forest values, which show a curve trend (Figure 3.7. left). In wet season's images TDF successional stages and riparian forest line up in the same direction following a linear trend. Vegetation spectral groups are even more overlapped than in dry season's images, with the most significant case at +55º (Figure 3.7. left).

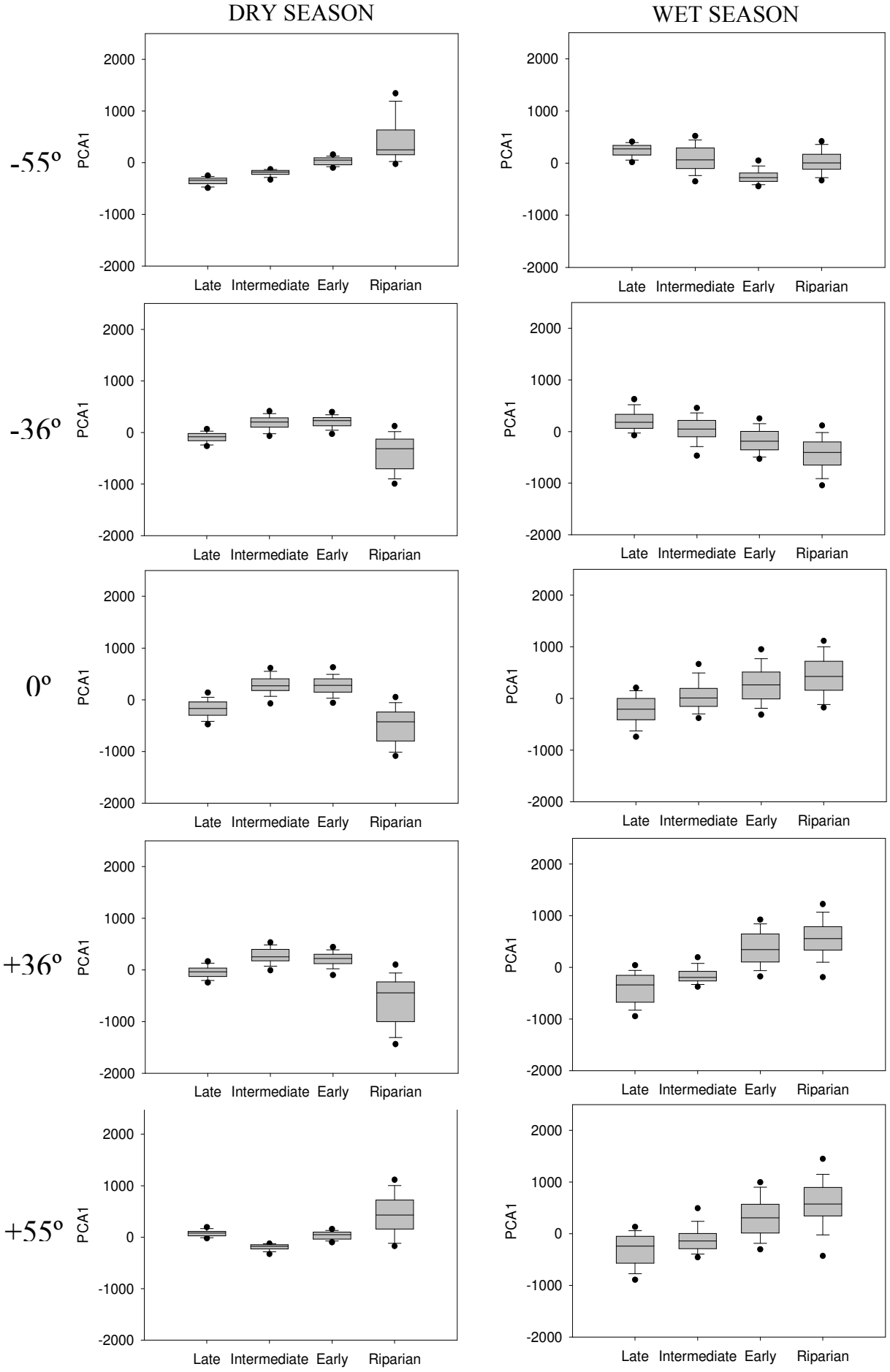

Figure 3.5. PCA1 scores of vegetation types in Mata-Seca for CHRIS/PROBA data acquired for the dry (left) and wet season (right) in five angles of observation.

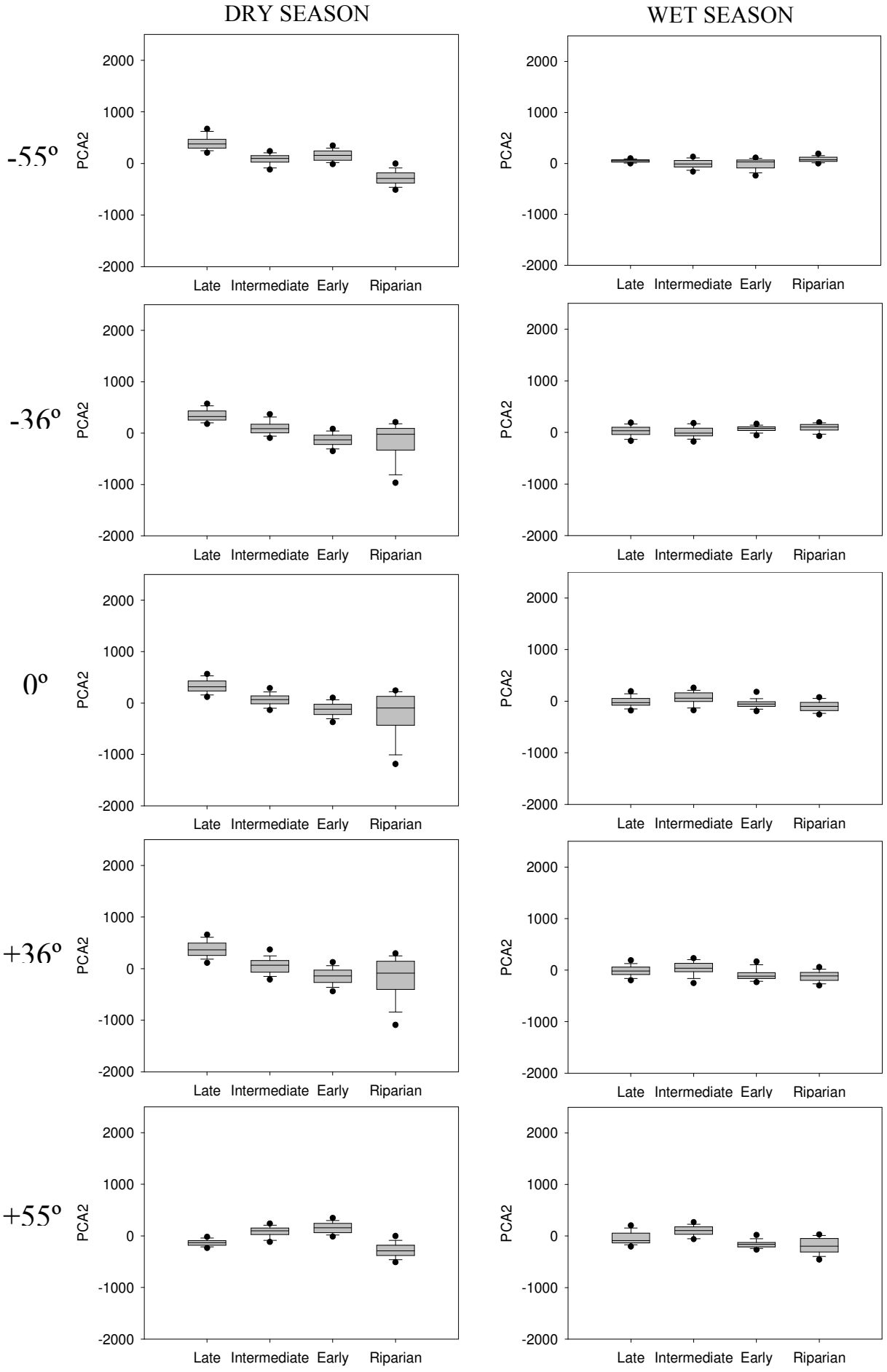

Figure 3.6. PCA2 scores of vegetation types in Mata-Seca for CHRIS/PROBA data acquired for the dry (left) and wet season (right) in five angles of observation

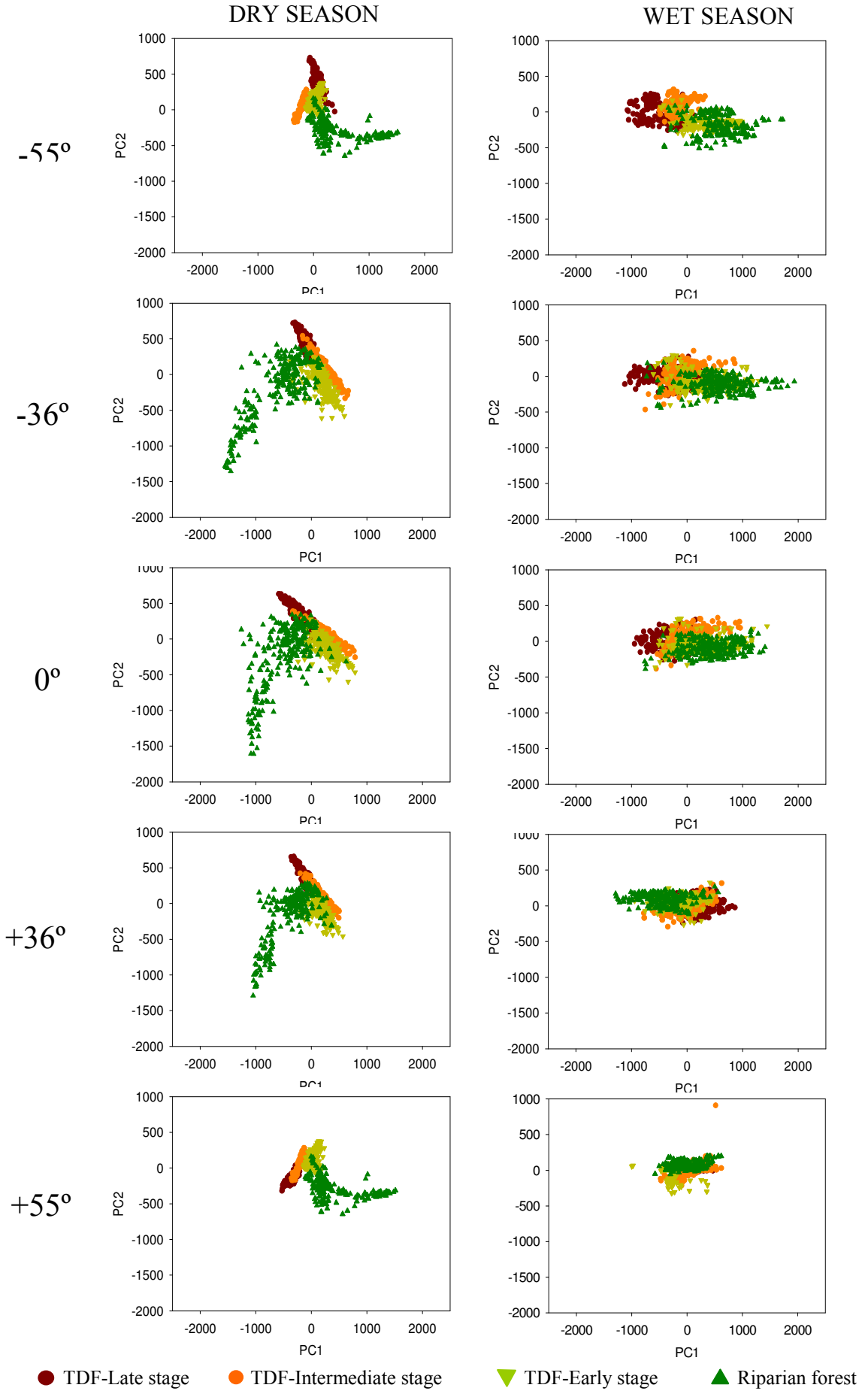

Figure 3.7. Spectral separability of vegetation types within Mata-Seca when using PC1 and PC2 together, for each CHRIS/PROBA image.

TABLE 3.4. Transformed Divergence for each CHRIS/PROBA image. Spectral separation of vegetation types by pairs, when using PC1 and PC2 combined.

	Dry season					Wet season				
	-55º	-36º	0º	+36º	+55º	-55º	-36º	0º	+36º	+55º
E-I	**1.95**	1.67	1.32	1.57	**1.88**	0.88	0.16	0.24	0.38	0.71
E-L	**1.95**	**1.76**	1.59	1.65	**1.90**	**1.82**	0.69	0.60	0.71	1.14
E-R	**2.00**	**1.98**	**1.98**	**1.98**	**2.00**	1.00	0.28	0.15	0.35	0.86
I-L	1.43	0.96	0.81	0.82	1.01	1.25	0.48	0.46	0.52	0.60
I-R	**2.00**	**2.00**	**2.00**	**2.00**	**2.00**	0.76	0.38	0.48	0.65	1.24
L-R	**2.00**	**2.00**	**2.00**	**2.00**	**2.00**	0.91	0.92	0.79	1.13	1.58

E: early stage, I: intermediate stage, L: late stage, R: Riparian forest

c. Accuracy assessment

Once the classifications were performed using different combinations of CHRIS/PROBA's angles of observation and seasons, map accuracies were tested using total and partial kappa coefficients (Figures 3.8. and 3.9.).

At a first sight, total kappa coefficients are higher when using both dry and wet seasons, around 77%. These scores are followed by classifications using dry season's images (72%) and the lowest scores are achieved by wet season's image classification, for all combinations of angles of observation (53%) (Table 3.5.).

TABLE 3.5. Mean and standard deviation for all combinations of angles involved in Mata-Seca's classification for the dry, wet and dry+wet seasons.

	Wet season	Dry season	Dry & Wet season
Total accuracy	61.65 ± 0.11 %	77. 91 ± 0.06 %	81.65 ± 0.10 %
Kappa coefficient	53.35 ± 0.11 %	72.70 ± 0.08 %	77.02 ± 0.13 %

When only one angle of observation is used for classification, better kappa accuracies are observed for shaded (negative) angles for the dry and dry+wet seasons, while better classification is observed for the sunlit (positive) angles when using wet season's images. In all cases, the weakest total kappa value is achieved at nadir angle (0º) (Figure 3.8.).

For the combination of two angles of observation, shaded angles (-36º/-55º) or the combination of shaded and nadir angles (0º/-36º and 0º/-55º) perform better results than sunlit angles (+36º/+55º) or the combination of sunlit and nadir angles (0º/+36º and 0º/+55º), for all season's combination. The use of extreme angles (±55º) for classification also presents a high kappa value for all season's combination. For the particular case of the dry

season, ±36º also shows a high kappa, while any combination with +36º (0º/+36º and ± 36º) shows the weakest score for the wet season and the combo dry+wet season. The addition of 0º to other angles of observation into the classification provokes different reactions depending on the season and angle. When using -55º in combination with 0º in comparison to using -55º alone, the total kappa improves for the wet season's classification, while it declines for the dry and dry+wet seasons. The addition of 0º to -36º do not produce any effect on the total accuracy, in comparison to the map classified only with -36º, to any season. Neither it provokes any effect on the total kappa coefficient when using +36º alone or 0º/+36º in dry season's classification, nor when comparing +55º or 0º/+55º in the dry season and dry+wet season's classification. Nevertheless, there is a decrease in total kappa when classifying with 0º/+36º using wet season and dry+wet season's images, and 0º/+55º in the wet season's classifications, in comparison to +36º and +55º alone, respectively (Figure 3.8.).

When using the combination of three angles of observation, the best performances are observed for nadir/shaded angles (0º/negative angles) and nadir/extreme angles (0º/±55º), except for the dry season, respect to extreme angles. When comparing classifications performed with two angles respect to three angles, we observe that the addition of 0º to shaded angles (-36º/-55º) and sunlit angles (+36º/+55º) do not significantly improves the total accuracy. In the case of close-to-nadir (±36º) and extreme angles (±55º), the addition of 0º provokes a reduction in total kappa coefficient, especially in dry and dry+wet season's classifications. It is observed that the highest score, reached by 0º/shaded angles (0º/-36º/-55º), is similar to the achieved with 0º/-55º, ±55º and -36º/-55º, which are the top kappa coefficients in the category of combination of two angles (Figure 3.8.).

In the case that all CHRIS/PROBA's angles of observation (five angles) are involved to produce Mata-Seca's land cover map, it is observed that there is not any improvement, respect to the use of three angles of observation. The total kappa value of five angles of observation is similar to the observed for 0º/±55º and weaker than the presented by 0º/negative angles (0º/-36º/-55º), for the dry and dry+wet seasons (Figure 3.8.).

The highest total kappa values are always achieved by those classification maps that involved both dry and wet seasons. The top scores, in order of ranking, are reached by 0º/-55º (90.57%), -55º (92.37%), five angles (93.60%), 0º/-36º/-55º (94.00%), -36º/-55º (94.04%), ±55º (94.64%) and 0º/±55º (94.64%) (Figure 3.8.).

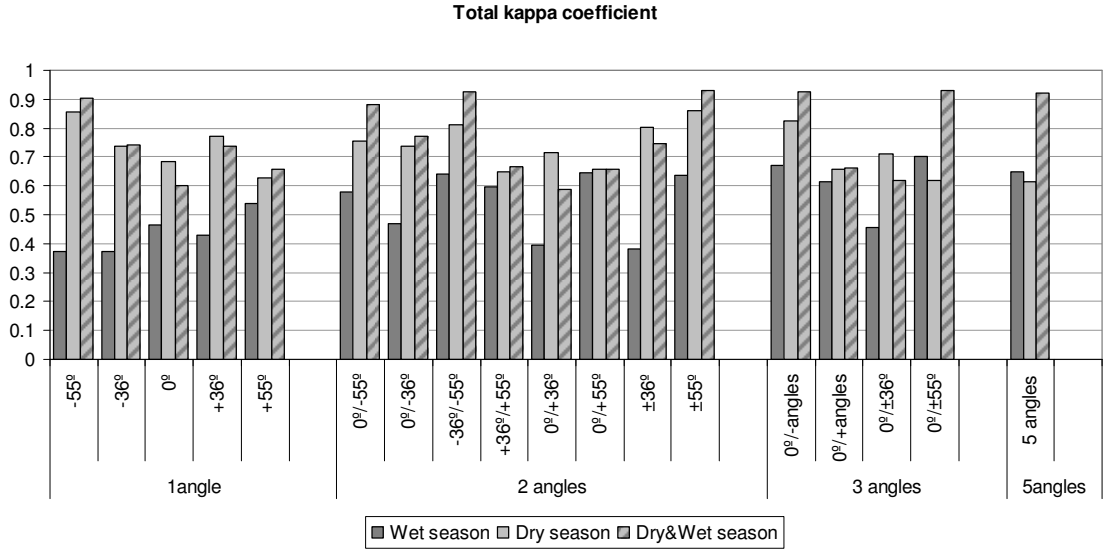

Figure 3.8. Total kappa coefficient for CHRIS/PROBA's classification maps in Mata-Seca's study site, for all angles combinations.

Once overall kappa accuracy has been evaluated, a partial kappa assessment for each vegetation type is described in following paragraphs. According to mean and standard deviation of partial kappa coefficients, the highest kappa values are reached using only dry season's images, while the weakest kappa value are achieved when using wet season's images alone, except for the riparian forest (Table 3.6.). The best classification are observed for the late stage of TDF when using dry season's images or the combination of dry and wet season, while riparian forest is better classified when using dry and wet seasons combined. The weakest kappa values are observed for the early stage of succession and the intermediate stage of TDF when using wet season's images (Table 3.6.).

TABLE 3.6. Kappa mean and standard deviation for all combinations of angles involved in Mata-Seca's classification for the dry, wet and dry+wet seasons, detailed for vegetation types

Kappa coefficient	TDF Late stage	TDF Intermediate stage	TDF Early stage	Riparian forest
Wet season	0.56 ± 0.28	0.38 ± 0.13	0.41 ± 0.28	0.69 ± 0.19
Dry season	0.88 ± 0.05	0.61 ± 0.15	0.49 ± 0.32	0.59 ± 0.18
Dry & Wet season	0.87 ± 0.05	0.57 ± 0.24	0.44 ± 0.35	0.81 ± 0.15

For the late stage of succession, classifications performed using dry season's images alone provide similar results to those performed dry and wet season's images combined. In most of cases, kappa values reach 80% of accuracy. On the other hand, classifications that used wet season's images alone as input variables show kappa values below 50% of accuracy, especially in single angles or the combination of two angles. Nevertheless, wet season's images provide high kappa values (comparable to dry season's and dry+wet season's images) when extreme angles are involved, such at 0º/-55º, 0º/+55º, -36º/-55º, ±55º, 0º/-36º/-55º, 0º/+36º/+55º, 0º/±55º and 5 angles (Figure 3.9.a.).

Kappa values for the intermediate and early stages of succession are considerable lower than for the late stage. For the intermediate stage of succession, wet season's images present the lowest kappa values for all cases, in comparison to land cover maps that used dry season's and dry+wet season's images. Dry season's images alone perform similar kappa accuracies than dry and wet season's combined for a single-angle classifications. When more than one angle is involved, dry+wet season's images perform higher kappa values than dry season's alone at negative values or extreme values combination (0º/-55º, 0º/-36º, -36º/-55º, 0º/±55º, 0º/-36º/-55º) and when using 5 angles of observation. On the other hand, dry season's images alone overcome kappa values for dry+wet season's images at positive angles and combinations with close-to-nadir angles (0º/+55º, 0º/+36º, +36º/+55º, 0º/±36º, 0º/+36º/+55º) (Figure 3.9.b).

For the early stage of succession, kappa presents null or negative values for the following cases, meaning that it has not been classified in the resulting vegetation map and it has been confused with other vegetation classes: at -36º when using only wet season's images, 0º/±55º and 5 angles of observation when using dry season's images alone, 0º/+55º and +36º/+55º in the case of dry season's and dry+wet season's images, 0º/+36º/+55º for dry season's and wet season's images, and ±55º for all seasons combination. In this vegetation type, dry season's images and dry+wet season's images provide similar kappa values, with some exceptions: dry season's images classifies better alone than in combination with wet season at 0º, 0º/+36º, 0º/+36º/+55º and 0º/±36º, while dry+wet season's images present better kappa accuracies at 0º/±55º and 5 angles of observation. On the other hand, wet season's images used alone classifies best at +36º/+55º, 0º/-36º/-55º and 0º/±55º. (Figure 3.9.c.).

For the riparian forest, most of the cases dry+wet season's images perform better classifications, especially in those angle's combination implying extreme angles (-55º, 0º/-55º, 0º/+55º, -36º/-55º, +36º/+55º, ±55º, 0º/-36º/-

55º, 0º/+36º/+55º, 0º/±55º and 5 angles of observation). Land cover maps that used wet season's images present their best kappa values in riparian forest's class. It presents the highest score at 0º/+55º, ±55º and 5 angles of observation (Figure 3.9.c.).

For a correct classification map, it is necessary that all classes are represented within a high percentage of accuracy. Kappa coefficient integrates the commission and omission error; a high kappa coefficient means the class under study is correctly classified and it is not confused with a different class. Kappa coefficients around a 75% or above for all vegetation classes are only achieved when using dry and wet season combined in classification, at -55º, 0º/-55º, -36º/-55º, ±55º, 0º/-36º/-55º and 0º/±55º (Figure 3.9 and Table 3.7).

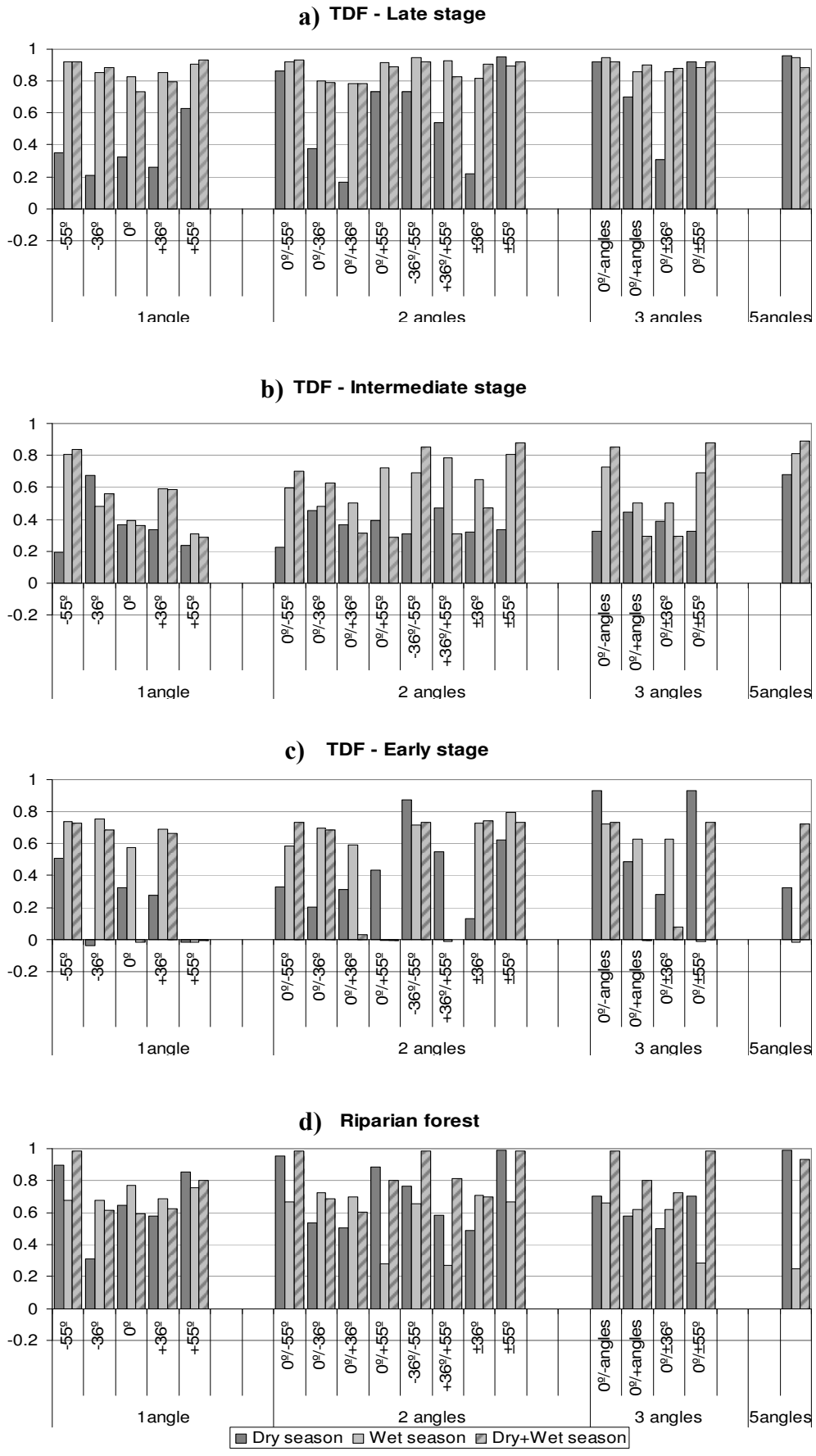

Figure 3.9. Partial kappa coefficient for each vegetation type for CHRIS/PROBA's classification maps in Mata-Seca's study site, for all angles combination.

TABLE 3.7. Best partial kappa scores for the four vegetation types in percentage

Dry & Wet Season	TDF Late stage	TDF Intermediate stage	TDF Early stage	Riparian forest	TOTAL
-55º	92.05	83.87	72.72	98.36	90.31
-36º/-55º	92.00	85.37	73.29	98.36	92.40
±55º	92.00	87.71	73.43	98.36	92.97
0º/-36º/-55º	92.00	85.37	73.29	98.36	92.40
0º/±55º	92.00	87.71	73.43	98.36	92.97

A proposal for accurately mapping tropical dry forests' succession

The analysis of spectral data of main Principal Components (PC), showed that only at -55º it is possible to spectrally separate four vegetation classes under study (three successional stages of TDF and riparian forest) in dry season's images, whether PC1 and PC2 are analyzed per separated (Figures 3.4. and 3.5.). For any other angle of observation, there is data range overlapping between at least two vegetation types, depending on the angle of observation. Spectral overlapping is more severe in wet season's images (Figures 3.4. and 3.5.).

However, when PC1 and PC2 are used together, riparian forests and tropical dry forests spectrally separate in dry season's images, at any angle of observation, as explained by transformed divergence values (Table 3.4.). This separation is due to a spectral difference in terms of phenology, since riparian forests remain green during the dry season, while TDF loses all their leaves. Neither riparian forests nor successional stages of succession are spectrally discriminated during the wet season; when both forests (riparian and TDF) are dressed up, spectral differences between them become inconspicuous.

According to transformed divergence values (Table 3.4.) and PC1 vs. PC2 correlation (Figure 3.7.), intermediate and late stages of succession do not separate in a hyperspace delimited by PC1 and PC2, at any angle of observation or season. This trouble has been encountered by many authors in the purpose of discriminating primary and secondary tropical rainforests with satellite imagery (Foody et al. 1996, Lu et al. 2003, Vieira et al. 2003, Liesenberg et al. 2009). Nevertheless, kappa values for the overall land cover map and for the partial class accuracies present successful results in the discrimination of both classes for the dry season and the combination of dry+wet season's images (Figures 3.8. and 3.9.). By the observation of decisional trees used for classification (Annex I and II), dry season's PC1 have been prioritized in front of PC2, meaning that not only the income

spectral data but also the non-parametric method selected have been determinant in the separation of intermediate and late stages of succession of TDF. Early stage of succession is spectrally separated from other stages of succession only at extreme angles in dry season's images (Table 3.4.) and presented the lowest kappa values in all land cover maps, at any combination of season and angle of observation (Figure 3.9.).

As explained in the methods, the first experiment was intended to Figure out whether it is possible to generate an accurate land cover map of TDF's succession by using a single CHRIS/PROBA angle of observation. Classifications performed with single-angle images provided moderated kappa results both for overall accuracy and partial vegetation classes' accuracy, above 60%, when using dry season or dry+wet season's images (Figures 3.8. and 3.9.). The best kappa accuracies were observed at -55 (Figures 3.8. and 3.9.). Results were weaker for wet season's classification, below 40% (Figures 3.8. and 3.9.).

The second experiment seeks to evaluate whether there is an improvement in land cover accuracy by the use of more than one angle of observation in the classification. According to the results, there is not an increment of kappa accuracy related to an increase in the number of angles used for classification (Figures 3.8. and 3.9.). Based on the overall and partial accuracies observed for kappa results, land cover accuracy is dependent on the nature of the angles that have been used for classification. The higher accuracies are achieved when negative angles (-36º and -55º) or extreme angles of observation (-55º or +55º) are involved in classification (Figures 3.8. and 3.9.). Furthermore, the addition of nadir observations (0º) into the classification do not improves classification, and in certain cases, it lowers the kappa value of the land cover map. In the case of single-angle classifications, nadir presents the lowest kappa value, as for the total accuracy as for the partial class accuracy (Figures 3.8. and 3.9.). In other words, nadir observations provides certain spectral separation between classes, but the spectral information provided by off-nadir angles is more relevant for the discrimination of successional stages of TDF. Other studies that used multi-angular images for land cover mapping also noticed that better results are obtained from off-nadir angles than nadir observation, especially related to vegetation classes (Sandmeier and Deering, 1999, Galvao et al. 2009, Liesenberg et al. 2009, Ducca et al. 2008, Chopping et al. 2006, Mahtab et al. 2008).

During the dry season, at nadir (0º) and close-to-nadir observations (±36º), CHRIS/PROBA images are providing information about canopy and understory elements, through gaps in the canopy. These differences, in terms of composition (non-photosynthetical elements of the forest such as

branches, trunks and lianas and understory elements such as litter, old pastures or bare soil) and structure (tree basal area, tree density, canopy openness) permit the discrimination of successional stages within TDF with moderate kappa accuracy, around a 50% at 0º (Figures 3.8. and 3.9.), at the spatial resolution of CHRIS/PROBA Mode-4 of 17m. Hyperspectral Proba sensor is more efficient in the discrimination of structural and compositional elements (both in canopy and understory) that characterize each successional stage of the TDF, as well as riparian forests, in front of other sensors with similar spatial resolution but coarser spectral resolution, such as Landsat (Castro-Esau et al. 2003, Kalacska et al. 2005a). As noticed by other authors, there is an important contribution of woody elements and understory in the definition of different growth stages in front of photosynthetic elements (Verrelst et al. 2009, Asner, 1998, Blackburn & Steele, 1999, Rautiainen et al. 2008) and these elements are conspicuous during the dry season.

Nevertheless, the best kappa values have been observed at -55º, above a 75% at all vegetation classes and overall accuracy (Figures 3.8. and 3.9.). At extreme angles, CHRIS/PROBA data is related to other structural elements, such as tree height, which present larger differences between successional stages at CHRIS/PROBA's pixel size. It would be expected that height differences between successional stages were able to be observed as for -55º as for +55º. However, successional stages of TDF are better separated at -55º (Figures 3.8. and 3.9.) and intermediate and early stages of succession presented very weak kappa values at +55º (Figure 3.9.). This observation leads to the idea that it is not tree height, but shadows projected by trees which is making the spectral difference between successional stages. At -36º there are tree shadows, but at -55º these are larger. Thus, negative angles provide better spectral separation between successional stages of TDF, especially at extreme observations. These results are alike to those obtained by Chopping et al. 2006 in the discrimination of shrubs in drylands. Shadows projected by shrubs were a crucial parameter to distinguish from other vegetation classes, since classical Spectral Vegetation Indices (SVI) were unsuitable for identify them, especially the vegetation with small Leaf Area Index (LAI). Rautiainen et al. 2008 experienced similar results in the discrimination of hemiboreal forests of Estonia, where geometrical parameters of trees and spatial arrangement of canopies defined specific shadow patterns. These shadows helped in the discrimination of deciduous and coniferous forests at different stand ages using CHRIS/PROBA images, especially in off-nadir pointing.

On the other hand, our results do not match neither with results achieved by Galvao et al. 2009 in Brazilian rainforests nor for Liesenberg et al. 2009 in

Indonesian peat swamps. They observed that better results are achieved using multi-angular approach (+55º, +36º, 0º and -36º) in front of single-angle approach. Moreover, best results were achieved in positive angles, were ground targets are sunlit. The main differences between rainforests and tropical dry forests are two: rainforests are green during the whole year, and they do not present emergent trees above the upper canopy layer in late stage of succession. So forth, shadows projected by trees in rainforests are not as large as in dry forests, so this element of differentiation between successional stages of TDF is not valid for rainforests. On the other hand, structural and compositional elements of TDF that are observed during the dry season are not visible in rainforests, since they are covered by green leaves all over the year. This may lead to the idea that CHRIS/PROBA data shall be interpreted and managed in a different manner for discriminating successional stages in TDF than in rainforests. Furthermore, Liesenberg at al. 2009 found weak spectral separation of primary forests and dense re-growth, such as we found trouble in separating the three successional stages of TDF when using wet season's images alone. The green canopy is masking extra information about structural parameters and composition of the understory, hindering differences between successional stages (Figures 3.8. and 3.9.). Moreover, during the wet season, light and shadows behave different than during the dry season, since green leaves absorb more radiation and scatter light in a more complex way than tree trunks, introducing noise into the signal captured by CHRIS/PROBA sensor.

The third approach of the study was to evaluate the effect of seasonality in the classification. According to kappa results (Figures 3.8. and 3.9.), land cover maps generated with dry season's images perform practically the same kappa accuracies than those that used dry and wet season's images together. Low kappa values for wet season's images alone point out that they do not contribute much to the combination of dry+wet season's images into classification and the most important information is provided by dry season's images (Annex I and II). Nevertheless, land cover maps that used wet season's images presented high kappa values for riparian forests, for late stage of succession at negative and extreme angles when combining more than one angle, and for early stage of succession at angle combinations cited in table3.7. (Figure 3.9.). These observations suggest that the spatial distribution of riparian forests in humid areas and early stage in drier areas helps in the discrimination of these two classes respect to late stage of succession. In a similar manner, wet season's images can indirectly help in the classification of intermediate stage of succession as well. For the intermediate stage of succession, wet season's images perform weak kappa accuracy for all angle combinations. However, kappa values for dry+wet season's images are higher than for dry season's images

alone when using extreme angles, negative angles and 5 angles of observation in classification, coinciding with the highest kappa values for early stage of succession. The fact that early stage and riparian forests are better defined in the classification model by their distribution associated to soil humidity reduces confusion in the classification. This discernment lead to the affirmation that, although dry season's images spectrally separates the three successional stages of TDF and riparian forests because their differences in terms of structure and composition, wet season's images are crucial for a proper discrimination of four vegetation classes by the contribution of information about soil humidity.

To sum up, in this study we observed that the discrimination of successional stages of TDF and riparian forests depend on hyperspectral, multi-angular and multi-temporal data, related to differences in composition, structure, phenology and environmental parameters between the vegetation types under study, respectively. The hyperspectral component provided the ability to discriminate compositional elements in the understory, visible during the dry season, that distinguish the three successional stages. The early stage of succession presents an opener canopy, through which it is possible to observe a larger area of understory. It is usually formed by old pastures or bare soil. The understory in the intermediate stage of succession is formed by a dense layer of seedlings and small trees, so the predominant element in an intermediate forest is lignin, both in the understory and the canopy. The late stage of succession is characterized by a single canopy of tall trees, with some emergent trees. Thus, there are not seedlings in lower layers and during the dry season it is possible to see litter of falling leaves through canopy gaps (Kalacska et al., 2005a). The hyperspectral sensor is also decisive in the determination of species composition, expressed as different phenology states for TDF and riparian forest during the dry season, since riparian forests keep their leaves while TDF loses them all. In this sense, hyperspectrality is the base for the differentiation of the three successional stages of TDF and riparian forest. The multi-angularity, though, provides a sharper spectral discrimination by the projection of shadows by trees, which is an indirect measure of tree height (table 3.1.). Trees are taller in late stage of succession (up to 15m) and emergent trees up to 25m come out the main canopy layer (Table 3.1.). Trees are smaller in the early stage of succession, around 5m height. Moreover, shadows projected by trees produce a different optical effect, depending on the successional stage. Emergent trees and main canopy layer in late stage of succession produce a heterogeneous shadowing pattern on top of the canopy. Intermediate stage also project shadows on top of the canopy, but in a repeatable manner, since the canopy height is homogeneous. In the case of early stage, most of shadows are projected on the ground, which provokes a different texture that the one projected on top

of a canopy. These results are comparable to other studies with multi-angular satellites, such as MIRS, which noticed the contribution of structural elements of the forest in off-nadir angles and the role of understory and tree crowns in nadir angles in forests characterization (Heiskanen 2006, Kimes et al. 2006, Gobron et al. 2000). The temporal component is the final touch to the discrimination of vegetation types within the study area. As derived by the visual interpretation of PCs, dry season's images are providing information about structure and composition of the successional stages of TDF and riparian forests, while wet season's images are contributing with information about soil humidity. Environmental parameters play a key role in the distribution of vegetation, and particularly in the spatial distribution of riparian forests in front of dry forests. Moreover, early stage of succession is a less dense forest with an opener canopy, which facilitates the lost of soil water through direct sun exposition. Thus, early forests are located in drier soil areas.

The main goal of this study was to find out the best combination of CHRIS/PROBA images, in terms of angles of observation and season, to generate a land cover map that satisfy an adequate separation of the thee successional stages of tropical dry forests and riparian forest within the Parque Estadual de Mata-Seca. As derived from Figure 3.9., early and intermediate stages of succession present the lowest kappa values, in comparison to late stage and riparian forests. The selection of the best angle and season combination has been based on those maps that classified intermediate and early stages with a reasonable kappa accuracy, above 75% (Table 3.7.). The highest kappa scores for the four vegetation types have been reached by land cover maps that used more than one angle of observation, at negative or extreme angles, and used dry and wet season's images combined (Table 3.7.).

Contributions of spectrodirectional platforms in the characterization of tropical dry forests' succession

In this chapter, CHRIS/PROBA hyperspectral, multi-angular and multi-temporal components have been evaluated in the generation of land cover maps of tropical dry forest succession in Brazil. Several image combinations have been tested for vegetation classification, considering different angles of observation and seasons, in order to find out which combination provides the best accuracy, for the overall map and for each vegetation class.

Land cover map accuracy is not related to the number of images employed in classification, but the nature of these images. Best results have been observed in land cover maps that use negative and extreme angles of

observation. The use of nadir observation (0º) does not improve classification, and in certain cases, it lowers map accuracy. However, most of satellites do not offer a multi-angular component.

The three successional stages of TDF differ in structure and composition, permitting the spectral discrimination by CHRIS/PROBA sensor. Structural parameters such as canopy openness, tree density and tree thickness, and compositional elements such as woody elements and understory (litter, bare soil, old pastures) are distinguished by hyperspectral Proba sensor at nadir observation. However, the most significant land cover accuracies have been reported for negative and extreme angles of observation, suggesting that shadows projected by trees are providing more spectral differences to discriminate forest succession.

Although dry season's images provide better map accuracy in most of cases, some vegetation classes, such as riparian forests and early stage of succession are better characterized when using wet season's images in conjunction with dry season's images. Phenological Differences between TDF stages of succession and riparian forests are better characterized by the contrast of wet and dry season. Moreover, wet season's images are providing information about soil humidity, which typifies riparian and early stage's spatial distribution.

As a final remark, we can state that the discrimination of successional stages of TDF and riparian forests are subdued to hyperspectral, multi-angular and multi-temporal data, due to differences in composition, structure, phenology and environmental parameters related to the vegetation types under study. In future, the contributions of multi-angular pointing shall be considered in the design of new space missions.

ANNEX I. Use of input variables in decision trees for classification. Wet and dry season

WET SEASON		
	PC1	PC2
-55º	74	100
-36º	100	80
0º	100	80
+36º	100	80
+55º	100	80

	1st	Angle	2nd	Angle
	PC1	PC2	PC1	PC2
0º/-55º	38	100	100	56
0º/-36º	78	78	79	100
-36º/-55º	53	100	66	48
+36º/+55º	21	61	100	80
0º/+36º	59	64	100	80
0º/+55º	26	32	100	80
+36º/-36º	100	75	67	78
+55º/-55º	100	100	19	0

	1st	Angle	2nd	Angle	3rd	Angle
	PC1	PC2	PC1	PC2	PC1	PC2
0º/-36º/-55º	41	89	39	100	71	45
0º/+36º/+55º	25	31	17	55	100	80
0º/+36º/-36º	21	58	100	73	67	72
0º/+55º/-55º	3	26	100	100	29	0

	1st	Angle	2nd	Angle	3rd	Angle	4th	Angle	5th	Angle
	PC1	PC2	PC1	PC2	PC1	PC2	PC1	PC2	PC1	PC2
0º/+36º/-36º/+55º/-55º	0	0	2	60	0	35	100	100	17	1

DRY SEASON		
	PC1	PC2
-55º	100	80
-36º	100	100
0º	100	100
+36º	100	89
+55º	100	67

	1st	Angle	2nd	Angle
	PC1	PC2	PC1	PC2
0º/-55º	54	25	100	47
0º/-36º	30	38	100	100
-36º/-55º	60	32	100	66
+36º/+55º	55	43	100	66
0º/+36º	62	100	72	59
0º/+55º	62	36	100	64
+36º/-36º	18	27	100	80
+55º/-55º	58	65	100	80

	1st	Angle	2nd	Angle	3rd	Angle
	PC1	PC2	PC1	PC2	PC1	PC2
0º/-36º/-55º	18	23	60	26	100	63
0º/+36º/+55º	31	6	36	67	100	64
0º/+36º/-36º	32	26	13	32	100	80
0º/+55º/-55º	54	17	45	59	100	63

	1st	Angle	2nd	Angle	3rd	Angle	4th	Angle	5th	Angle
	PC1	PC2	PC1	PC2	PC1	PC2	PC1	PC2	PC1	PC2
0º/+36º/-36º/+55º/-55º	19	0	2	0	61	21	66	61	100	43

ANNEX II. Use of input variables in decision trees for classification. Wet+Dry seasons

	WET & DRY SEASON			
	Wet season		Dry season	
	PC1	PC2	PC1	PC2
-55º	4	0	100	100
-36º	20	58	100	80
0º	62	46	80	100
+36º	38	52	100	89
+55º	24	71	100	68

	Wet Season				Dry season			
	1st Angle		2nd Angle		1st Angle		2nd Angle	
	PC1	PC2	PC1	PC2	PC1	PC2	PC1	PC2
0º/-55º	0	50	0	0	0	0	100	100
0º/-36º	14	30	27	47	27	28	100	80
-36º/-55º	0	0	1	0	63	0	100	86
+36º/+55º	4	4	17	36	32	61	100	64
0º/+36º	24	26	52	49	41	100	55	22
0º/+55º	0	18	26	34	50	33	100	64
+36º/-36º	45	49	21	28	10	29	100	58
+55º/-55º	0	24	0	0	39	0	100	61

	Wet season						Dry season					
	1st Angle		2nd Angle		3rd Angle		1st Angle		2nd Angle		3rd Angle	
	PC1	PC2	PC1	PC2	PC1	PC2	PC1	PC2	PC1	PC2	PC1	PC2
0º/-36º/-55º	0	0	0	0	1	0	14	0	63	0	100	86
0º/+36º/+55º	0	0	1	2	19	35	34	4	3	56	100	64
0º/+36º/-36º	13	3	0	47	21	24	6	24	7	18	100	58
0º/+55º/-55º	0	24	0	0	0	0	0	0	39	0	100	61

	1st Angle		2nd Angle		3rd Angle		4th Angle		5th Angle	
	PC1	PC2	PC1	PC2	PC1	PC2	PC1	PC2	PC1	PC2
	Wet season									
0º/+36º/-36º/+55º/-55º	0	0	0	0	0	0	0	0	0	0
	Dry season									
0º/+36º/-36º/+55º/-55º	0	0	0	24	24	0	39	0	100	61

Chapter 4.

IMPLICATIONS OF INTERPRETING TROPICAL DRY FOREST SUCCESSION AFTER RADIOMETRIC CORRECTION OF CHRIS/ PROBA

Abstract

In the present chapter, we evaluate the effect of self-shadows in the classification of three successional stages of tropical forest in Mexico using hyperspectral and multiangular CHRIS/PROBA images. A simple algorithm based on the cosine of the angle formed between the normal to the terrain and the incident sunlight is applied to correct the effect of topography on CHRIS/PROBA's reflectance. Previous to the correction of topographic effects, CHRIS/PROBA images were atmospherically corrected in BEAM software. Vegetation maps of the study site were generated using non-parametric decisional trees, defining four main classes: late, intermediate and early stages of succession within a tropical dry forest, and riparian forests. By the comparison of resultant vegetation maps before and after the correction of topography in CHRIS/PROBA's spectral data, we found that late stage of succession and riparian forests are overestimated in non-corrected images while intermediate and early stages of succession are underestimated. Errors in classification are more important in extreme CHRIS/PROBA's angles of observation. Thus, the radiometric correction of topography is necessary for an accurate classification of succession in tropical dry forests.

Limitations for mapping forests in rugged areas

In the aim to understand global climate change, the precise estimation of the extent of secondary and primary forests is a key element to know the existing forest biomass, phenology dynamics and real forest capacity to sequester carbon (Eaton et al. 2007, Canadell et al. 2007). Remote sensing is the most suitable science to study forests worldwide, although it is not an easy task (Schaepman et al. 2004).

Satellite images need first to be atmospherically corrected, since the sensor is also capturing light from the atmosphere, located between the observed target on Earth's surface and the sensor, and the atmosphere itself modifies the beams through scattering and absortion. The incident sun light changes its physical behaviour when interacts with the atmosphere, both in its sun-Earth as in its Earth-sensor paths. The contribution of the atmosphere into the radiance that reaches the sensor is dependent on the position of the sensor respect to the sun, the position of the sun respect to the Earth (dependent on the day and the hour) and the atmospheric conditions at the moment of the image acquisition (e.g. presence of clouds, water vapour content and aerosol optical thickness) (Pons & Sola-Sugrañes, 1994). In rugged areas, there is an extra parameter to include in the described viewing geometry: topography.

Topography makes that light reaching a given object is reflected in a different direction than expected by the physic-chemical characteristics of the object itself and the angle of incident sunlight. At the sensor, the same object may present different values of radiance due to the topography, depending on the orientation of the slope respect to the sun and the sensor, driving to a wrong interpretation of the observed object. In shaded slopes, radiance values are apparently lower than the nominal observed target while objects in sunlit slopes present higher radiance values (Vicente-Serrano et al. 2008). Furthermore, some pixels can present higher radiance values because of the light reflected from adjacent slopes (Proy et al. 1989).

Generally, the correction of topographic effects is coupled with the correction of atmospheric radiance. Empirical models consider few parameters that are easy to retrieve (top-of-atmosphere radiance, solar azimuth and zenith angle, calibration parameters of the sensor) and are based on general assumptions about the sun-earth-sensor system (e.g. Lambertian scattering of light on forested canopies, homogeneous distribution of the atmosphere in layers). These methods are also called "simplified methods" (e.g., Dark Object Subtraction (DOS)-based methods

(Chavez, 1996), radiometric correction, (Pons & Sola-Sugrañes, 1994)). Physical models are much more complex and are based on in situ measurements at the moment of image acquisition. In the case of forests, they consider the structure of the canopy (e.g. tree height, tree density, shape of the crowns, canopy gaps, structure of the understory), composition of the observed targets (e.g. water content, photosynthetic pigments, non-photosynthetic components) and topographic parameters (digital elevation model and their derivates). They are also called "radiative transfer models" (e.g. SMAC (Rahman & Dedieu, 1994), 6S (Vermote et al., 1994), MODTRAN (Berk et al., 1999), and ATCOR (Richter, 1996).

Radiative transfer models require to be feed with ancillary data collected on field at the simultaneous overpass of the sensor, such as reflectance of different land covers (collected using a field spectrometer) or fraction of Active Photosynthetic Absorbed Radiation (fAPAR) within forests (collected using hemispherical photographs or LiCor spectrometers). In the case of studies focused on the estimation of the Bidirectional Reflectance Distribution Function (BRDF) or those which use multiangular satellite imagery, field reflectances of a given target are recorded in several angles of observation with goniometers. Some countries have coordinated research projects such as AERONET or FLUXNET which collect data about atmospheric conditions in a continuum that can be used to model atmospheric correction of satellite images. Some other research projects involve airborne campaigns to collect images simultaneously to satellite overpass so it is possible to separate forests reflectances from atmospheric contributions in the radiance captured by the satellite (e.g. MISR and AirMISR; CHRIS/PROBA and ROSIS).

Despite radiative transfer models are more realistic than simplified models, many times it is not possible to retrieve all the data they need due to the lack of technical and financial support, especially in developing countries. In other cases, such as in natural catastrophes studies, it is not able to coordinate field campaigns with the satellite overpass. Some other times, it is difficult to reach the study site to collect field data (e.g. dense tropical forests with no road access). In the particular case of forest, it would be necessary to collect data on top of the canopy, by means of eddy covariance towers or spectrometers on trails, which is much more complicated than retrieving data with portable equipment (e.g. LiCor, ASD, hemispherical cameras, goniometers), especially in canopies of up to 25 m height. In these cases, simplified methods for atmospheric and topographic correction are useful. Furthermore, some comparative studies concluded that simplified and radiative transfer models present similar accuracy errors (Pons & Sola-Sugrañes, 1994), due to certain assumptions and uncertainties

of the later (e.g. assumption of the Lambertian scattering, not well-defined shape of tree crowns, light scattering in edges and adjacent slopes, etc.) (Laurent et al. 2011b).

Some simplified models have been proposed to correct effects of topography in satellite images (Minnaert, 1941, Smith et al. 1980, Teillet et al. 1982, Gu & Gillespie, 1998, Civco, 1989, Pons & Sola-Sugrañes, 1994, Vincini et al. 2002, Chen et al. 2005b). They correct the overestimation of radiance in sun-exposed slopes and the underestimation in shaded slopes using the cosine of the angle between the solar incident angle and the surface normal (Vincini & Frazzi, 2003). These simplified methods have been extensively used to correct Landsat and sensors with similar spectral and spatial resolution (e.g. ASTER, SPOT). On the other hand, scarce literature has been reported about simplified methods for the correction topographic effects of hyperspectral sensors (Feng et al. 2003). To our knowledge, multi-angular pointing satellites (e.g. MISR, CHRIS/PROBA) have been always corrected with complex radiative transfer models that have been supported with field campaigns and airborne data (Kneubühler et al. 2005, Kuus et al. 2008, Chopping et al. 2012).

Most studies on tropical forests have focused in the Amazonas, which present flat terrain. However, other tropical biomes, such as tropical dry forests, are located in mountainous areas (i.e. Central-America or pre-Andean mountains). In these cases the correction of topographic effects becomes crucial, especially whether the scope of study relies in forest dynamics, such as forest succession (Vicente-Serrano et al. 2008, Song & Woodcock, 2003, Schroeder et al. 2006).

In the present chapter, we used a simplified algorithm proposed by Pons & Sola-Sugrañes in 1994 based on the cosine of the angle between the solar incident angle and the surface normal to correct topographic effects on CHRIS/PROBA imagery. We asses the effects of topography on the classification of three successional stages (late, intermediate and early) within a Mexican tropical dry forest as a function of five CHRIS/PROBA angles of observation (0º, ±36º and ±55º) and seasonality (dry and wet season).

A simplified algorithm for correcting the effects of topography in satellite images

a. Chamela- Cuixmala Biosphere Reserve

The Chamela- Cuixmala Biosphere Reserve is located on the coast of the State of Jalisco, with central coordinates 19º29'55" N, 105º02'39" W (Figure 4.1.). The reserve protects 13,142 ha of natural areas, mainly comprised of tropical dry forest, riparian forest and marshes (Sánchez-Azofeifa et al. 2009). The site has a mean annual temperature of 24ºC and an average annual rainfall of 919 mm. The altitude in the study site ranges between 0 and 500 m, with maximum slopes of 30º (Figure 4.2.). The reserve was initially designed as a protected area by the Biological Research Station of the Universidad Autonoma de Mexico, and afterwards was enlarged and administratively recognized by the federal government. The initial protected area is presumed to have been pristine for hundreds of years (Maass & Martinez-Yrizar 2001). The area protected in the second phase have been shaped by human activities like cattle ranching, slash and burn to open agricultural lands and selective timber extraction of fine woods (Lara and Taboada 1996).

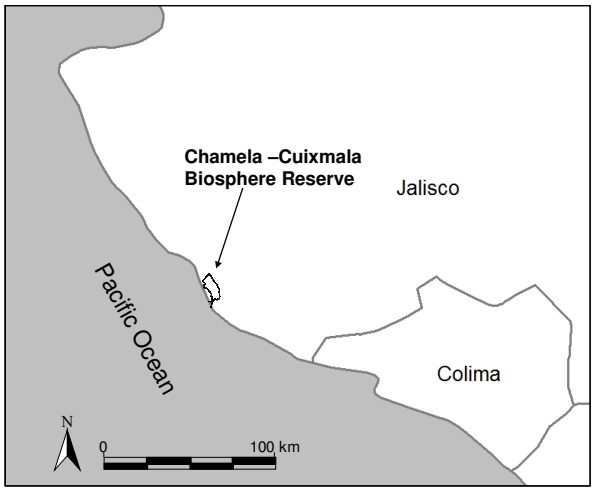

Figure 4.1. Chamela-Cuixmala Biosphere Reserve, Mexico

Three successional stages were identified within the study area: early, intermediate and late. Successional stages are defined in terms of structure and composition (Kalacska et al., 2004b) (Table 4.1.).

TABLE 4.1. Structure and composition parameters of three successional stages within Chamela's dry forest.

	Early stage	Intermediate stage	Late stage
# stems (0.1 ha)	65.7± 53.6	169.3± 44.3	200.7± 25.4
# species (0.1 ha)	9.3± 3.8	35.0± 3.0	40.0± 3.6
# families (0.1 ha)	5.0± 2.0	16.7± 0.6	19.0± 2.6
Averaged Height (m)	5.2± 1.8	11.8± 1.4	9.5± 0.3
Averaged Basal Area (m^2/ha)	15.7± 15.8	42.0 ± 29.9	36.2 ± 8.2
Dominant Family (%)	Leguminosae (83.8)	Leguminosae (31.7)	Leguminosae (47.2)
Dominant Species (%)	Acacia farnesiana (36.7)	Cnidosculus spinosus (12.4)	Apoplanesia paniculata (12.5)
HCI	11.8 ± 16.9	309.4 ± 219.5	284.4 ± 106.9

b. Image acquisition and pre-preprocessing

Mode-4 of CHRIS instrument was selected for this study. CHRIS/PROBA images were acquired for two dates, corresponding to the dry (31st March, 2006) and the wet season (30th October, 2010) (Figure 4.3.). Figure 4.3., demonstrates that the sun is in line with CHRIS/PROBA satellite at -36º, especially in October 2010 (wet season). That means that at -36º there was less shadow projection that in the rest of acquired scenes. In March 2006 (dry season), the sun was in between 0º and -36º (closer to 0º), producing a similar spectral behavior for both angles of observation, and larger shadows in off-nadir angles.

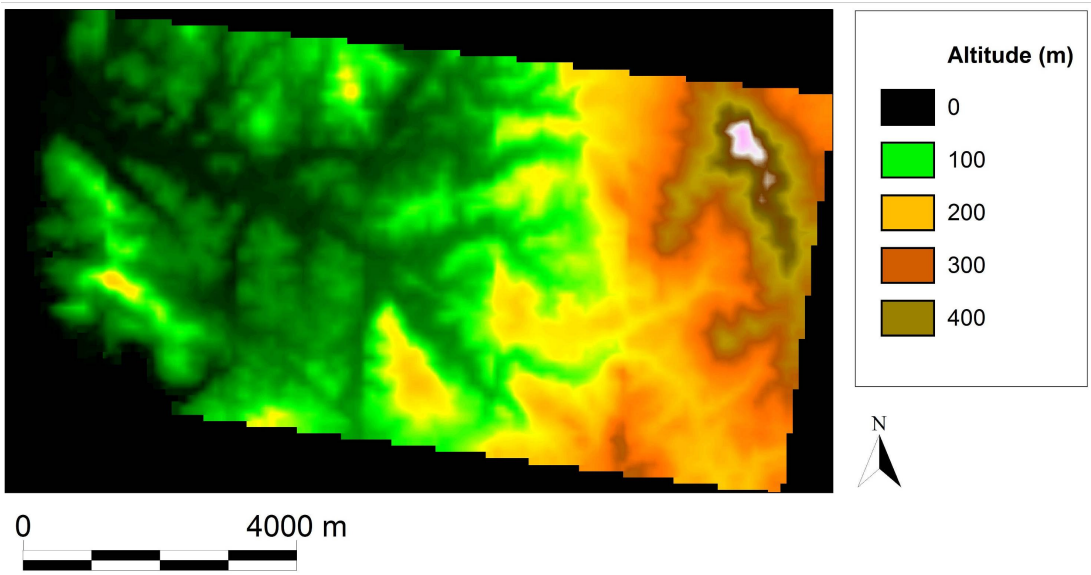

Figure 4.2. Digital Elevation Model (DEM) for the study site in Chamela, Mexico.

CHRIS/PROBA images are delivered in Top-of-Atmosphere (TOA) radiances (Level 1). In order to convert these values into reflectance (Level 2) we performed an atmospheric correction using BEAM 4.6.1. / Chris-Proba Tool-Box 4.7.1. (Kaufman and Sendra 1988, Gomez-Chova et al. 2006, 2008), an open-source toolbox developed by Brockmann-Consults and supported by the European Spatial Agency (ESA) (Alonso et al., 2009).

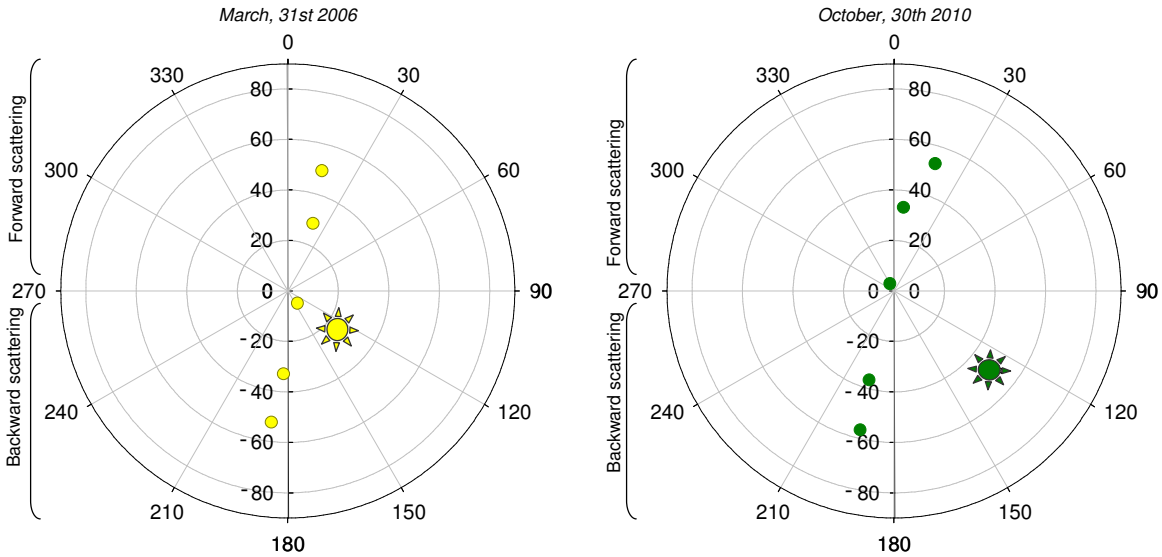

Figure 4.3. Geometry of the CHRIS/PROBA image acquisition

c. Radiometric correction

Most of correction models perform atmospheric and topographic correction in the same process, since both components are linked through the viewing geometry sun-Earth-sensor. Nevertheless, we consider BEAM's atmospheric correction as the most suitable for CHRIS/PROBA's case since it considers sensor's calibration parameters and AOT for the moment of acquisition. Unfortunately, BEAM does not consider the topographic factor, so we decided to correct it using a simplified algorithm based on the cosine of the angle of solar incidence on the terrain Pons & Sola-Sugrañes (1994).

Depending on the position of the sun and the sensor, in a rugged terrain the sensor will capture higher radiance of those slopes facing the sun and less radiance of those slopes with a different orientation (Pons & Sola-Sugrañes (1994). The effect of the topography is less evident in low sun and sensor zenith angles (Song & Woodcock, 2003). Topographic effects were corrected by dividing each pixel reflectance value by the absolute cosine of the incident angle (ρ), formed by the normal vector (N) respect to the maximum slope plane and the solar vector, for each pixel of the CHRIS/PROBA image (Fig. 3). The solar vector is dependent on the position of the sun at the date and hour the image was captured, which is defined by the solar elevation and azimuth. Topographic information was extracted from the ASTER digital elevation model (DEM) with a spatial resolution of 15m.

The algorithm is an adaptation of Pons & Sole-Sugrañes, (1994) (1) and was applied to every pixel of each CHRIS/PROBA image using Miramon software 7.x. (Pons, 2000).

$$\rho = \frac{\pi * [L - L_a] * d^2}{\cos\theta * E_0 * \tau_1 * \tau_2} \quad (1)$$

$$\tau_1 = e^{\left(\frac{-\tau_0}{\cos(s)}\right)} \quad (2)$$

$$\tau_2 = e^{\left(\frac{-\tau_0}{\cos(\nu)}\right)} \quad (3)$$

where:
ρ: Reflectance at ground level
E_0: Exoatmospheric solar irradiance ($W*m^{-2}$)

τ_1/ τ_2: Atmospheric transmittance coefficient through the path Sun-Earth / Earth-sensor

L_a: Radiance received by the sensor from an area where only atmospheric contribution exists (for example, shadows of water, depending on the spectral region, can provide an approximation)

L: Radiance at sensor level

θ: Incidence angle between the solar zenith and the normal vector of the terrain

d: Sun-Earth distance, in Astronomical Units

τ_0: Atmospheric optical depth.

s: Zenithal solar angle.

v: Angle between the normal vector of a plain terrain and the vector of the sensor vision.

d. Classification of forest types

In order to evaluate the effect of topography on CHRIS/PROBA's reflectance, we compared vegetation maps that were created using CHRIS/PROBA's images before and after radiometric correction. Four vegetation classes were identified in a supervised classification based on non-parametric decisional tree classification: late, intermediate and early stages of succession within the dry forest, and riparian forest. Non-forest classes were previously masked in CHRIS/PROBA's images in order to reduce spectral variability and enhance differences between targets of interest (e.g. roads, bare soil, water, marshes and crops). A total of 20 vegetation maps were created: one for each CHRIS/PROBA's angle of observation, for each season (dry and wet season) and before and after radiometric correction.

e. Comparing images before and after radiometric correction

Vegetation maps corresponding to a determined season and angle of observation (i.e. vegetation map generated using CHRIS/PROBA's image corresponding to the dry season at nadir pointing) were compared before and after radiometric correction by overlapping both maps. The resulting class' matches and errors of pixel-by-pixel comparison were recorded in a confusion matrix. These results were used to validate the radiometric correction we performed using kappa coefficient (Congalton, 1991). In opposition to other validation coefficients, such as Tau coefficient, kappa coefficient considers all marginal distributions of the confusion matrix, thus comprehending the errors of commission and omission and avoiding to consider those successes obtained by chance (Stehman, 1999).

Quantifying errors in classification of tropical dry forests' succession in rugged areas

Results from the comparison of vegetation maps before and after radiometric correction are evaluated with kappa coefficient for the late, intermediate and early stages of succession as a function of seasonality and CHRIS/PROBA's angle of observation (Figure 4.4.). The late stage of succession presents an opposite spectral behavior for the dry and the wet season, respect to the angle of observation (Figure 4.4.a.). For dry season's images, the highest kappa accuracy is reached in nadir observations (0º). The lower kappa values are observed in extreme angles, with the same magnitude at forward and backward angles. On the other hand, during the wet season, the highest accuracy is reached in extreme angles, while the lowest kappa values are observed in sunlit angles (0º and +36). Nevertheless, partial kappa values for late stage are under 0.4, both for dry and wet season.

In opposition to the observed for the late stage of succession, kappa accuracy before and after radiometric correction is independent of the season, for the intermediate (Fig. 4.b.) and early stages (Fig. 4.c.). Curves for the dry and wet season are parallel, although higher kappa values are observed for the wet season for both the intermediate and the early stages of succession. In both seasons and stages of succession, the highest kappa accuracies are observed for 0º in wet season and 0º and -36º in dry season. The lowest kappa values are reached for -55º and +36º in dry season, and +36º in the wet season. Kappa values for both intermediate and early stage are negative, in opposition to results observed for the late stage. Kappa values for the early stage are even lower (more negative) than for the intermediate stage.

The percentage of pixels that belong to the same vegetation class in both radiometrically-corrected and non-corrected maps are shown in Figure 4.5., for the three successional stages of tropical dry forest. Attention must be paid, since this percentage do neither considers the error of commission nor the error of omission, as kappa coefficient do. The percentage of matches for the late stage is higher for the dry (85-95%) than for the wet season (75-85%). In the dry season, positive angles present higher percentage of matching pixels than 0º and negative angles of observation. For the wet season, the highest percentage of matches is reached by -36º, while the lowest percentage is observed for 0º. In the case of intermediate stage, there

is a higher percentage of matches in the wet season (20-45%) than in the dry season (5-25%). In both seasons, the highest match is achieved in -36º and the lowest in -55º. For the early stage, the lowest percentage is observed for the dry season at 0º and the highest at ±55º. In the wet season, negative angles remain with a lower percentage of matching than 0º and positive angles.

Analyzing confusion matrices resulted of the comparison of vegetation maps before and after radiometric correction, we observed that the three stages of succession (late, intermediate and early) were wrongly classified as "late stage" when CHRIS/PROBA images were not radiometrically corrected previous to land cover classification. Figure 4.6. presents the percentage of pixels from intermediate or early stage that classified as "late stage" in maps generated with images that were not radiometrically corrected. For the intermediate stage, the percentage of wrong classification is higher for the dry season (50-95%) than the wet season (25-50%). In the dry season, the lowest percentage of error is observed at 0º, while the highest error is committed by -55º, followed by +36º. In the wet season, 0º and +36º present the highest percentage of error, closely followed by -55º. The lowest errors correspond to -55º and -36º. In the case of the early stage, the percentage of error varies between 10-70%. The error is higher in the wet season for negative angles and lower for 0º and positive angles. For the dry season, lower errors are observed in positive angles.

Besides the highest percentage of pixels of the intermediate stage is wrongly classified as "late stage" when using non-corrected CHRIS/PROBA images, a 25% of pixels are properly classified as "intermediate stage" in dry season's images at -36º and positive angles (Table 4.2.). At 0º, the percentage of pixels classified as "late stage" was smaller than for the rest of angles (50% in front of 70-90% in off-nadir angles, Figure 4.6.), but also it is wrongly classified as "riparian forest" in a 25% (Table 4.2.). Thus, the percentage of misclassification of intermediate forests in dry season's images is similar to the other angles of observation for the same season. In the wet season, around a 20-25% of pixels of the intermediate stage matches both maps using corrected and non-corrected CHRIS/PROBA images at -55º, 0º and +36º (Table 4.2.). On the other hand, intermediate stage is wrongly classified in non-corrected maps as "late stage" (35%) or "early stage" (25%) in -36º and +55º, respectively (Table 4.2.). According to spectral signatures during the wet season (Figure 4.7.), there is a small spectral difference between intermediate and late stages. Since both classes do not separate in the wet season, they cannot be properly classified. Then misclassification is assumed to be due both to topographic and phenological issues.

The early stage forest is classified as such both in corrected and non-corrected maps using dry season's images in around a 20-30% at negative angles (Table3). However, it is wrongly classified as "riparian forest" in non-corrected maps (around a 15-25%) in nadir and positive angles (Table 4.2.). In those maps generated with wet season's non-corrected images, the early stage is correctly classified in a 20% in 0º and positive angles, while it is wrongly classified as "riparian" or "intermediate stage" in negative angles, around a 15% (Table 4.2.). According to Figure 4.6. and table 4.2., we observe that in non-corrected images the early stage is classified only as "late stage" or as "early stage" in shaded angles (especially in the wet season), while there is confusion with several vegetation classes in sunlit angles (late stage, intermediate stage or riparian forest). It seems that when there is an important reduction of the reflectance because of topographic shadowing, reflectance in non-corrected CHRIS/PROBA images shifts to a spectral signature similar to late stage, so early stage's pixels classify only as late or as early stage. In the case the shadows are not very intense, the reduction of reflectance is weaker, so early stage can be classified as early, intermediate, late or riparian, introducing more confusion into the decisional tree of classification and reducing the probability of a pixel to be properly classified as "early stage" (Figure 4.7.).

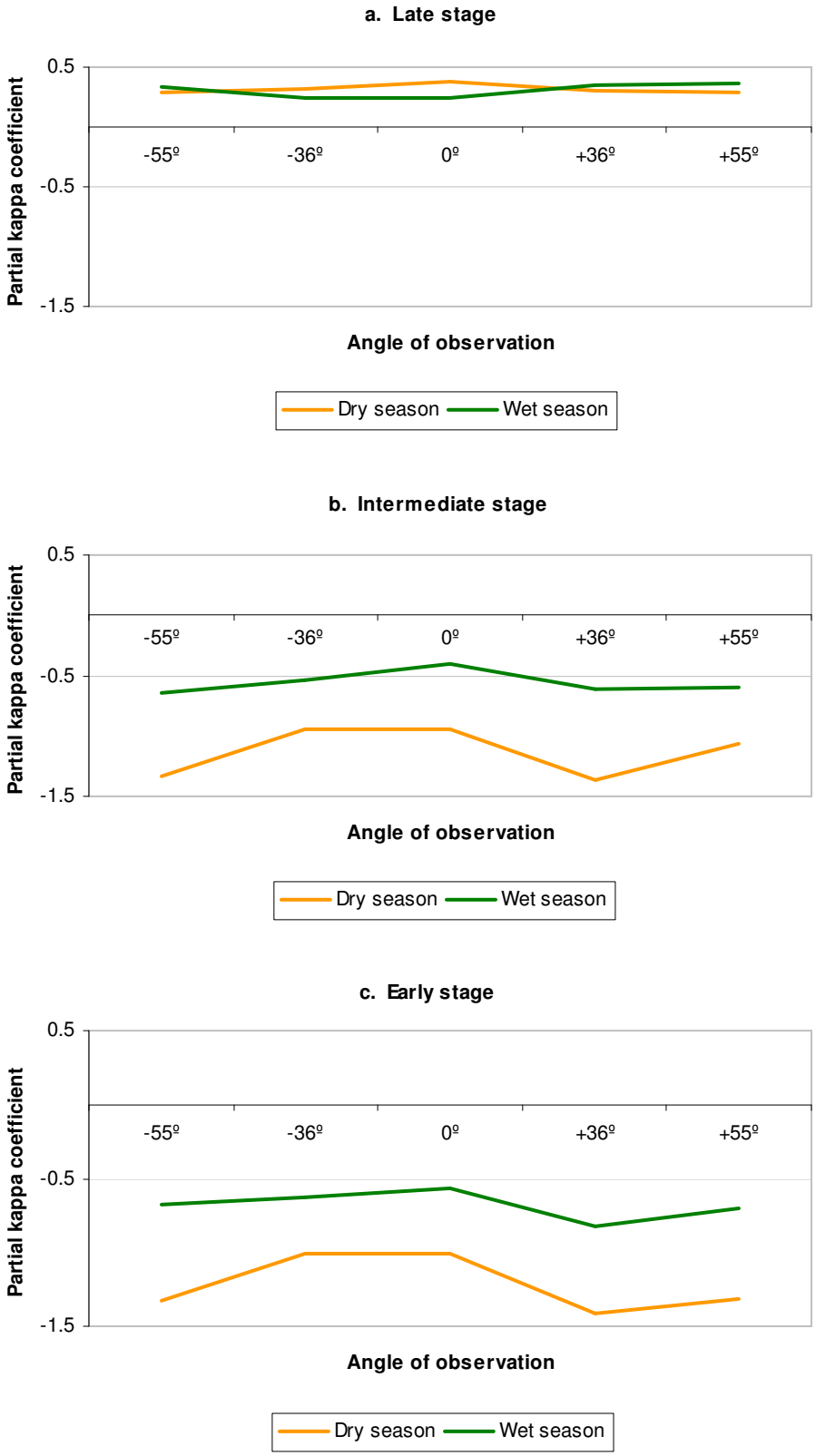

Figure 4.4. Kappa coefficient comparing vegetation maps based on CHRIS/PROBA images before and after radiometric correction for the late, intermediate and early stages of succession.

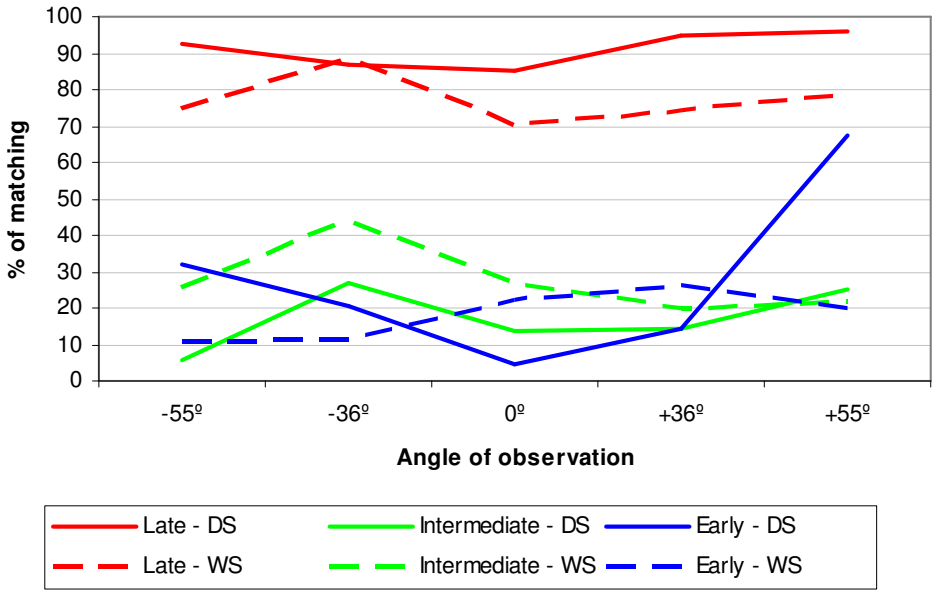

Figure 4.5. Percentage of pixels that belong to the same vegetation class before and after radiometric correction.

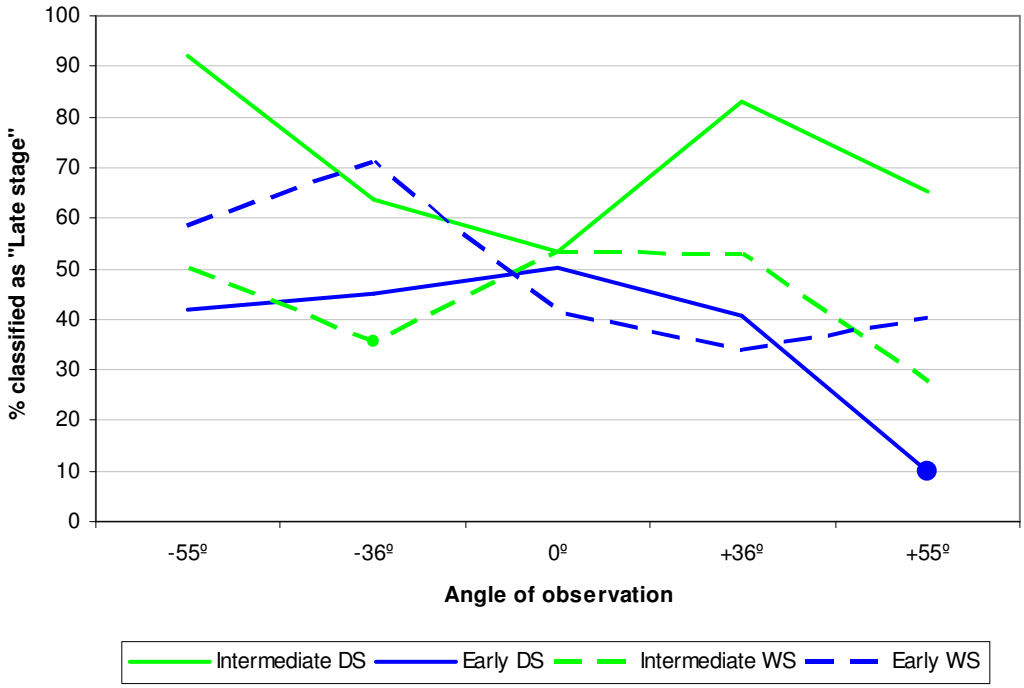

Figure 4.6. Percentage of pixels classified as “Late stage” for the three successional stages.

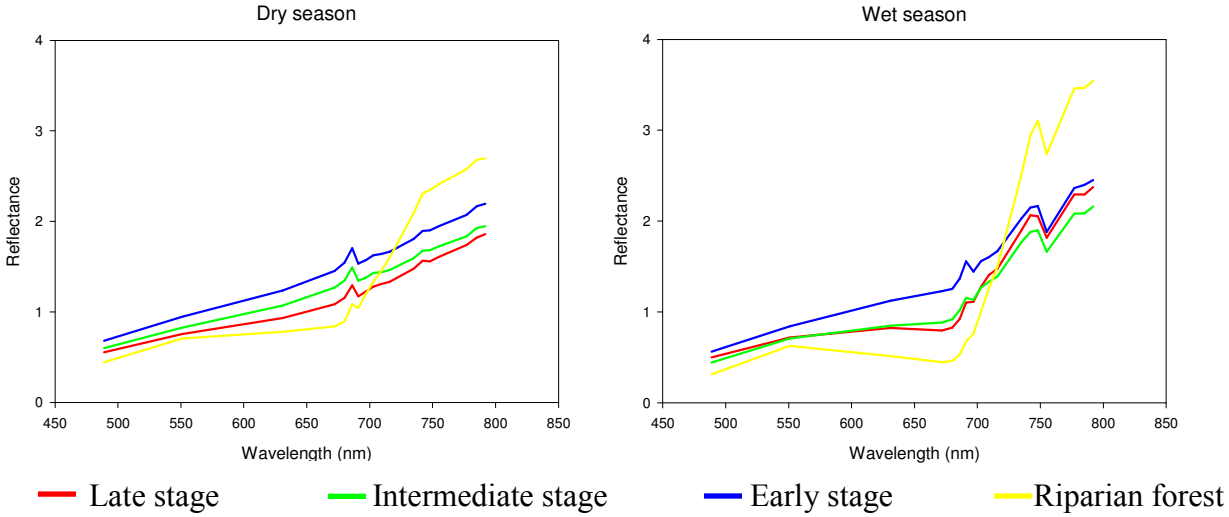

Figure 4.7. Spectral signature of vegetation types in Chamela-Cuixmala Biosphere Reserve for the dry season (left) and wet season (right)

TABLE 4.2. Confusion matrix resulted of the comparison vegetation maps generated with radiometrically-corrected and non-corrected CHRIS/PROBA images. Values are expressed in percentage. Only values above of 15% are displayed.

DRY SEASON	-55º		-36º		0º		+36º		+55º	
LATE	Late	92.4	Late	87.1	Late	85.1	Late	95.0	Late	95.7
INTERMEDIATE	Late	92.1	Late	63.5	Late	53.4	Late	82.9	Late	65.1
	-	-	Intermediate	27.0	Riparian	26.9	Intermediate	14.2	Intermediate	25.3
EARLY	Late	41.7	Late	44.9	Late	50.2	Late	40.6	Late	9.7
	Early	32.2	Early	20.4	Riparian	26.0	Riparian	25.5	Riparian	17.4

WET SEASON	-55º		-36º		0º		+36º		+55º	
LATE	Late	74.8	Late	88.8	Late	70.3	Late	74.0	Late	79.1
					Riparian	19.2	Riparian	19.3		
INTERMEDIATE	Late	50.1	Intermediate	44.1	Late	53.5	Late	53.2	Late	27.6
	Intermediate	25.5	Late	35.7	Intermediate	26.8	Intermediate	19.9	Early	25.5
EARLY	Late	58.3	Late	71.1	Late	41.6	Late	34.2	Late	40.2
	Riparian	15.0	Intermediate	15.1	Early	22.0	Early	26.2	Early	19.8

Implications of correcting topography for an accurate determination of tropical dry forests' succession

According to kappa coefficients (Figure 4.4.) and the percentage of coincident pixels (Figure 4.5.), the lack of radiometric correction of CHRIS/PROBA images leads to important errors in land cover classification (Vicente-Serrano et al. 2008, Kobashi & Sanga-Ngoie 2009, Zhang et al. 2011). Similar results were found in boreal forest succession (Song & Woodcock, 2003) and in Mediterranean forest succession after fire (Diaz-Delgado et al. 2003).

Errors in forest classification are dependent on the angle of observation and seasonality (Figures 4.4.-4.6., Table 4.2.). Topographic effects are minimized at small solar zenith angles (Song & Woodcock, 2003) and

sensor zenith angle. For this reason, a smaller error has been reported for nadir observation and higher inaccuracies have been observed for extreme angles of observation. Moreover, illumination conditions vary depending on the viewing geometry of the sun and the sensor, which is different from one image acquisition to another (Vicente-Serrano et al. 2008, Vincini & Frazzi, 2003). Thus, it is not only the differential phenology in dry and wet season that generates different errors in classification in non-corrected images, but also the position of the sun depending on the date of the year.

For our study case, the late stage of succession within the Mexican dry forest has a lower reflectance than intermediate stage, and the early stage a lower reflectance than the intermediate stage (Figure 4.7., left). This pattern is similar along TDFs in America and CHRIS/PROBA's angles of observation, as observed in chapter 2 of this thesis (Figure 2.4.). The reason of this pattern is that a higher solar radiance is absorbed in forests with higher biomass: the higher the number of stems, tree density and canopy layers (in late stage of succession), the lowest the reflectance (table 4.1). Riparian forest's reflectance is different to the dry forest because it keeps the leaves during the dry season: leaves are absorbing visible light for photosynthesis and reflecting in near-infrared range because of the water evapo-transpirated from trees. Shadows projected by topography in CHRIS/PROBA images generates a decrease in the reflectance of pixels in shaded slopes, shifting spectral signatures to vegetation classes with nominal lower reflectance values (i.e. late stage of dry forest or riparian forests). Moreover, shadows projection are larger in off-nadir angles of observation, therefore higher errors in classification are produced in extreme angles. Thus, radiometric correction is needed for the correct separation of spectral classes, which will allow the accurate selection of endmembers for map classification (Feng et al. in 2003).

The late stage of succession is the less affected by topography effects. The percentage of matches between corrected and non-corrected maps are very high for both seasons (Figure 4.5.). The results are slightly lower in the wet season, especially in those angles of observation with larger shadow projection. The error of omission is small in classifying late stage of succession using non-corrected CHRIS/PROBA images (Figure 4.5.). However, the error of commission is very high since intermediate and early stages of dry forest are classified as "late stage" when a radiometric correction is not performed (Figure 4.6.). For this reason the percentage of matches for late stage is very high (Figure 4.5.), but kappa value for this class in small (Figure 4.4.). The negative kappa values for intermediate and early stages indicate these classes are underestimated when using non-corrected images (Figure 4.4.) in the benefit of the late stage (Figure 4.6.).

Our results differ with the findings of Song & Woodcock in 2003, which reported that late stage of coniferous forests are more affected by topography than earlier stands.

The percentage of pixels that coincide in both radiometrically-corrected and non-corrected vegetation maps is remarkable smaller in the intermediate and early stages, if compared to the late stage (Figure 4.5.). The percentage of matches in the intermediate stage is higher in angles of observation with smaller shadow projection –0º in the dry season, -36º in the wet season– (Figure 4.5.) and in the early stage in wet season's images (0º). However, in dry season's images the early stage of succession is presents smaller error of classification in extreme angles of observation (Figure 4.5.), probably to random classification.

Most of studies about forest succession point out the negative effect of topography on forest characterization, but none of them estimated the percentage of error provoked by relief (Diaz-Delgado et al. 2003, Xu et al. 2009, Song et al., 2002, Lawrence & Ripple, 2000, Verrelst et al. 2008). Only Song & Woodcock, 2003 assessed several algorithms for topography correction in the accurate classification of successional stages of coniferous forest using Landsat ETM+. Some strategies to skip the effects of topography have been used, such as stratifying thematic classes into sunlit / shaded classes within a given class (Helmer et al., 2000, Thenkabail, 1999) or selected pixels only in flat areas within a mountainous region (Verrelst et al. 2008), but these solutions are partial.

Spectrodirectional sensing in front of topographic shadowing in tropical dry forests' succession mapping

The effects of topographic shadowing on the land cover classification of three successional stages of tropical dry forest were evaluated by comparing forest cover maps created using seasonal and multi-angular CHRIS/PROBA remote sensing data sets for a region in the Pacific coast of Mexico.

Important errors in tropical dry forest stage classification were observed when radiometric correction is lacking. In the case of late stage, the most important mistake is made on errors of commission, while intermediate and early stages are on errors of omission. In the classification, there is a transfer of pixels from intermediate and early stages to late stage, and in a smaller extent, to riparian forest. Shadows on scene provoke a spectral

reduction, motivating the spectral shift to vegetation types with smaller spectral signatures.

We observed more important errors in classification in those images with larger shadows on scene, coinciding with larger angle of observation respect to the normal to the sun.

Errors in wet season's images relate to smaller spectral differences between the three successional stages, making them more sensitive to changes in pixel shadowing. Differences between angles of observation, and thus between shadow projection, are more evident during the dry season because successional stages are better spectrally differentiated.

Chapter 5.

GENERAL CONCLUSIONS
(English version)

This research has been motivated by the need to improve our knowledge about tropical dry forests (TDFs) succession. Successional stages within TDFs have been little explored using remote sensing. Up to date, the spectral separation of three successional stages was achieved with the combined use of multispectral Landsat ETM+ and IKONOS imagery (Arroyo-Mora et al. 2005), and with multiangular MISR (Liesenberg et al. 2007). Succession has been also defined by its compositional and structural components; canopy height, above biomass and species diversity were correlated to spectral vegetation indices extracted from Hyperion images, which were at the same related to successional stages of TDFs (Kalacska et al. 2007a). However, Hyperion was not suitable for the estimation of stem or species density (Kalacska et al. 2007a). Airborne HYDICE hyperspectral images succeeded in the identification of tree and lianas species (Kalacska et al. 2007b), which can also be used for the discrimination of successional stages of TDFs.

This thesis contributes in the research on tropical dry forests' succession with the evaluation of the latest technology in optical remote sensing. CHRIS/PROBA's spectrodirectional data (combined multi-angular and hyperspectral data) has been explored for the analysis of biochemical and structural canopy properties of secondary tropical dry forests in the Americas. The main challenge in this dissertation was the generation of maps of succession for this biome, in order to support landscape management and studies on climate change.

Based on this dissertation the following overall conclusions can be reached:

- It is possible to spectrally separate three successional stages (late, intermediate and early) within the American tropical dry forest using CHRIS/PROBA data (Chapter 2 and 3).

- The patterns of reflectance for the three successional stages of TDFs are similar in three study sites along the Americas (Mexico, Nicaragua and Brazil) (Chapter 2). This observation consolidates that the definition of succession in terms of structure and species composition is valid for studies using remote sensing.

- The spectral separation of successional stages within TDFs is dependent on phenology traits. The dry season has been confirmed as the most suitable season for discriminating succession (Chapters 2 and 3).

- CHRIS/PROBA's hyperspectral component contributed in the estimation of biochemical traits of TDFs' succession, particularly non-photosynthetic elements within the forest (e.g. woody elements of the canopy: trees and lianas; understory composition: bare soil, litter, dry pasture, etc.) that can be observed during the dry season (Chapters 2 and 3).

- CHRIS/PROBA's multiangular component helps in the characterization of structural parameters of TDFs that define the three successional stages, such as Leaf area index (LAI) and tree height (chapters 2 and 3).

- The multiangular domain is decisive in the discrimination of TDFs' succession since a better spectral separation of the three proposed successional stages is better achieved at extreme angles (Chapters 2 and 3). Thus, it can be stated that multi-angular spectroscopy has the ability to capture forest information that can not be reached by single angular optical sensor.

- Non-parametric statistics help in the spectral separation of the three TDFs' successional stages defined for the study (Chapters 2 to 4).

- The proposed methodology for the spectral separation of successional stages of TDFs and classification is valid for different geographical areas (Chapters 2 and 3).

- Our findings in the spectral separation succession within TDFs at the plot level (chapter 2) have been successfully extrapolated to a landscape level by the generation of land cover maps (chapter 3).

- There is correlation between our results in the spectral analysis of CHRIS/PROBA data and classification statistics: the best spectral separation of TDF's succession and best land cover map accuracies are achieved with extreme angles or negative angles of observation (Chapters 2 and 3).

- Topography interferes in the correct spectral separation of the three successional stages of TDFs in rugged areas (Chapter 2 and 4).

- The higher CHRIS/PROBA's angle of observation, the higher the error in succession classification (Chapter 4).

- Early and intermediate stages of succession are underestimated by the effect of topography while late stage of succession is overestimated, whether topography is not corrected in CHRIS/PROBA images (chapter 4).

- It is feasible to correct the effect of topography in CHRIS/PROBA images using simplified methods, facilitating the use of these images to users with low financial and technical support. It also encourages the research on remote areas (Chapter 4).

As explained in the introduction (Chapter 1), PROBA-1 was an exploratory mission (Barnsley et al. 2004). During its eleven years of operation, important research has been conducted in several topics, and particularly in forestry and ecology (Chopping et al. 2008b, Rautianien et al. 2008, Galvao t al. 2008, Mottus et al. 2009, Liesenberg et al. 2009, Verrelst et al. 2009, 2010). CHRIS/PROBA has largely helped in the characterization of the Bidirectional Reflectance Distribution Function (BRDF) and forest traits and dynamics. These studies also enlightened about the limitations of the sensor and the platform, which is very valuable information for the design of future space missions. In the frame of the present thesis, we have identified certain limitations when working with CHRIS/PROBA:

- CHRIS/PROBA do not cover Short Infrared Wavelength (SWIR) wavelength, which is important for vegetation studies. Based in our observations of TDFs' succession reflectances (chapter 2), better spectral separation of successional stages is expected for (SWIR) both in dry and wet season, since their spectral signatures show higher separation in Near Infrared (NIR) bands. This is also supported by the fact that best spectral separation was experienced for the dry season, were non-photosynthetic elements are observed. Biochemical compounds in woody elements and litter present absorption peaks in the SWIR region (e.g. lignin, cellulose) (Fourty et al. 1996), which shall help in the discrimination of successional stages. Also bare soil and litter perform a differential reflectance in SWIR region, respect to vegetation, enhancing spectral separation of TDFs' succession. Furthermore, the assessment of woody element through proxy estimations of lignin or cellulose content will help in generation of aboveground biomass maps and in the characterization of biochemical cycles in forests.

- CHRIS/PROBA presents a swath width of 13 km, which is very limited for ecological research at a landscape scale. Moreover, one of

the main interests in simultaneous multi-angle observations is the characterization of BRDF of targets on Earth surface, for which it is required the co-registration and superposition of images corresponding to more than one angle of observation. In the case of CHRIS/PROBA's images, up to a 60% of the observed area coincides in five angles of observation, significantly reducing the area of interest.

- Satellite's pitch and roll for the acquisition of images with several viewing angles generates important perspective distortions of the land surface, especially in images with larger zenith angles. The accurate geometric correction and co-registration of CHRIS/PROBA images is very time consuming, which discourage to use them. For an easy use of CHRIS/PROBA images there shall be interfaces that perform semi-automatic corrections using nadir images as reference. The BEAM software (Alonso et al. 2009) overcame some of these pre-processing limitations by the application of an orbital parametric algorithm based on CHRIS/PROBA geometry of acquisition and telemetry data.

- Although we consider the BEAM software the most suitable interface for CHRIS/PROBA pre-processing (since it has been designed in consideration of the platform particularities), we found some limitations in the radiometric correction of topographic effects on surface reflectance. The software is able to orthorectify CHRIS/PROBA images using digital elevation models (DEM) of the study site, but geometric correction and surface relief is not considered in the process of converting Top-Of-Atmosphere (TOA) radiances into reflectances. For this reason, a simplified algorithm of correction had to be applied after BEAM's atmospheric correction (chapter 4).

PROBA-1 mission was intended to evaluate innovations on satellite features and operation in order to guide future operational missions (Barnsley et al. 2004). The most remarkable contributions of CHRIS/PROBA were its flexible spectral acquisition sets in different wavelength regions depending on the study scope (five modes of acquisition), hyperspectral data and multi-angular observations. In this frame, SPECTRA mission was proposed to follow on the line of CHRIS/PROBA overcoming some of the limitations exposed in previous paragraphs (Berger et al. 2001). SPECTRA proposed a swath width of 50 km, 50 m pixel size, seven angles of observation (0º, ± 30º, ± 50º, ± 60º), a spectral range comprising visible, VNIR and SWIR and a regular re-visit of

one week on scheduled study sites. Unfortunately, SPECTRA proposal was not accepted for the Earth Observation Envelope Programme (EOEP) of the European Space Agency (ESA) for the next decade. The conclusions of the present thesis encourage promoting operational missions in the line of CHRIS/PROBA and SPECTRA, since it has been largely proved the contributions of spectrodirectional data on the characterization and monitoring of forests worldwide, and particularly succession in tropical dry forests.

European Space Agency (ESA) agenda such as the Environmental Mapping and Analysis Program (EnMAP) and the Fluorescence Explorer mission (FLEX) will continue research based on spectrodirectional Earth Observation. EnMAP mission is scheduled to be launched on 2012 (Kaufman et al. 2008). Despite the success of putting hyperspectral sensors on orbit (EnMAP), it is very important to promote multiangular pointing platforms for future space missions. The Fluorescence Explorer mission (FLEX) plans to put in orbit a hyperspectral and multi-angular platform. This mission is currently a candidate of the Living Planet Program of the ESA (Guanter et al. 2010).

The results of this thesis opens new paths in the research of TDFs. Based in our findings, we expect to generate maps of aboveground biomass linked to successional stages that will be very useful for an accurate estimation of TDFs contribution to the carbon cycle and climate change. Among other projects, we also would like to generate maps of lithology using CHRIS/PROBA and link soil properties to the regeneration rate of TDFs after deforestation.

Capítulo 5.

CONCLUSIONES GENERALES
(Versión española)

La investigación llevada a cabo en el marco de esta tesis ha estado motivada por la necesidad de mejorar el conocimiento científico acerca de la sucesión en bosques tropicales secos (BTS). La literatura acerca de la sucesión del BTS mediante el uso de sensores remotos es escasa. Por el momento, se ha logrado la caracterización espectral de tres estados sucesionales (tardío, intermedio y temprano) mediante el uso combinado de imágenes multiespectrales Landsat ETM+ e imágenes hiperespaciales IKONOS (Arroyo-Mora et al. 2005) o mediante imágenes multiangulares MISR (Liesenberg et al. 2009). Por otro lado, los estados de sucesión se definen a partir de sus características estructurales y de composición; algunos de estos parámetros como la altura del canopy, la biomasa aérea y la diversidad de especies están correlacionadas con índices espectrales de vegetación calculados a partir de valores de reflectancia de Hyperion (Kalacska et al. 2007a). Sin embargo, las imágenes Hyperion no son adecuadas para la estimación de otros parámetros estructurales y composicionales que diferencian estados sucesionales entre sí, como son la densidad de especies y las densidad de árboles (Kalacska et al. 2007a). También imágenes de sensores aerotransportadas hiperespectrales HYDICE se utilizaron con éxito para la identificación de especies de lianas y árboles, lo que se podría utilizar para diferenciar entre estados sucesionales del BTS (Kalacska et al. 2007b).

Esta tesis ha contribuido al conocimiento de la sucesión de los BTS mediante la evaluación de tecnología punta en sensores remotos ópticos. La información espectrodireccional (información hiperespectral y multidireccional) del satélite CHRIS/PROBA se ha utilizado para analizar las propiedades bioquímicas y estructurales del canopy del bosque tropical seco secundario en América. Nuestra aportación ha consistido en la generación de mapas de sucesión de BTS que apoyarán la gestión de este bioma a nivel de paisaje y de estudios de cambio climático. En base a los estudios realizados en el marco de esta tesis, se puede concluir que:

- Es posible distinguir espectralmente tres estados sucesionales (tardío, intermedio y temprano) del bosque tropical seco americano utilizando la información proporcionada por las imágenes CHRIS/PROBA (capítulos 2 y 3).

- Los patrones de reflectancia de tres estados sucesionales de BTS son similares en tres zonas de estudio repartidas por el continente americano (México, Nicaragua y Brasil) (capítulo 2). Esta observación consolida que la definición de sucesión en términos de estructura y composición de especies es válida para estudios de teledetección.

- La separación espectral de estados sucesionales del BTS depende de la fenología del bosque. Los tres estados sucesionales del BTS se discriminan mejor espectralmente durante la época seca (capítulos 2 y 3).

- La componente hiperespectral de CHRIS/PROBA permite la estimación de parámetros bioquímicos de los estados sucesionales del BTS, especialmente de elementos no fotosintéticos del bosque (por ejemplo, materiales leñosos de la cubierta: árboles y lianas; composición del sotobosque: suelo desnudo, hojarasca, pasto seco, etc.) que se pueden observar durante la época seca (capítulos 2 y 3).

- La componente multiangular permite la caracterización de parámetros estructurales del BTS que definen los tres estados sucesionales, tales como el índice de área foliar (LAI) y la altura de los árboles (capítulos 2 y 3).

- La componente multiangular es decisiva en la discriminación de la sucesión del BTS, ya que se consigue una mejor separación espectral de los tres estados sucesionales en ángulos extremos (capítulos 2 y 3). Por tanto, se puede afirmar que la espectroscopía multiangular puede capturar información del bosque que no puede obtenerse con sensores ópticos mono-angulares.

- La estadística no paramétrica ayuda a la separación espectral de tres estados sucesionales del BTS definidos en este estudio (capítulos 2 al 4).

- La metodología propuesta para la separación espectral de los estados sucesionales del BTS y su clasificación es válida para zonas geográficas diferentes (capítulos 2 y 3).

- Nuestros resultados acerca de la separación espectral de los estados sucesionales del BTS a escala de parcela experimental (capítulo 2) se han extrapolado exitosamente a escala de paisaje a través de la generación de mapas de cobertura forestal (capítulo 3).

- Existe correlación entre los resultados acerca del análisis espectral de CHRIS/PROBA y las estadísticas de validación de los mapas de clasificación: la mejor separación espectral de la sucesión del BTS y los mapas de cobertura vegetal con mayor precisión se obtienen con ángulos de observación extremos o negativos (capítulos 2 y 3).

- La topografía interfiere en la correcta separación espectral de los tres estados sucesionales de BTS en zonas con relieve (capítulos 2 y 4).

- Cuanto mayor es el ángulo de observación de la imagen CHRIS/PROBA, mayor es el error en la clasificación de los estados sucesionales de BTS (capítulo 4).

- Los estados temprano e intermedio de sucesión son infraestimados debido al, mientras que el estado tardío se sobreestima, si no se corrige el efecto de la topografía en la reflectancia de las imágenes CHRIS/PROBA (capítulo 4).

- Es posible corregir el efecto de la topografía de las imágenes CHRIS/PROBA usando métodos simplificados, facilitando así el uso de estas imágenes por parte de usuarios con bajo presupuesto y soporte tecnológico. Estas técnicas también motiva la investigación en áreas remotas (capítulo 4).

Tal como se explicó en el capítulo de introducción, PROBA-1 fue una misión exploratoria (Barnsley et al. 2004). Durante sus once años en funcionamiento, se han llevado a cabo investigaciones en diferentes campos, entre otros, estudios forestales y ecológicos (Chopping et al. 2008b, Rautianien et al. 2008, Galvao t al. 2008, Mottus et al. 2009, Liesenberg et al. 2009, Verrelst et al. 2009, 2010). CHRIS/PROBA ha ayudado ampliamente en la caracterización de la Función Bidireccional de Distribución de la Reflectancia (BRDF) así como de las propiedades de los bosques y sus dinámicas ecológicas. Estos estudios también han puesto de manifiesto ciertas limitaciones del sensor y la plataforma espacial, información muy valiosa para el diseño de misiones espaciales venideras. En el marco de la presente tesis, hemos identificado ciertas limitaciones al trabajar con CHRIS/PROBA:

- CHRIS/PROBA no cubre la región del infrarrojo de onda corta (SWIR), a cual es importante en estudios de vegetación. En base a nuestras observaciones de las reflectancias de la sucesión del BTS (capítulo 2), es de esperar que se produzca una mejor separación espectral de los estados sucesionales en la región del infrarrojo corto (SWIR) tanto en la época seca como en la época de lluvias, ya que las firmas espectrales muestran mayor separación en las bandas del infrarrojo cercano (NIR). Esto también se ve respaldado por el hecho de que una mejor separación espectral se aprecia en las imágenes de la época seca, en las cuales se observan elementos no fotosintéticos.

Los compuestos bioquímicos presentes en elementos leñosos y la hojarasca muestran picos de absorción en la región del SWIR (por ejemplo, la lignina o la celulosa) (Fourty et al. 1996), pudiendo mejorar la discriminación de los estados sucesionales. También el suelo descubierto presenta una reflectancia en el rango del SWIR diferente a la de la vegetación, aumentando la separación espectral entre estados sucesionales del BTS. Además, la estimación indirecta de elementos leñosos a través de la determinación del contenido de lignina y celulosa puede ayudar a la generación de mapas de biomasa aérea y la caracterización de los ciclos bioquímicos de los bosques.

- CHRIS/PROBA presenta un swath de 13 km^2, la cuál es demasiado reducida para estudios ecológicos a escala de paisaje. Además, uno de los principales objetivos de la toma de imágenes con diferentes ángulos de observación de manera simultánea es la caracterización del BRDF de objetos sobre la superficie terrestre, para lo cual es necesario el co-registro y superposición de imágenes correspondientes a más de un ángulo de observación. En el caso de las imágenes CHRIS/PROBA, sólo un 60% como máximo de la superficie observada coincide en los cinco ángulos de observación, reduciendo significativamente el área de interés.

- El cabeceo y alabeo del satélite que se produce al adquirir las imágenes con diferentes ángulos de observación genera importantes deformaciones en la perspectiva de la superficie terrestre, especialmente en las imágenes con mayor ángulo zenital. Se necesita mucho tiempo para lograr una corrección geométrica y un co-registro de precisión, lo que desmotiva al usuario a utilizar imágenes Chris Proba. Para poder trabajar eficazmente con imágenes CHRIS/PROBA, son necesarios programas informáticos que realicen correcciones semi-automáticas tomando las imágenes de nadir como referencia. El software BEAM (Alonso et al. 2009) ha superado algunas de las limitaciones en la fase de pre-procesamiento mediante la aplicación de un algoritmo orbital paramétrico basado en la geometría de adquisición y la telemetría de CHRIS/PROBA en el momento de adquisición de las imágenes.

- Aunque consideramos que BEAM software es el programa informático más apropiado para pre-procesar las imágenes CHRIS/PROBA (ya que ha sido diseñado considerando las particularidades del satélite), encontramos ciertas limitaciones en la corrección radiométrica de la topografía. Dicho software permite ortorectificar las imágenes CHRIS/PROBA utilizando un modelo

digital de elevaciones (DEM) de la zona de estudio, pero no se tienen en cuenta ni la superficie del terreno ni la corrección geométrica en el proceso de convertir la radiación en la cubierta de la atmósfera (TOA) a reflectancia. Por esta razón, es necesario aplicar un algoritmo simplificado de corrección de la topografía después de la corrección atmosférica con BEAM (capítulo 4).

La misión espacial PROBA-1 tenía como propósito evaluar innovaciones en las prestaciones satelitales y en los modos de operación para guiar futuras misiones (Barnsley et al. 2004). Las innovaciones más significativas de CHRIS/PROBA han sido que es capaz de adquirir diferentes configuraciones espectrales en función del objeto de estudio (cinco modos de adquisición), ofrece bandas hiperespectrales y observaciones multiangulares. En este marco, se propuso la misión SPECTRA para poner en pie un satélite con las características principales de CHRIS/PROBA, pero que a su vez superaba algunas de las limitaciones que se han explicado en párrafos anteriores (Berger et al. 2001). Se pretendía que SPECTRA tuviera un swath de 50 km, un tamaño de píxel de 50m, siete ángulos de observación (0º, ± 30º, ± 50º, ± 60º) y un periodo de revista de una semana para zonas de estudio previamente programadas. Desafortunadamente, la propuesta de SPECTRA no fue aceptada para el Programa Conjunto de Observación de la Tierra (EOEP) de la Agencia Espacial Europea (ESA) para la próxima década. Las conclusiones de la presente tesis recomiendan la promoción de misiones operacionales en la línea de CHRIS/PROBA y SPECTRA, ya que han quedado ampliamente demostrada las aportaciones de la información espectrodireccional para la caracterización y monitoreo de los bosques a nivel global, y particularmente de la sucesión ecológica en los bosques tropicales secos.

La ESA tiene planificado continuar la observación de la Tierra con espectrómetros direccionales a través de ciertas misiones, como el Programa de Mapeo y Análisis Ambiental (EnMAP) y la misión de Exploración de la Fluorescencia (FLEX). El lanzamiento de EnMAP está programado para el año 2012 (Kaufmann et al. 2008). A pesar de que sea un éxito el lanzamiento de sensores hiperespectrales en órbita (EnMAP), es muy importante también promocionar plataformas de observación multiangular en misiones espaciales futuras. La misión FLEX planea poner en órbita una plataforma hiperespectral y multiangular. Esta misión es en la actualidad una candidata para el Programa del Planeta Vivo de la ESA (Guanter et al. 2010).

Los resultados de esta tesis abren nuevas líneas de investigación para los bosques tropicales secos. En base a nuestras averiguaciones, esperamos

poder generar mapas de biomasa aérea para diferentes estados sucesionales que serán de gran utilidad para una correcta estimación de la aportación de los BTS al ciclo del carbón y al cambio climático. Entre otros proyectos, también planeamos generar mapas litológicos con imágenes CHRIS/PROBA y vincular las propiedades del suelo con la tasa de regeneración del BTS después de un periodo de deforestación.

REFERENCES

Achard, F., H. D. Eva, H. J. Stibig, P. Mayaux, J. Gallego, T. Richards, And J. P. Malingreau. 2002. Determination of deforestation rates of the world's humid tropical forests. Science 297: 999–1002.

Alonso, L. and Moreno, J. (2004). Quasi-automatic geometric correction and related geometric issues in the exploitation of CHRIS/PROBA data. Proceedings of the 2nd CHRIS/PROBA Workshop, 21-23 March 2004, ESA/ESRIN, Frascati, Italy.

Alonso, L., Gomez-Chova, L., Moreno, J., Guanter, L., Brockmann, C., Fomferra, N., Quast, R.and Regner, P. (2009). CHRIS/PROBA toolbox for hyperspectral and multiangular data explotaitions. IEEE International Geoscience and Remote Sensing Symposium IGARSS, 1-5:453-456.

Alves, D. S., Soares, J. V., Amaral, S., Mello, E. M. K., Almeida, S. A. S., da Silva, O. F., and Silveira, A. M. (1997). Biomass of primary and secondary vegetation in Rondonia, Western Brazilian Amazon. Global Change Biology, 3:451–461.

Alves, R. (2008). Zonamento ambiental e os desafios da implementação do Parque Estadual Mata Seca, Municipio de Manga, Norte de Minas Gerais. Instituto de geociencias da Universidade Federal de Minas Gerais. Belo Horizonte, Brasil.

Arroyo-Mora, J.P., Sanchez-Azofeifa, G.A, Kalacska, M.E.R., Rivard, B., Calvo-Alvarado, J.C., Janzen, D.H. (2005). Secondary Forest Detection in a Neotropical Dry Forest Landscape Using Landsat 7 ETM+ and IKONOS Imagery. Biotropica 37:4, 497–507 doi:10.1111/j.1744-7429.2005.00068.x

Asner, G.P. and Warner, A.S. (2003). Canopy shadow in IKONOS satellite observations of tropical forests and savannas. Remote Sensing of Environment 87:4, 521-533.

Asner, G. P. (1998). Biophysical and biochemical sources of variability in canopy reflectance. Remote Sensing of Environment, 64, 234-253.

Asner, G.P., Braswell, B.H., Schmiel, D.S. and Wessman, C.A. (1998). Ecological research needs from multiangle remote sensing data. Remote Sensing of Environment, 63(2), 155-165.

Bachmann, C. M. T. F. D., Dubois, K., Fusina, R. A., Bettenhausen, M., Porter, J. H., Truitt, B. R. (2001). Automatic detection of an invasive plant species on a barrier island in the Virginia. Proceedings of IGARSS, Toronto, Canada, 2001.

Barducci, A., Guzzi, D., Marcoionni, P. and Pippi, I. (2009). Investigating the angular and spectral properties of natural targets using CHRIS-PROBA images of San Rossore test site',International Journal of Remote Sensing,30:3,533-553.

Barker-Schaaf, C., and A. H. Strahler, 1994: Validation of bidirectional and hemispherical reflectances from a geometricoptical model using ASAS imagery and pyranometer measurements of a spruce forest. Remote Sensing of Environment, 49, 138–151.

Barnsley, M.J., Settle, J.J., Cutter, M.A., Lobb, D.R., Teston, F., 2004. The PROBA/CHRIS mission: a low-cost smallsat for hyperspectral multiangle observations of the Earth surface and atmosphere. IEEE Transactions Geoscience and Remote Sensing, 42, 1512–1520.

Berger, M., Rast, M., Wursteisen, P., Attema, E., Moreno, J., Müller, A., Beisl, U., Richter, R., Schaepman, M., Strub, G., Stoll, M.P., Nerry, F., Leroy, M. (2001). The DAISEX Campaigns in Support of a Future Land-Surface-Processes Mission. ESA bulletin 105, February 2001.

Berk, A., Anderson, G. P., Bernstein, L. S., Acharya, P. K., Dothe, H., Matthew,M.W., Adler-Golden, S. M., Chetwynd, J. H., Richtsmeier, S. C., Pukall, B., Allred, C. L., Jeong, L. S., & Hoke, M. L. (1999). MODTRAN4 radiative transfer modeling for atmospheric correction. Proceedings of SPIE Optical Spectroscopic Techniques and Instrumentation for Atmospheric and Space Research III, Denver, Co, USA, 18 July 1999.

Bhattacharyya, A. (1943). On a measure of divergence between two statistical populations defined by their probability distributions Bulletin Calcutta Mathematics Society, vol. 35, no. 99-109, pp.4.

Blackburn, G. A., & Steele, C. M. (1999). Towards the remote sensing of matorral vegetation physiology: Relationships between spectral reflectance, pigment, and biophysical characteristics of semiarid bushland canopies. Remote Sensing of Environment, 70, 278-292.

Boardman, J. W., Kruse, F. A., and Green, R. O. (1995). Mapping target signatures via partial unmixing of AVIRIS data: in Summaries, Fifth JPL Airborne Earth Science Workshop, JPL Publication 95-1, vol. 1, p. 23-26.

Braswell, B.H., Hagen, S.C., Frolking, S.E., Salas W.A. (2003). A multivariable approach for mapping sub-pixel land cover distributions using MISR and MODIS: Application in the Brazilian Amazon region. Remote Sensing of Environment. Vol. 87, No. 2-3, pp. 243-256.

Brondizio, E., Moran, E., Mausel, P., and Wu, Y., 1996, Land cover in the Amazon Estuary: linking of the Thematic Mapper with botanical and historical data. Photogrammetric Engineering and Remote Sensing, 62, 921–929.

Brown, S. A., Hall, C. A. S., Knabe, W., Raich, J., Trexler, M. C., and Woomer, P. (1993). Tropical forests: their past present and potential future role in the terrestrial carbon budget, Water Air Soil Pollution, 70, 71-94.

Calvo-Alvarado, J., McLennan, B., Sanchez-Azofeifa, G.A., Garvin, T. 2009. Deforestation and forest restoration in Guanacaste, Costa Rica: Putting conservation policies in context. Forest Ecology and Management. 258, 931–940

Canadell, J.G., Le Quere, C., Raupach, M.R., Field, C.B., Buitenhuis, E.T., Ciais, P., Conway, T.J., Gillett, N.P., Houghton, R.A., Marland, G. (2007). Contributions to accelerating atmospheric CO2 growth from economic activity, carbon intensity, and efficiency of natural sinks. Proceedings of the National Academy of Sciences,104, 18866–18870.

Castillo, A., Godinez, C., Schroeder, N., Galicia, C., Pujadas-Botey, A., Hernandez, L.M. 2009. The dry tropical forest at risk: conflicts between agricultural and cattle use, tourism development, and provision of ecosystemic services in the coast of Jalisco, Mexico. Interciencia, 34:12, 844-850.

Castro, K. L., Sanchez-Azofeifa, G. A. and Rivard, B. (2003). Monitoring secondary tropical forests using space-borne data: implications for Central America. International Journal of Remote Sensing, 24:9, 1853 – 1894

Castro-Esau, K.L., Sánchez-Azofeifa, G.A., Rivard, B. (2006). Comparison of spectral indices obtained using multiple spectroradiometers. Remote Sensing of Environment, 103, 276–288.

Castro-Esau, K.L., Sanchez-Azofeifa, G.A., and Caelli, T. (2004). Discrimination of lianas and trees with leaf-level hyperspectral data. Remote Sensing of Environment, 90, 353–372

Chavez, P. S. (1996). Image-based atmospheric corrections-revisited and improved. Photogrammetric Engineering and Remote Sensing, 62, 1025-1036.

Chazdon, R.L., Denslow, J., (2002). Floristic composition and species richness. In: Chazdon, R.L., Whitmore, T.C. (Eds.), Foundations of Tropical Forest Biology. Classic Papers with Commentaries, University of Chicago Press, Chicago, IL, pp. 513–522.

Chen, J.M., Menges, C.H., Leblanc, S.G. (2005a). Global mapping of foliage clumping index using multi-angular satellite data. Remote Sensing of Environment, 97:4, 447-457.

Chen, X., Vierling, L., & Deering, D. (2005b). A simple and effective radiometric correction method to improve landscape change detection across sensors and across time. Remote Sensing of Environment, 98, 63-79.

Chen, J.M., Li, X., Nilson, T., and Strahler, A. (2000). Recent advances in geometrical optical modelling and its applications. Remote Sensing Reviews. Vol. 18. pp. 227 – 262.

Chen, J. M., and Cihlar, J. (1995), Plant canopy gap-size analysis theory for improving optical measurements of leaf area index. Applied Optics, 34, 6211–6220.

Chopping, M., North, M., Chen, J., Schaaf, C.B., Blair, J.B., Martonchik, and Michael, J.V., and Bull, A. (2012). Forest Canopy Cover and Height From MISR in Topographically Complex Southwestern US Landscapes Assessed With High Quality Reference Data. IEEE Journal of Selected Topics in Applied Earth Observations and Remote Sensing, 5(1), February 2012.

Chopping, M., Nolin, A., Moisen, G.G., Martochnick, J.V. and Bull, M. (2009). Forest canopy height from the Multiangle Imaging SpectroRadiometer (MIRS) assessed with high resolution discrete return lidar. Remote Sensing of Environment, 113, 2172-2185.

Chopping, M., Moisen, G.G., Su, L., Laliberte, A., Rango, A., Martochnick, J.V., and Peters, D.P.C. (2008a). Large area mapping of

southwestern forest crown cover, canopy height and biomass using the NASA Multiangle Imaging SpectroRadiometer. Remote Sensing of Environment, 112, 2051-2063.

Chopping, M., Su L., Laliberte, A., Rango A., Peters, D.P.C., Kollikkathara, N. (2008b). Mapping shrub abundance in desert grasslands using geometric-optical modeling and multi-angle remote sensing with CHRIS/PROBA. Remote Sensing of Environment 104, 62–73.

Chopping, M., Su, L., Laliberte, A., Rango, A., and Peters, D.P.C. and Kollikkathara, N. (2006). Mapping shrub abundance in desert grasslands using geometric-optical modelling and multi-angle remote sensing with CHRIS/PROBA. Remote Sensing of Environment, 104, 62-73.

Chopping, M. J., Rango, A., Havstad, K.M., Schiebe, F.R., Ritchie, J.C., Schmugge, T.J., French, A. N., Su, L., McKee, L., Davis, M.R. (2003). Canopy attributes of desert grassland and transition communities derived from multiangular airborne imagery. Remote Sensing of Environment 85, 339–354.

Cincotta, R.P., Wisnewski, J., Engelman, R. (2000). Human population in the biodiversity hotspots. Nature 404, 990–992.

Civco, D. L. (1989). Topographic normalization of Landsat Thematic Mapper digital imagery. Photogrammetric Engineering & Remote Sensing, 55, 1303-1309.

Clark, M., Roberts D.A., Clark, D.B. (2005). Hyperspectral discrimination of tropical rain forest tree species at leaf to crown scales. Remote Sensing of Environment. 96:375–398. doi:10.1016/j.rse.2005.03.009

Cochrane, M.A. (2000) Using vegetation reflectance variability for species level classification of hyperspectral data. International Journal of Remote Sensing 21, 2075–2087. doi:10.1080/01431160050021303

Congalton, R. G. (1991). A review of assessing the accuracy of classifications of remotely sensed data. Remote Sensing of Environment, 37, 35-46

Congalton R. G., Oderwald, R. G., and Mead, R. A. (1983). Assessing Landsat classification accuracy using discrete multivariate analysis statistical techniques. Photogrammetric Engineering and Remote Sensing, 49, 1671-1678. 1983.

Cross, A. M., Settle, J. J., Drake, N. A, Paivinen R.T.M. (1991). Subpixel measurement of tropical forest cover using AVHRR data. International Journal of Remote Sensing, 12:5, 1119-1129.

Curran, P. J. (1994). Imaging spectrometry. Progress in Physical Geography, 18(2), 247– 266.

Cutter, M. & Sweeting, M. A. (2007). Hyperspectral imaging mission for small satellites – five years orbit experience. Proceedings of the IEEE. 2007. I – 4244 – 1057 – 6/07.

Dennison, P. E. and Roberts, D. A. (2004). Examining Seasonal Changes in Canopy Moisture Using AVIRIS Time Series Data. Remote Sensing of Environment, 93: 3, 359-367.

Díaz-Delgado, R., Lloret, F., & Pons, X. (2003). Influence of fire severity on plant regeneration by means of remote sensing imagery. International Journal of Remote Sensing, 24, 1751-1763.

Diner, D.J., Asner, G.P., Davies, R., Knyazikhin, Y., Muller, J.P., Nolin, A.W., Pinty B, Schaaf C.B., Stroeve J. (1999). New directions in earth observing: Scientific applications of multiangle remote sensing. Bulletin of the American Meteorological Society, 80:11, 2209-2228.

Dixon, R. K., Brown, S., Houghton, R. A., Solomom A. M., Trexler, M. C., and Wisniewski, J. (1994). Carbon pools and flux of global forest ecosystems, Science, 263:185-190.

Duca, R. and Del Frate, R. (2008). Hyperspectral and Multiangle CHRIS–PROBA Images for the Generation of Land Cover Maps. IEEE Transactions on Geoscience and Remote Sensing,. 46:10, 2857.

Dyk, A., Goodenough, D.G., Li, J.Y., Niemann, K.O., Guan, A., Chen, H. and Duong, J. (2006). Multi-Temporal, Multi-Angle Evaluation with CHRIS of Coastal Forests. IEEE International Geoscience and Remote Sensing Symposium (IGARSS). Denver (USA).

Eaton, J. M., Lawrence, D. (2009). Loss of carbon sequestration potential after several decades of shifting cultivation in the Southern Yucatan. Forest Ecology and Management 258, 949–958.

Eva, H.D., Belward, A.S., De Miranda, E.E., Di Bella, C.M., Gond, V., Huber, O., Jones, S., Sgrenzaroli, M., Fritz, S. (2004). A land cover map of South America. Global Change Biology, 10:5, 731–744.

Ewel, J.J. (1999). Natural systems as models for the design of sustainable systems of land use. Agroforestry Systems 45, 1–21.

Fahsi, A., Tsegaye, T. and Coleman, T. (2000). Incorporation of digital elevation models with Landsat-TM data to improve land cover classification accuracy. Forest Ecology Management. 128: 57-64.

Fajardo, L., González, V., Nassar, J., Lacabana, P., Portillo, Q., Carrasquel, F., Rodríguez, J.P. (2005). Tropical dry forests of Venezuela: characterization and current conservation status. Biotropica 37:4, 531–546.

Fearnside, P. M., and Guimaraes, W. M. (1996). Carbon uptake by secondary forests in Brazilian Amazonia. Forest Ecology and Management, 80, 35–46.

Feeley, K.J., Gillespie, T. W. and Terborgh, J.W. (2005). The Utility of Spectral Indices from Landsat ETM+ for Measuring the Structure and Composition of Tropical Dry Forests. Biotropica, 37:4, 508–519.

Feng, J., Rivard, B., Sanchez-Azofeifa, A. (2003). The topographic normalization of hyperspectral data: implications for the selection of spectral end members and lithologic mapping. Remote Sensing of Environment, 85, 221–231

Fisher, Ronald A. (1918). The Correlation between Relatives on the Supposition of Mendelian Inheritance. Philosophical Transactions of the Royal Society of Edinburgh, 52, 399–433.

Foody, G. M. (2003). Remote sensing of tropical forest environments: towards the monitoring of environmental resources for sustainable development. International Journal of Remote Sensing, 24: 20, 4035 – 4046.

Foody, G.M., D. S. Boyd, and M. E. J. Cutter. (2003). Predictive relations of tropical forest biomass from Landsat TM data and their transferability between regions. Remote Sensing Environment, 85: 463–474.

Foody, G.M., Palunbiskas, G., Lucas, R.M., Curran, P.J., Honzak, M. (1996). Identifying terrestrial carbon sinks: classification of successional

stages in regenerating tropical forest from Landsat TM data. Remote Sensing of Environment, 55, 205–216.

Foody, G. M., and Curran, P. J. (1994). The use of remote sensing to characterise the regenerative states of tropical forests. In Environmental Remote Sensing from Regional to Global Scales, edited by G. M. Foody and P. J. Curran (Chichester: John Wiley), pp. 44–83.

Fourty, Th., Baret, F., Jacquemoud, S., Schmuck, G., & Verdebout, J. (1996). Leaf optical properties with explicit description of its biochemical composition: direct and inverse problems. Remote Sensing of Environment, 56, 104– 117.

Friedman, Milton. (1940). A comparison of alternative tests of significance for the problem of m rankings. The Annuals of Mathematical Statistics 11 (1): 86–92. (March 1940).

Galvao, L. S., Ponzoni, F. J., Liesenberg, V., Santos, J. R. (2009). Possibilities of discriminating tropical secondary succession in Amazonia using hyperspectral and multiangular CHRIS/PROBA data. International Journal of Applied Earth Observation and Geoinformation 11, 8–14.

Gamon, J. A., Kitajima, K., Mulkey, S. S., Serrano, L. and Wright, S. J. (2005). Diverse Optical and Photosynthetic Properties in a Neotropical Dry Forest during the Dry Season: Implications for Remote Estimation of Photosynthesis. Biotropica, 37, 547–560. doi: 10.1111/j.1744-7429.2005.00072.x

Gao, B. C., and Goetz, A. F. H. (1994), Extraction of dry leaf spectral features from reflectance spectra of green. Remote Sensing of Environment, 47:3, 369–374.

Gastellu-Etchegorry, J. P., Zagolski, F., Marty, G., and Giordano, G. (1995). An assessment of canopy chemistry with AVIRIS: A case study in the Landes Forest, South West France. International Journal of Remote Sensing, 16:3, 487–501.

Gedney, N. & Valdes, P.J. (2000). The effect of Amazonian deforestation on the northern hemisphere circulation and climate. Geophysical Research Letters, 27:19.

Gentry, A. (1995). Diversity and floristic composition of Neotropical dry forests. In: Bullock, S.H., Mooney, H.A., Medina, E. (Eds.), Seasonally

Dry Tropical Forests. Cambridge University Press, Cambridge, pp. 146–194.

Gentry, A.H. (1982). Neotropical floristic diversity: phytographical connections between Central and South America, Pleistocene climatic fluctuations, or an accident of the Andean orogeny? Annual Missouri Botanical Garden 69, 557–593.

Gerard, F. F., & North, P. R. J. (1997). Analyzing the effect of structural variability and canopy gaps on forest BRDF using a geometric-optical model. Remote Sensing of Environment, 62, 46-62.

Gillespie, T. W., Zutta, B. R., Early, M. K. and Saatchi, S. (2006). Predicting and quantifying the structure of tropical dry forests in South Florida and the Neotropics using spaceborne imagery. Global Ecology and Biogeography, 15: 225–236. doi: 10.1111/j.1466-8238.2005.00203.x

Gillespie, T. W., Brock, J. and Wright, C. W. (2004). Prospects for quantifying structure, floristic composition and species richness of tropical forests, International Journal of Remote Sensing, 25:4, 707-715.

Gillespie, T.W. (1999). Life history characteristics and rarity of wood plants in tropical dry forest fragments of Central America. Journal of Tropical Ecology 15, 637–649.

Gobron, N., Pinty, B., Verstraete, M.M., Martonchik, J.V., Knyazikhin, Y. and Diner, D.J. (2000). Potential of multiangular spectral measurements to characterize land surfaces: Conceptual approach and exploratory application. Journal of Geophysical Research, 105:D13, 17 539-17 549.

Goel, N. S. (1988). Models of vegetation canopy reflectance and their use in estimation of biophysical parameters from reflectance data. Remote Sensing Reviews, 4:1–212.

Gómez-Chova L., Alonso L., Guanter L., Camps-Valls G., Calpe J. and Moreno J. (2008). Correction of systematic spatial noise in push-broom hyperspectral sensors: application to CHRIS/PROBA images. Applied Optics, 47, 28.

Gomez-Chova, L., Camps-Valls, G., Amoros-Lopez, J., Calpe, J., Guanter, L., Alonso, L., Fortes, J.C., Moreno, J. (2006). Cloud Probability mask for Proba / Chris Hyperspectral images. IEEE International Geoscience and Remote Sensing Symposium (IGARSS). Denver (USA).

Gomez-Chova, L., Amoros, J., Camps-Valls, G., Martín, J.D., Calpe, J., Alonso, L., Guanter, L., Fortes, J.C., Moreno, J.F. (2005). Cloud Detection for CHRIS/PROBA Hyperspectral images. Proceedings of the SPIE Remote Sensing. 19-22 September 2005, Bruges (Belgium).

Goodin, D. G., Gao, J., and Henebry, G.M. (2004). The effect of solar illumination angle and sensor view angle on observed patterns of spatial structure in tallgrass prairie. IEEE Transactions on Geoscience and Remote Sensing, 42:1.

Grace, J., Lloyd, J., Mcintyre, J., Miranda, A. C., Meir, P., Miranda, H. S., Meir, P., Miranda, H., Moncrieff, J., Massheder, J., Wright, I., Gash, J. (1995). Carbon-dioxide uptake by an undisturbed tropical rain-forest in southwest Amazonia, 1992 to 1993. Science, 270, 778– 780.

Grace, J., Malhi, Y. Lloyd, J. (1996). The use of eddy covariance to infer the net carbon dioxide uptake of Brazilian rain forest. Global Change Biology, 2:3, 209 – 217.

Green, R. O., Eastwood, M. L., Sarture, C. M., Chrien, T. G., Aronsson, M., Chippendale, B. J., Faust, J.A., Pavri, B .E., Chovit, C.J., Solis, M., Olah, M.R. and Williams, O. (1998). Imaging spectroscopy and the Airborne Visible/Infrared Imaging Spectrometer (AVIRIS). Remote Sensing of Environment, 65, 227–248.

Green, K. M. (1983). Using Landsat to monitor tropical forest ecosystems realistic expectations of digital processing technology. Sutton, S. L., T. C. Whitmore and A. C. Chadwick (Ed.). British Ecological Society Special Publications Series, Vol.2. Tropical Rain Forest: Ecology And Management. Blackwell Scientific Publications: Palo Alto, California, USA, pp. 397-410.

Gu, D., & Gillespie, A. (1998). Topographic normalization of Landsat TM images of forest based on subpixel sun-canopy-sensor geometry. Remote Sensing of Environment, 64:166-175.

Guanter, L., Alonso, L., Gomez-Chova, L., Meroni, M., Preusker, R., Fischer, J., Moreno, J. (2010). Developments for vegetation fluorescence retrieval from spaceborne high-resolution spectrometry in the O-2-A and O-2-B absorption bands. Journal of Geophysical Research-Atmospheres, 115. D19303. DOI: 10.1029/2009JD013716

Guanter, L., Richter, R. and Moreno, J. (2006). Spectral calibration of hyperspectral imagery using atmospheric absorption features. Applied Optics, 45, 2360-2370

Guanter, L., L. Alonso, J. Moreno. (2005). A method for the surface reflectance retrieval from PROBA/CHRIS data over land: application to ESA SPARC campaigns. IEEE Transactions in Geoscience Remote Sensing 43, 2908–2917.

Guerschman, J.P., Paruelo, J.M., Bella, C.D., Giallorenzi, M.C. and Pacin, F. (2003). Land cover classification in the Argentine Pampas using multi-temporal Landsat TM data. International Journal of Remote Sensing, 24, 3381–3402.

Gunal, S. & Edizkan, R. (2008). Subspace based feature selection for pattern recognition. Information Sciences 178, 3716–3726.

Hansen, M. C., and DeFries, R. (2004). Detecting long-term global forest change using continuous fields of tree-cover maps from 8-km advanced very high resolution radiometer (AVHRR) data for the years 1982–99. Ecosystems, 7, 695–716.

Heiskanen, J. (2006). Tree cover and height estimation in the Fennoscandian tundra-taiga transition zone using multiangular MIRS data. Remote Sensing of Environment, 103, 97-114.

Helmer, E. H., Brown, S., and Cohen, W. B. (2000). Mapping montane tropical successional stage and land use with multi-date Landsat imagery. International Journal of Remote Sensing, 21, 2163–2183

Hill, M.J., Averill, C, Jiao, Z, Schaaf C.B., Armston J.D. 2008. Relationship of MISR RPV parameters and MODIS BRDF vegetation patterns in an Australian tropical savanna. Canadian Journal Of Remote Sensing, 34, S247-S267.

Hoekstra, J., Boucher, T., Ricketts, T., Roberts, C. (2005). Confronting a biome crisis: global disparities of habitat loss and protection. Ecology Letters 8, 23–29.

Holdridge, L., Grenke,W.C., Hatheway,W.H., Liang, T., Tosi Jr., J. (1971). Forest Environments in Tropical Life Zones: A Pilot Study. Pergamon Press, New York 747.

Huber, S., Koetz, B. Psomas, A., Kneubuehler, M., Schopfer, J.T., Itten, K.I. and Zimmermann, N.E. (2010). Impact of multiangular information on empirical models to estimate canopy nitrogen concentration in mixed forest. Journal of Applied Remote Sensing, 4, 043530.

Ingram, J. C., Dawson, T. P., Whittaker, R. J. (2005). Mapping tropical forest structure in southern Madagascar using remote sensing and artificial neural networks. Remote Sensing of Environment, 94, 491 – 507.

Innes, J. L., and B. Koch. (1998). Forest biodiversity and its assessment by remote sensing. Glob. Ecol. Biogeogrraphy, 7: 397–419.

Jacquemoud, S., F. Baret, and J. F. Hanocq. (1992). Modeling spectral and bidirectional soil reflectance. Remote Sensing of Environment, 41, 123–132.

Janzen, D.H., (1988). Tropical dry forests. The most endangered major tropical ecosystem. In: Wilson, E.O. (Ed.), Biodiversity. National Academy Press, Washington, pp. 130–137.

Janzen, D. H. & Wilson, D. E. (1983). Mammals. pp.426 -442. Costa Rican Natural History. Chicago University Press, Chicago, USA.

Jensen, J. R. (2000a). Remote Sensing of the Environment: An Earth Resource Perspective 2000. Upper Saddle River, New Jersey: Prentice-Hall Inc.

Jensen, G. L. Peterson,J. Q., Greenman, M. (2000b). Measurement results from flight measurements with the hyperspectral imaging polarimeter. Conference on Polarization Analysis, Measurement and Remote Sensing 4133:3, 214 – 220.

Jensen, J. R. (1996). Introductory Digital Image Processing (Upper Saddle River, NJ: Prentice Hall).

Jin, H., Li, P., Cheng, T., & Song B. (2012). Land cover classification using CHRIS/PROBA images and multi-temporal texture, International Journal of Remote Sensing, 33:1, 101-119.

Johansen K., Coops N.C., Gergel S.E., Stange Y. (2007). Application of high spatial resolution satellite imagery for riparian and forest ecosystem classification. Remote Sensing of Environment, 110, 29–44. doi:10.1016/ j.rse.2007.02.014

Joly, A.B., (1970). Conheça a vegetaçao brasileira, EDUSP e Polígono, Sao Paulo, Brazil.

Jones, J.R. (2001). Processing of digital data for the Central American Ecosystem map.

Kalacska, M., Sanchez-Azofeifa, G.A., Rivard, B., Caelli, T., White, H. P., Calvo-Alvarado, J.C. (2007a). Ecological fingerprinting of ecosystem succession: Estimating secondary tropical dry forest structure and diversity using imaging spectroscopy. Remote Sensing of Environment, 108,82–96.

Kalacska, M., Bohlman, S., Sanchez-Azofeifa, G.A., Castro-Esau, K., Caelli, T. (2007b). Hyperspectral discrimination of tropical dry forest lianas and trees: Comparative data reduction approaches at the leaf and canopy levels. Remote Sensing of Environment, 109, 406–415.

Kalacska, M. E. R., Sánchez-Azofeifa, G.A., Calvo-Alvarado, J.C., Rivard, B., and Quesada, M. (2005a). Effects of season and successional stage on Leaf Area Index and spectral vegetation indices in three Mesoamerican tropical dry forests. Biotropica 37:4, 486-496.

Kalácska, M., Sánchez-Azofeifa, G.A., Caelli, T., Rivard, B. and Boerlage, B. (2005b). Estimating Leaf Area Index from satellite imagery using Bayesian Networks. IEEE Transactions on Geoscience and Remote Sensing, 43:8.

Kalacska, M., Sanchez-Azofeifa, G.A., Rivard, B., Calvo-Alvarado, J.C., Journet, A.R.P., Arroyo-Mora, J.P., Ortiz-Ortiz, D. (2004a). Leaf area index measurements in a tropical moist forest: A case study from Costa Rica. Remote Sensing of Environment, 91, 134–152.

Kalacska, M.E.R, Sanchez-Azofeifa, G.A., Calvo-Alvarado, J.C., Quesada, M., Rivard, B., Janzen, D.H. (2004b). Species composition, similarity and diversity in three successional stages of a seasonally dry tropical forest. Forest Ecology and Management, 200, 227–247

Kaufmann, H., Segl, K., Guanter, L., Hofer, S., Foerster, K.-P., Stuffler, T., Mueller, A., Richter, R., Bach, H., Hostert, P., Chlebek, C. (2008). Environmental Mapping and Analysis Program (Enmap) – Recent advances and status. IEEE. IGARSS, Boston, 2008.

Kaufman Y. J. and Sendra C. (1988). Algorithm for atmospheric corrections. Inte rnational Journal of Remote Sensing, 9, 1357–1381.

Kayitakire F, Hamel C, Defourny P. (2006). Retrieving forest structure variables based on image texture analysis and IKONOS-2 imagery. Remote Sensing of Environment, 102, 390–401. doi:10.1016/j.rse.2006.02.022

Kimes, D.S., Ranson, K.J, Sun, G, and Blair J.B. (2006). Predicting lidar measured forest vertical structure from multi-angle spectral data. Remote Sensing of Environment. 100:4, 503-511.

Kimes, D. S. , Nelson, R. F. , Salas, W. A. and Skole, D. L. (1999). Mapping secondary tropical forest and forest age from SPOT HRV data. International Journal of Remote Sensing, 20: 18, 3625-3640.

Kimes, D. S. (1983). Dynamics of directional reflectance factor distributions for vegetation canopies. Applied Optics, 22, 1364-1372.

Kneubühler, M., Koetz, B., Huber, S., Zimmermann, N.E. and Schaepman, M. (2008). Space-based spectrodirectional measurements for the improved estimation of ecosystem variables. Canadian Journal of Remote Sensing, 34, 192-205.

Kneubühler, M., Koetz, B., Richter, R., Schaepman, M., and Itten, K. (2005). Geometric and radiometric pre-Processing of CHRIS/PROBA data over mountainous terrain. Proceedings of the Third CHRIS/PROBA Workshop, ESRIN, Frascati, Italy.

Knyazikhin, Y., Schull, M., Hu, L., Myneni, R. and Latorre-Carmona, P. (2009). Canopy spectral invariants for remote sensing of canopy structure. IEEE 1st Workshop on Hyperspectral Image and Signal Processing - Evolution in Remote Sensing. Grenoble, (France).

Kobayashi, S., Sanga-Ngoie, K. (2009). A comparative study of radiometric correction methods for optical remote sensing imagery: the IRC vs. other image-based C-correction methods. International Journal Of Remote Sensing, 30:2, 285-314.

Koetz, B., Kneubühler, M., Widlowski, J. L., Morsdorf, F., Schaepman, M. and Itten, K. (2005).Assessment of canopy structure and heterogeneity frommultiangular CHRIS-PROBA data. The 9th International Symposium on Physical Measurements and Signatures in Remote Sensing (ISPMSRS) (pp. 73-78). Beijing, China.

Krishnaswamy, J., Kiran, M. C. and K. Ganeshaiah, N. (2004). Tree model based eco- climatic vegetation classification and fuzzy mapping in diverse tropical deciduous ecosystems using multi-season NDVI. International Journal of Remote Sensing, 25, 1185–1205.

Kuusk, A., Kuusk, J., Lang, M. (2009). A dataset for the validation of reflectance models Remote Sensing of Environment, 113, 889–892.

Landgrebe, D. (1997). On information extraction principles for hyperspectral data.
http://dynamo.ecn.purdue.edu/wlandgreb/ whitepaper.pdf.

Lara G. and Taboada M., (1996). Historias de mis abuelos Mexico DF (Mexico): Desarrollo Educativo y Cultural Costa Alegre, A.C.

Lass, L. W., Thill, D. C., Shafii, B. and Prather, T. S. (2002). Detecting Spotted Knapweed (Centaurea maculosa) with Hyperspectral Remote Sensing Technology. Weed Technology, 16, 426 - 432.

Laurance, W. F. (1999). Reflections on the tropical deforestation crisis. Biological Conservation, 91, 109–117.

Laurent, V. C. E., Verhoef, W., Clevers, J. G. P. W. and Schaepman, M. E. (2011a). Inversion of a coupled canopy-atmosphere model using multi-angular top-of-atmosphere radiance data: A forest case study. Remote Sensing of Environment, 115, 2603–2612.

Laurent, V.C.E., Verhoef, W., Clevers, J.G.P.W., Schaepman, M.E. (2011b). Estimating forest variables from top-of-atmosphere radiance satellite measurements using coupled radiative transfer models. Remote Sensing of Environment 115, 1043–1052.

Lawrence, D., D'Odorico, P., DeLonge, M., Diekmann, L., Das, R., Eaton, J.M. (2007). Ecological feedbacks following deforestation create the potential for a catastrophic ecosystem shift in tropical dry forest. Proceedings of the National Academy of Sciences 104, 20696–20701.

Lawrence, R.L., Ripple, W.J. (2000). Fifteen years of revegetation of Mount St. Helens: A landscape-scale analysis. Ecology, 81:10, 2742-2752.

Leblanc, S.g., Chen, J.M., White, H.P., Latifovic, R., Lacaze, R. and Roujean, J.L. (2005). Canada-wide foliage clumping index mappinf from

multiangular POLDER measurements. Canadian Journal of Remote Sensing, 31, 364-376.

Levin N., Shmida A., Levanoni O., Tamari H., Kark, S. (2007). Predicting mountain plant richness and rarity from space using satellite-derived vegetation indices. Diversity Distribution, 13:692–703

Li, X., and Strahler, A. H. (1985). Geometric-optical modelling of a coniferous forest canopy. IEEE Transactions on Geoscience and Remote Sensing, 23:207–221.

Li, X., Strahler, A. H., and Woodcock, C. E. (1995). A hybrid geometric optical-radiative transfer approach for modeling albedo and directional reflectance of discontinuous canopies. Transactions on Geoscience and Remote Sensing, 33:466–480.

Liesenberg, V., Boehm, H-D. V., and Gloaguen, R. (2009). The contribution of CHRIS/PROBA data for tropical peat swamp landscape discrimination purposes. IEEE International Geoscience and Remote Sensing Symposium (IGARSS). Cape Town (South Africa).

Liesenberg, V., Galvao, L.S., Ponzoni, F.J. (2007). Variations in reflectance with seasonality and viewing geometry: implications for classification of Brazilian savanna physiognomies with MISR/Terra data. Remote Sensing of Environment, 107, 276–286.

Lo, T.H.C., Scarpace, F.L., Lillesand, T.M. (1986). Use of multitemporal spectral profiles in agricultural land-cover classification. Photogrammetric Engineering and Remote Sensing, 52, 535-544.

Lobo, J.A., Quesada, M., Stoner, K.E., Fuchs, E.J., Herrerias-Diego, Y., Rojas-Sandoval, J., Saborio-Rodriguez, G. (2003). Factors affecting phenological patterns of Bombacaceous trees in seasonal forests in Costa Rica and Mexico. American Journal of Botany, 90, 1054–1063.

Lu, D., Mause, P., Brondizio, E., Moran, E. (2003). Classification of successional forest stages in the Brazilian Amazon basin Forest Ecology and Management, 181, 301–312.

Lucas, R. M. , Honzák, M. , Amaral, I. D., Curran, P. J. and Foody, G. M. (2002). Forest regeneration on abandoned clearances in central Amazonia. International Journal of Remote Sensing, 23: 5, 965-988.

Lucas, R. M., Honzak, M., Curran, P. J., Foody, G. M., Milne, R., Brown, T., and Amaral, S. (2000). Mapping the regional extent of tropical forest regeneration stages in the Brazilian Legal Amazon using NOAA AVHRR data. International Journal of Remote Sensing, 21, 2855–2881.

Lugo, A. E. and E. Helmer. (2004). Emerging forests on abandoned land: Puerto Rico's new forests. Forest Ecology Management 190: 145–161.

Maass, M., and A. Martinez-Yrizar. (2001). NPP Tropical Forest: Chamela, Mexico, 1982–1995. Data set. Available online [http://www.daac. ornl.gov] from Oak Ridge National Laboratory Distributed Active Archive Center, Oak Ridge, Tennessee.

Mahtab, A., Sridhar, V.N., Navalgund, R.R. (2008). Impact of surface anisotropy on classification accuracy of selected vegetation classes: an evaluation using multidate multiangular MISR data over parts of Madhya Pradesh, India. IEEE Transactions in Geoscience and Remote Sensing, 46, 250–258.

Malenovsky, Z., Martin, E., Homolova, L., gastellu-Etchegory, J.P., Zurita-Milla, R., Schaepman, M.E., Pokorny, R., Clevers, J.G.P.W., Cudlin, P. (2007). Influence of woody elements of a Norway spruce canopy on nadir reflectance simulated by the DART model at very high spatial resolution. Remote Sensing of Environment, 112:1, 1–118.

Malingreau, J. P., Tucker, C.J., Laporte, N. (1989). AVHRR for monitoring global tropical deforestation. International Journal of Remote Sensing, 10 :4-5, 855-867.

Mares, M. A. (1992). Neotropical mammals and the myth of Amazonian diversity. Science, 255: 976-979.

Martin, M. E., Newman, S. D., Aber, J. D., and Congalton, R. G. (1998). Determining forest species composition using high spectral resolution remote sensing data. Remote Sensing Environment, 65:249–254.

Martin, M. E., and Aber, J. D. (1997). High spectral resolution remote sensing of forest canopy lignin, nitrogen, and ecosys tem processes. Ecological Applications, 7:2, 431–443.

Mas J.F., Velazquez A., Palacio-Prieto J.L., Bocco G., Peralta A., Prado J. (2002). Assessing forest resources in Mexico: Wall-to-wall land use/cover

mapping Photogrammetric Engineering and Remote Sensing, 68:10, 966-968.

Mayaux, P., Holmgren, P., Achard, F., Eva, H., Stibig, H.J., Branthomme, A. (2005). Tropical forest cover change in the 1990's and options for future monitoring. Philosophical Transactions of the Royal Society Bulletin, 360, 373-384.

Meyer, D., Verstraete, M.M., and Pinty, B. (1995). The effect of surface anisotropy and viewing geometry on the estimation of NDVI from AVHRR. Remote Sensing Reviews. 12: 1, 3-27.

Miles, L., Newton, A., DeFries, R., Ravilious, C., May, I., Blyth, S., Kapos, V., Gordon, J. (2006). A global overview of the conservation status of tropical dry forests. Journal of Biogeography, 33, 491–505.

Minnaert, M. (1941). The reciprocity principle in lunar photometry. Astrophysical Journal, 93:3, 403-410.

Mitchell, T. M. (1997). Machine learning. New York: McGraw-Hill.

Moran, EF; Brondizio, ES; Tucker, JM, da Silva-Forsberg MC, McCracken S, Falesi I. (2000). Effects of soil fertility and land-use on forest succession in Amazonia. Forest Ecology And Management, 139: 1-3, 93-108.

Moran, E. F., Brondizio, E., Mausel, P., and Wu, Y. (1994). Integrating Amazonian vegetation, land-use, and satellite data: attention to differential patterns and rates of secondary succession can inform future policies. BioScience, 44, 329–338.

More, G. & Pons, X. (2007). Influencia del número de imágenes en la calidad de la cartografía detallada de vegetación forestal. Revista de Teledetección.ISSN: 1133-0953. 28: 61-68.

Mõttus, M. and Rautiainen, M. (2009). Direct retrieval of the shape of leaf spectral albedo from multiangular hyperspectral Earth observation data. Remote Sensing of Environment 113, 1799–1807.

Murphy, P. G., and A. E. Lugo. (1986). Ecology of tropical dry forest. Annual Review of Ecology Evolution and Systematics, 17: 67–88.

Myneni, R. B., and Asrar, G. (1993). Radiative transfer in three-dimensional atmosphere–vegetation media. Journal of Quantitative Spectroscopy and Radiative Transfer, 49:585–598.

Myneni, R. B., Ross, J., and Asrar, G. (1989). A review on the theory of photon transport in leaf canopies. Agricultural and Forest Meteorology, 45, 1–153.

Nagendra, H. (2001). Using remote sensing to assess biodiversity. International Journal of Remote Sensing, 22, 2377–2400. doi:10. 1080/01431160117096

Nagendra, H. and Rocchini, D. (2008). High resolution satellite imagery for tropical biodiversity studies: the devil is in the detail. Biodiversity and Conservation, 17, 3431–3442 DOI 10.1007/s10531-008-9479-0

Nicodemus, F.E., Richmond, J.C., Hsia, J.J., Ginsberg, I.W., Limperis, T., (1977). Geometrical Considerations and Nomenclature for Reflectance, Rep. No. 160. National Bureau of Standards, US Department of Commerce, Washington, DC. Olson, D.M. et al., 2001. Terrestrial ecoregions of the world: a new map of life on earth. BioScience, 51, 933–938.

Opler, P.A., Baker, H.G., Frankie, G.W. (1980). Plant reproductive characteristics during secondary succession in neotropical lowland forest ecosystems. Biotropica 12, 40–46.

Ostrom, E., Nagendra, H. (2006). Insights on linking forests, trees, and people from the air, on the ground and in the air. Proceedings of the National Academy of Sciences. USA, 103, 19224–19231, doi:10.1073/pnas.0607962103

Pacheco, A. (1998). Inventario Florístico durante la sucesión del bosque tropical seco, Parque Nacional Santa Rosa, Guanacaste. Informe de Practica de Especialidad, p. 114. ITCR- Departamento de Ingeniería Forestal.

Palà, V. & X. Pons (1995). Incorporation of relief into geometric corrections based on polynomials. Photogrammetric Engineering & Remote Sensing, 61:7, 935-944.

Pax-Lenney, M. & Woodcock, C.E. (1997). Monitoring Agricultural Lands in Egypt with Multitemporal Landsat TM Imagery: How many Images are needed?. Remote Sensing of the Environment, 59, 522-529.

Pennington, T., Lewis, G., Ratter, J. (2006). Neotropical Savannas and Seasonally Dry Forests: Plant Diversity, Biogeography and Conservation. CRC Press, FL, USA.

Perz, S.G. and Skole, D.L. 2003. Social determinants of secondary forests in the Brazilian Amazon. Social Science Research Network. 32, 25–60.

Pinty, B., Widlowski, J. -L., Gobron, N., Verstraete, M. M., & Diner, D. J. (2002). Uniqueness of multiangular measurements—Part I: An indicator of subpixel surface heterogeneity from MISR. EEE Transactions on Geoscience and Remote Sensing, 40:7, 1560-1573.

Pocewicz, A., Vierling, L. A., Lentile, L. B., & Smith, R. (2007). View angle effects on relationships between MISR vegetation indices and leaf area index in a recently burned ponderosa pine forest. Remote Sensing of Environment, 107, 322-333.

Pons, X., (2000). MiraMon. Geographic Information System and Remote Sensing software. Centre de Recerca Ecològica i Aplicacions Forestals, CREAF. Bellaterra (Barcelona).

Pons, X. & Solé-Sugrañes, L. (1994). A Simple radiometric correction model to improve automatic mapping of vegetation from multispectral satellite data. Remote Sensing of Environment, 48, 191-204.

Ponzoni, F. J. Galvão, L. S. Liesenberg, V. & Santos, J. R. (2010). Impact of multi-angular CHRIS/PROBA data on their empirical relationships with tropical forest biomass, International Journal of Remote Sensing, 31:19, 5257-5273.

Portillo-Quintero, C. A., Sánchez-Azofeifa, G. A. (2010). Extent and conservation of tropical dry forests in the Americas. Biological Conservation, 143, 144-155.

Powell, R. L., Matzke, N., de Souza Jr., C., Clark, M., Numata, I., Hess, L. L., et al. (2004). Sources of error in accuracy assessment of thematic land-cover maps in the Brazilian Amazon. Remote Sensing of Environment, 90, 221–234.

Proy, C., Tanre, D., & Deschamps, P. Y. (1989). Evaluation of topographic effects in remotely sensed data. Remote Sensing of Environment, 30, 21-32.

Queiroz, L.P. (2006). The Brazilian caatinga: phytogeographical patterns inferred from distribution data of the leguminosae. In: Pennington, R.T., Ratter, J.A., Lewis, G.P. (Eds.), Neotropical Savannas and Seasonally Dry Forests: Plant Biodiversity, Biogeography and Conservation. CRC Press, Boca Raton, FL.

Rahman, H., & Dedieu, G. (1994). SMAC: a simplified method for the atmosphericcorrection of satellite measurements in the solar spectrum. International Journal of Remote Sensing, 15, 123-143.

Rautiainen, M., Lang, M., Mõttus, M., Kuusk, A., Nilson, T., Kuusk, J., Lükk, T. (2008). Multi-angular reflectance properties of a hemiboreal forest: An analysis using CHRIS PROBA data Remote Sensing of Environment, 112, 2627–2642.

Redford, K. H., A. Taber, and J. A. Simonetti. 1990. There is more biodiversity than tropical rain forests. In defense of non-rain forests ecosystems. Conservation Biology. 4, 1-3.

Richards, J. A. and Jia, X. (2005). Remote Sensing Digital Image Analysis: An Introduction, Springer-Verlag New York, Inc., Secaucus, NJ, USA.

Richards, J.A. (1993). Remote Sensing Digital Image Analysis. Springer-Verlag. Berlin. pp. 240.

Richter, R. (1998). Correction of satellite images over mountainous terrain. Applications in Optics, 37, 4004–4015.

Roberts, D. A., Green, R. O., Sabol, D. E., and Adams, J. B. (1993). Temporal changes in endmember abundances, liquid water and water vapor over vegetation at Jasper Ridge. In Summaries of the Fourth Annual JPL Airborne Geoscience Workshop, Jet Propulsion Laboratory, Pasadena, CA, pp. 153–156.

Rocchini, D. (2007). Effects of spatial and spectral resolution in estimating ecosystem _-diversity by satellite imagery. Remote Sensing of Environment, 111:423–434. doi:10.1016/j.rse.2007.03.018

Ross, J. K. (1981). The Radiation Regime and Architecture of Plant Stands, Kluwer Boston, Hingham, MA.

Roujean, J.L., Lacaze, R. (2002). Global mapping of vegetation parameters from POLDER multiangular measurements for studies of surface-atmosphere interactions: A pragmatic method and its validation. Journal of Geophysical Research-Atmospheres, 107(D12):4150.

Ruiz, J., Fandiño, M. C. and Chazdon, R. L. 2005. Vegetation Structure, Composition, and Species Richness Across a 56-year Chronosequence of Dry Tropical Forest on Providencia Island, Colombia. Biotropica, 37: 520–530. doi: 10.1111/j.1744-7429.2005.00070.x

Running, S. W., C. O. Justice, and D. Carneggie, (1994). Terrestrial remote sensing science and algorithms planned for EOS/ MODIS. International Journal of Remote Sensing, 15, 3587–3602.

Rzedowski, J. (1991). El endemismo en la flora fanerogamica mexicana: una apreciacion analitica preliminar. Acta Botanica Mexicana 15, 47–64.

Saatchi, S.S., Harris, N.L., Brown, S., Lefsky, M., Mitchard, E.T.A., Salas, W., Zutta, B.R., Buermann, W., Lewis, S.L., Hagen S., Petrova, S., White, L., Silman, M., Morel, A. (2010). A Benchmark map of forest carbon stocks in tropical regions across three continents. Proceedings of the National Academy of Sciences of the United States of America 2011, 108:9899-9904.

Sabol Jr, D.E., Gillespie, A.R., Adams, J.B., Smith, M.O. and Tucker, C.J. (2002). Structural stage in Pacific Northwest forests estimated using simple mixing models of multispectral images. Remote Sensing of Environment, 80, 1-16.

Sader, S.A., Waide, R.B., Lawrence, W.T., Joyce A.T. (1989). Tropical forest biomass and successional age class relationships to a vegetation index derived from Landsat TM data. Remote Sensing of Environment. 28, 143-156.

Saldarriaga, J.G., West, D.C., Tharp, M.L., Uhl, C., (1988). Longterm chronosequence of forest succession in the Upper Rio Negro of Colombia and Venezuela. Jorunal of Ecology, 76, 938–958.

Sánchez-Azofeifa, G. A., Quesada, M., Cuevas-Reyes, P., Castillo A., and Sánchez-Montoya, G. (2009). Land cover and conservation in the area of

influence of the Chamela-Cuixmala Biosphere Reserve, Mexico. Forest Ecology and Management, 258: 6, 907-912.

Sánchez-Azofeifa, G.A., Quesada, M., Rodriguez, J.P., Nassar, J.F., Stoner, K.E., Castillo, A., Garvin, T., Zent, E.L., Calvo-Alvarado, J.C., Kalacska, M.E.R., Fajardo, L., Gamon, J.A. and Cuevas-Reyes, P. (2005). Research priorities for Neotropical dry forests. Biotropica, 37:4, 477–485.

Sanchez-Azofeifa G.A., Castro K.L., Rivard B., Kalascka M.R., Harriss R.C. (2003a). Remote sensing research priorities in tropical dry forest environments. Biotropica, 35:134–142

Sanchez-Azofeifa, G. A., Daily, G. C., Pfaff, A. S. P., & Busch, C. (2003b). Integrity and isolation of Costa Rica's national parks and biological reserves: examining the dynamics of land-cover change. Biological Conservation, 109, 123-135.

Sandmeier, S., and Deering, D. W. 1999. Structure analysis and classification of boreal forests using airborne hyperspectral BRDF data from ASAS. Remote Sensing of Environment. 69:281–295.

Schaepman, M.E., Ustin, S.L., Plaza, A.J., Painter, T.H., Verrelst, J., Liang, S. (2009). Earth system science related imaging spectroscopy – An assessment Remote Sensing of Environment,113, S123–S137.

Schaepman, M. E. (2007). Spectrodirectional remote sensing: From pixels to processes. International Journal of Applied Earth Observation and Geoinformation, 9, 204–223.

Schaepman, M.E., Koetz, B., Schaepman-Strub, G., Itten, K.I., (2005). Spectrodirectional remote sensing for the improved estimation of biophysical and chemical variables: two case studies. International Journal of Applied Earth Observation and Geoinformation. 6, 271–282.

Schaepman, M. E., Koetz, B., Schaepman-Strub, G., Zimmermann, N. E. and Itten, K. I. (2004). Quantitative retrieval of biogeophysical characteristics using imaging spectroscopy – a mountain forest case study. Community Ecology, 5:1, 93-104.

Schaepman-Strub, G., Schaepman, M.E., Painter, T.H., Dangel, S., and Martonchik, J.V. (2006). Reflectance quantities in optical remote sensing definitions and case studies. Remote sensing of Environment, 103, 27– 42.

Schroeder, T. A., Cohen, W. B., Song, C., Canty, M. J., & Yang, Z. (2006). Radiometric correction of multi-temporal Landsat data for characterization of early successional forest patterns in western Oregon. Remote Sensing of Environment, 103:16-26.

Sedano, F., Gomez, D., Gong, P, Biging G.S. (2008). Tree density estimation in a tropical woodland ecosystem with multiangular MISR and MODIS data. Remote Sensing of Environment, 112: 5, 2523-2537.

Shriever, J. R. & Congalton, R. G. (1993). Mapping forest cover types in New Hampshire using multi-temporal Landsat Thematic Mapper data. ASPRS/ACSM Ann. Conv. Exp., New Orleáns. 333–342.

Sidak, Z. (1967). Rectangular Confidence Regions for the Means of Multivariate Distributions, Journal of American Statistics Association. 62, 626-633.

Skole, D. L., and Tucker, C. J. (1993). Tropical deforestation and habitat fragmentation in the Amazon: satellite data from 1978 to 1988. Science, 260, 1905–1910.

Smith, J. A., Tzeu Lie Lin, T. L., and Ranson, K. J. (1980). The Lambertian assumption and Landsat data. Photogrammetric Engineering and Remote Sensing, 46, 1183–1189.

Snedecor, George W. & Cochran, William G. (1989). Statistical Methods (8th ed.). Ames, Iowa: Blackwell Publishing Professional. ISBN 0-8138-1561-4.

Song, C., & Woodcock, C. E. (2003). Monitoring forest succession with multitemporal Landsat images: Factors of uncertainty. IEEE Transactions on Geoscience and Remote Sensing, 41, 2557-2567.

Song, C.H., Woodcock, C.E., Li, X.W. (2002). The spectral/temporal manifestation of forest succession in optical imagery - The potential of multitemporal imagery. Remote Sensing of Environment, 82:2-3, 285-302.

Stehman, S.V., Sohl, T.L., Loveland, T.R. (2003). Statistical sampling to characterize recent United States land-cover change. Remote Sensing of Environment, 86, 517–529

Stehman, S. V. (1999): Comparing thematic maps based on map value, International Journal of Remote Sensing, 20:12, 2347-2366

Steininger, M. K. (2000). Satellite estimation of tropical secondary forest above ground biomass: data from Brazil and Bolivia. International Journal of Remote Sensing, 21, 1139–1157.

Steininger, M. K. (1996). Tropical secondary forest regrowth in the Amazon: age, area and change estimation with Thematic Mapper data. International Journal of Remote Sensing, 17, 9–27.

Stoms D.M., Estes J.E. (1993). A Remote-Sensing Research Agenda for Mapping and Monitoring Biodiversity. International Journal of Remote Sensing, 14, 1839-1860.

Swain, P. H., & Davis, S. M. (1978). Remote sensing: the quantitative approach. New York: McGraw-Hill.

Teillet, P. M., Guindon, B. and Goodenough, D. G. (1982). On the slope-aspect correction of multispectral scanner data. Canadian Journal of Remote Sensing, 8:2, 84–106.

Thenkabail, P.S., Enclona, E.A., Ashton, M.S. and Van Der Meer, B. (2004a). Accuracy assessments of hyperspectral waveband performance for vegetation analysis applications. Remote Sensing of Environment, 91, 354–376.

Thenkabail, P.S., Enclona, E.A., Ashton, M.A., Legg, C., Dieu, M.J.D. (2004b). Hyperion, IKONOS, ALI and ETM+ sensors in the study of African rainforests. Remote Sensing Environment, 90, 23–43. doi:10.1016/j.rse.2003. 11.018

Thenkabail, P. S. (2003). Biophysical and yield information for precision farming from near-real-time and historical Landsat TM images. International Journal of Remote Sensing, 24:14, 839– 877.

Thenkabail, P. S. (1999). Characterization of the alternative to slash-and-burn benchmark research area representing the Congolese rainforests of Africa using near-real-time SPOT HRV data, International Journal of Remote Sensing, 20: 5, 839 — 877.

Townsend, A.R., Asner, G.P., Cleveland, C.C. (2008). The biogeochemical heterogeneity of tropical forests. Trends Ecol Environ 43:8, 424–431. doi:10.1016/j.tree.2008.04.009

Uhl, C., Bushbacher, R., and Serrao, E. A. S. (1988), Abandoned pastures in Eastern Amazonia. I. Patterns of plant succession. Journal of Ecology, 76, 663–681.

Underwood, E., Ustin, S. and DiPietro, D. (2003). Mapping nonnative plants using hyperspectral imagery, Remote Sensing of Environment, 86, 150-161.

Ustin, S.L., Jacquemoud, S., and Asner, G.P. (2004). Remote sensing of environment: state of the science and new directions. In Remote sensing for natural resource management and environmental monitoring. Manual of remote sensing. Edited by S.L. Ustin. John Wiley & Sons, Hoboken, N.J. pp. 679-729.

Ustin, S. L., Smith, M. O., Roberts, D., Gamon, J. A. and Field, C. B. (1992). Using AVIRIS images to measure tem poral trends, in abundance of nonphotosynthetic canopy components. In Summaries of the Third Annual JPL Air borne Geoscience Workshop, Jet Propulsion Laboratory, Pasadena, CA, pp. 5–7.

Verhoef, W. and Bach, H. (2007). Coupled soil–leaf-canopy and atmosphere radiative transfer modeling to simulate hyperspectral multi-angular surface reflectance and TOA radiance data. Remote Sensing of Environment, 109, 166–182

Vermote, D., Tanre, J. L., Deuze, M., Herman, and Morcrette, J. J. (1994) Second simulation of the satellite signal in the solar spectrum (6S). User Guide Apr. 18, NASA GSFC, Greenbelt MD, pp.183.

Verrelst, J., Clevers, J.G.P.W., Schaepman, M.E. (2010). Merging the Minnaert-k parameter with Spectral Unmixing to map forest heterogeneity with CHRIS/PROBA data. IEEE Transactions on Geoscience and Remote Sensing, 48:11, 4014-4022.

Verrelst, J., Schaepman, M.E., Malenovský, Z., Clevers, J.G.P.W. (2009). Effects of woody elements on simulated canopy reflectance: Implications for forest chlorophyll content retrieval. Remote Sensing of Environment, 114, 647–656

Verrelst, J., Schaepman, M. E., Koetz, B., & Kneubühler, M. (2008). Angular sensitivity analysis of vegetation indices derived from CHRIS/PROBA data. Remote Sensing of Environment, 112, 2341-2353.

Verstraete, M.M., Pinty, B., Myneni, R.B. (1996). Potential and limitations of information extraction on the terrestrial biosphere from satellite remote sensing. Remote Sensing of Environment, 58, 201– 214.

Vicente-Serrano, S. M., Pérez-Cabello F., Lasanta, T. (2008). Assessment of radiometric correction techniques in analyzing vegetation variability and change using time series of Landsat images. Remote Sensing of Environment, 112, 3916–3934

Vieira, I. C. G., Silva de Almeida, A., Davidson, E. A., Stone, T. A. Reis de Carvalho, C. J., Guerrero, J. B. (2003). Classifying successional forests using Landsat spectral properties and ecological characteristics in eastern Amazonia. Remote Sensing of Environment, 87, 470–481.

Vincini, M., & Frazzi, E. (2003). Multitemporal evaluation of topographic normalization methods on deciduous forest TM data. IEEE Transactions on Geoscience and Remote Sensing, 41, 2586-2590.

Vincini, M., Reeder, D., and Frazzi, E. (2002). An empirical topographic normalization method for forest TM data. Proceedings IGARSS, Toronto, ON, Canada, June 24th 2002. 28, 2091–2093.

Vreugdenhil, D., J. Meerman, A. Meyrat, L. Diego Gómez, and D. J. Graham. (2002). Map of the Ecosystems of Central America: Final Report. World Bank, Washington, D.C.

Wessels, K.L., DeFries, R.S., Dempewolf, J., Anderson, L.O., Hansen, A.J. Powell, S.L. and Moran, E.F. (2004). Mapping regional land cover with MODIS data for biological conservation: Examples from the Greater Yellowstone Ecosystem, USA and Parao State, Brazil. Remote Sensing of Environment, 92, 67-83.

Widlowski, J.L., Pinty, B., Gobron, N., Verstraete, M., Diner, D.J., & Davis, B. (2004). Canopy structure parameters derived from multi-angular remote sensing data for terrestrial carbon studies. Climatic Change, 67, 403-415.

Widlowski, J.L., Pinty, B., Gobron, N., Verstraete, M., & Davis, B. (2001). Characterization of surface heterogeneity detected at the MIRS/Terra subpixel scale. Geophysical Research Letters, 28, 4639-4642.

Wilson, E.O. (1989). Threats to biodiversity. Scientific American, 261:3, 108.

Wilson, E. O. (1988). Biodiversity. Washington, DC7 National Academy of Sciences.

Wolter, P. T., Mladenoff, D. J., Host, G. E. & Crow, T. R.. (1995). Improved forest classification in the northern Lake States using multitemporal Landsat imagery. Photogrammetric Engineering & Remote Sensing. 61:1129–1143.

Woodwell, G. M., Houghton R. A., Stone T. A. 1986. Deforestation in the Brazilian amazon basin measured by satellite imagery. PRANCE, G. T. (ED.). AAAS Selected Symposium, 101. Tropical Rain Forests and The World Atmosphere. New York, USA, May 27, 1984. pp.23-32.

Wright, S. J., Muller-Landau H. C. (2006). The Future of Tropical Forest Species. Biotropica, 38:3, 287–301.

Wright, S. J. (2005). Tropical forests in a changing environment. Trends in Ecology Evolution, 20, 553–560.

Xu, J.W., Liang, Y., Wang, Y.Q. (2009). Examining Effects of Past Volcanic Eruptions on Forests of the Changbai Mountain with in situ and Remote Sensing Observations. 17th International Conference on Geoinformatics, Vol. 1 and 2, 547-552.

Zhang, Z.M., De Wulf, R.R.,Van Coillie, F.M.B.,Verbeke, L.P.C., De Clercq, E.M., Ou, X.K. (2011). Influence of different topographic correction strategies on mountain vegetation classification accuracy in the Lancang Watershed, China. Journal Of Applied Remote Sensing, 5.